#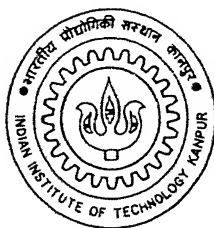 DEVELOPMENT OF 3-D EM SIMULATOR FOR DESIGNING MICROWAVE CIRCUITS USING MATERIAL INDEPENDENT PERFECTLY MATCHED LAYERS AS ABC

By

Amitabh Chowdhary

To the

DEPARTMENT OF ELECTRICAL ENGINEERING

INDIAN INSTITUTE OF TECHNOLOGY, KANPUR

July 1999

DEVELOPMENT OF 3-D EM SIMULATOR FOR DESIGNING MICROWAVE CIRCUITS USING MATERIAL INDEPENDENT PERFECTLY MATCHED LAYERS AS ABC

By

Amitabh Chowdhary

To the

DEPARTMENT OF ELECTRICAL ENGINEERING

INDIAN INSTITUTE OF TECHNOLOGY, KANPUR

July 1999

DEVELOPMENT OF 3-D EM SIMULATOR FOR DESIGNING MICROWAVE CIRCUITS USING MATERIAL INDEPENDENT PERFECTLY MATCHED LAYERS AS ABC

A Thesis Submitted

In Partial Fulfillment of the Requirements

For the Degree of

Master of Technology

By

Amitabh Chowdhary

To the

DEPARTMENT OF ELECTRICAL ENGINEERING

INDIAN INSTITUTE OF TECHNOLOGY, KANPUR

July 1999

Certificate

It is certified that work contained in the thesis entitled, **DEVELOPMENT OF 3-D EM SIMULATOR FOR DESIGNING MICROWAVE CIRCUITS USING MATERIAL INDEPENDENT PERFECTLY MATCHED LAYER AS ABC,** by **Amitabh Chowdhary,** Has been carried out under my supervision and this work has not been submitted elsewhere for a degree.

6 JULY 1999

(DR. Animesh Biswas)

Associate Professor

Department of Electrical Engineering

I.I.T. Kanpur

Co-Guides

(DR. Joseph John)

Associate Professor

Department of Electrical Engineering

I.I.T. Kanpur

(Shri Akhilesh Jain)

Scientific Officer 'D'

C.A.T., D.A.E,

Indore

Acknowledgements

Acknowledgements

Abstract

DEVELOPMENT OF 3-D EM SIMULATOR FOR DESIGNING MICROWAVE CIRCUITS USING MATERIAL INDEPENDENT PERFECTLY MATCHED LAYERS AS ABC

Thesis Supervisor   **Dr. Animesh Biswas**

Co-guide   **Dr. Joseph John**
   Akhilesh Jain

An improved version of unsplit perfectly matched layers (PML), which is material independent, has been formulated for the simulation of microwave circuits embedded in lossy, isotropic or anisotropic, dielectric and magnetic 3-D media. Advantage of using PML is that it provides virtually reflection free absorption, which gives highly accurate solutions for circuit parameters. It has been demonstrated that because of accuracy of material independent perfectly matched layers (MIPML), the usual oscillatory behavior observed in dispersion relations of characteristic impedance and relative effective dielectric constant in FDTD analysis is drastically reduced. The other advantage of MIPML formulation is that for various types of geometries and material, there is no modification in the algorithm for the calculation of flux components in perfectly matched layers and in working domain. By adding a little structural details in the subroutines; responsible for setting up PEC in working domain, for calculating E and H fields from flux components and for specifying source stimulus, the program can calculate circuit parameters. This greatly enhances potential for calculating responses of complex circuits and radiating structures without any major changes in the program. Though the scheme, which has been adapted here requires more memory but it lends it self for uniformity of the algorithm throughout the computing domain, reduces number of subroutines and makes it easier for developers to debug the program. A collection of sample problems have been included to demonstrate the working potential of the program and to validate calculated results with published data. Samples include patch antenna on an anisotropic substrate, propagation of a Gaussian pulse in a microstrip, wave propagating in a uniform anisotropic 3-D medium. It has been found that calculated and published results are in excellent agreement. Dispersion relationships of characteristic impedance and relative effective dielectric constants of microstrip on an arbitrary anisotropic substrate, which are very useful for CAD have been worked out. Here these responses have been calculated by both, conventional method of multiple cells and a new single cell method based upon transmission line analogy. It has been successfully demonstrated that new method developed in this thesis further reduces oscillations observed in dispersion relations. Improvement is quite distinctive at lower frequency side.

Chapter 1

Introduction

Finite difference time domain method was introduced by Yee K. S. [1] back in 1966. Method did not receive much attention due to several reasons. Prominent of them was high cost of computation. Although with time, cost of computation came down, there was a lack of proper absorbing boundary conditions, which were inherent in the original scheme for open boundary problems. After researchers proposed several ABCs, there has been a tremendous growth of activity in FDTD making it the most popular method in electromagnetics problems. There are numerous advantages of the FDTD method. In present scenario of computation, it enjoys popularity because it lends itself to be programmed on parallel processors and thus analysis of very complex geometries is possible. Further being a time domain technique, in a single run it gives response of the geometry over a wide frequency range. Another reason for its popularity is that very little analytical preparation is required and standard algorithms can be developed which cover a wide range of the problems. The scope of FDTD method covers almost entire field of electromagnetics, so it is difficult to cover all of them. The FDTD method has been extensively used for Microwave CAD, mostly for isotropic medium. In this thesis FDTD method has been chosen over other methods (TLM or Bergeron's) because it is extremely efficient, its implementation is quite straight forward, and it may be derived directly from Maxwell's equation. X.Zhang et al. [2,3] had used FDTD with Super Absorbing Boundary conditions to analyze frequency dependent characteristics of microstrip transmission lines and discontinuities. They had used electric wall source, which resulted in a sharp magnetic field tangential to the source wall. This results in some distortion of the launched pulse. Sheen et al. [11], for characterizing microstrip discontinuities, also used FDTD method with Mur's first order ABC and used magnetic wall in source plane, which was imposed using image theory which avoided induced magnetic field. Here electric field components on source plane were obtained using finite difference equations. However, method of excitation was complicated but it was better than Xhang et al. In addition, ABC used by them was simpler. In FDTD analysis, frequency dependence of microstrip parameters shows oscillatory behavior [12]. One of the contributors to

oscillatory behavior is mixed modes of propagation and evanescent waves contained in excitation source. Advanced excitation source scheme proposed by Zhao in [26,27] is quite simple and much better. Major contribution to oscillatory behavior comes from imperfect ABCs and the Mur's ABC, used by above researchers is not perfect. Also computation domain required by these pioneering works was large as ABCs used, required scatterer to be placed quite far, so impinging waves on interface become plane waves and near normal incident. In October 1994, Berenger created waves by introducing Perfectly Matched Layer [13], which was far superior, compared to existing ABCs. The innovation of Berenger's PML is that plane waves of arbitrary incidence, polarization, and frequency are matched at the boundary. This helped in reducing size of computing domain enormously. Though Berenger's original paper was for two-dimensional isotropic space but Katz [25] et al. validated it for 3-D space. Its wide band performance was validated by Reuter et al. [26]. Among other researchers who put forward rigorous analysis of absorption characteristics of PML, were Prescott et al. [29,30] who compared PML with other ABCs in a two-part article. Extensive research by Fang et al. [15,16] overcame certain disadvantages of PML formulation, mainly absorption of evanescent waves and inclusion of lossy materials. They also optimized parameters for PML. Others who did similar works were Cangellaris et al. [14]. All above works focussed on split formulations. Later Chew and Weedon [18] introduced stretched co-ordinate approach, which provided pathways to map PML in cylindrical and other co—ordinates systems. Also using stretched co-ordinate transformation, PML equations could be transformed to unsplit form, which is Maxwellian and more familiar. An alternative formulation for FEM, which was unsplit PML without co-ordinate transformation, was proposed by Sacks et al. [19]. Cangellaris et al. [17] and Gedney [20] adapted this unsplit formulation for FDTD. Gedney later also developed it for lossy and dispersive media [21]. He also analyzed patch antenna on isotropic substrate. Work of these researchers was for isotropic media.

Garcia et al. [31] derived matching condition on a single interface between anisotropic medium and isotropic PML for an extra ordinary wave in 2-D space. However, it was of no practical use and could not be extended for 3-D space. Zhao et al. [32] proposed split formulation which they called Material Independent Perfectly Matched layer (MIPML) in

2-D dielectric space. They gave theoretical proof later [22] for this split formulation, which was very similar to what was proposed by Berenger. The proposed MIPML was used for 2-D arbitrary anisotropic magnetic media by Zhao [33] with almost similar approach by just replacing dielectric quantities with magnetic ones. Later Zhao et al. used the same MIPML for arbitrary dielectric and magnetic media for 2-D [23]. Zhao et al. [24] then extended this split formulation for 3-D but without any proof. They used matching conditions similar to those of 2-D in three dimensions.

In fact, it was Gedney's work [20,21], which first time clearly hinted, and in his personal communication to us, he confirmed that UPML could be used to absorb hybrid waves. Prompted by this, UPML has been adopted for our work on anisotropic media in this thesis. Using formulation for isotropic medium proposed by Gedney, It has been demonstrated that UPML equations are material independent if permittivity and permeability in Maxwell equations are combined with field quantities for replacing them with flux quantities. Then it has been shown numerically that this new UPML formulation matches Hybrid waves propagating in 3-D homogeneous and non-homogeneous arbitrary anisotropic mediums. For 2-D, a general proof has been developed for Split formulation to show that PML matches to anisotropic media. Zhao et al. [22] have also proposed a proof for matching PML to 2D anisotropic dielectric media using flux components. Proof in this thesis is without using flux components and it is for the media which is anisotropic in permittivity and permeability both. The proof has been done with field components only. In a publication Zhao et al. [24] have shown matching of 3-D anisotropic media to PML numerically but they have used split formulation which is quite memory intensive and secondly they have extended no theoretical proof. In our work, it has been clearly shown that MIPML with unsplit formulation is far more efficient in terms of memory requirement. It has also been proved that extension of UPML to any media in 3D is possible, as UPML equations are inherently material independent.

By adapting to MIPML, reflections from truncation boundary have been reduced. Its virtual reflection free performance gives highly accurate time domain results. By developing unsplit formulation, memory requirements have been reduced. By using Zhao's advanced excitation scheme, source specification in FDTD code has been

simplified and reduction of errors in time domain results. This all together provides oscillation free frequency dependent characteristics of microstrip on an anisotropic substrate.

Need for characteristics of planar circuits on arbitrary anisotropic substrate come from various reasons. One of the practical design difficulties of using isotropic substrates, such as alumina, is the significant variation in dielectric permittivity from different manufacturers or even from batch to batch from the same manufacturer. This essentially means that repeated measurements are required for accurate design of microstrip circuits. The use of anisotropic substrate with stable electrical properties, such as sapphire, alleviates this difficulty. Also sapphire has pot free structure and its flat surface makes it best known anisotropic substrate for MICs. But its anisotropic behavior requires new techniques to characterize microstrip devices on sapphire substrate. The TEM approach was used by Owens et al. [34] and Alexopoulos et al. [35] to determine Quasi-static characteristics of microstrip lines on anisotropic substrate with diagonal dielectric tensor. These characteristics are not accurate enough for high-speed pulse applications. In TEM approach dispersion is not considered which is significant at high frequencies. Mariki et al. [36] used TLM method to analyze enclosed microstrip on anisotropic substrate. Later Koike [37] et al. used Bergeron's method in time domain. A unique problem with this method is that the dielectric interface and perfectly conducting strips are misaligned by half a space step.

Our method is simple of all and takes dispersion into account. As stated earlier FDTD is efficient than other methods. MIPML is virtually reflection free. Advanced source excitation has been used so no spurious fields are induced. Use of new single cell method has removed whatever oscillatory behavior is there in the multiple cell method. These features make our results highly accurate compared to other methods.

1.1 MIPML and Its Application to Present Work

During recent years, great interests have been shown in using microstrip lines deposited on anisotropic substrates since substrate anisotropy could have important implications on the operation of microstrip circuits. With increasing complexity of geometry and material property, designing these circuits require more and more dedicated and sophisticated computer aided–design tools to predict the characteristics or performance of the circuits

4

as most of these structures do not lead themselves to analytical solutions Therefore, the natural choice has been the FDTD method But in the past most of the simulation has focussed upon isotropic materials and also perfectly matched layers have been developed with independent derivations for TE and TM modes of propagation, assuming isotropic material. During the literature survey, It was discovered that all the derivations and theoretical proofs pertaining to perfectly matched layers have been done for TE and TM modes separately and then it has been assumed that in isotropic materials any propagating hybrid mode is superimposition of propagating TE and TM modes. so these derivations will hold good for propagating hybrid modes also. However, in a 3-D arbitrary anisotropic medium it is not possible to split any propagating hybrid mode into propagating TE and TM modes. So attempt had been made by us to carry forward these proofs to propagating hybrid modes within an anisotropic medium, as derivations and ultimate Maxwellian equations in PML for isotropic medium indicated that unsplit PML (UPML) should hold for anisotropic mediums also. Material independent nature of the coefficients of FDTD equations in UPML has been demonstrated, so it can be extended to anisotropic medium. By trying the same matching conditions, which work for isotropic materials, numerically it has been prove that UPML works for anisotropic materials. This has opened possibility of using FDTD and PML combinations for circuits and radiators on anisotropic materials and predict their performance accurately. Here a generalized electromagnetic simulator 'MIPML' using FDTD and Unsplit Perfectly Matched Layers has been developed, which can analyze any material and geometry. This simulator is material independent and for each geometry and material, there is no need to rewrite whole algorithm. For each new geometry, one has to add boundary conditions for PEC in the working volume, specify dielectric permittivity tensor for all points in the working volume for the calculating electric fields from electric flux. In the algorithm of MIPML simulator, we deal with fluxes rather than fields.

Towards the end of the thesis, dispersion characteristics of characteristic impedance and effective relative dielectric constant of microstrip have been worked out. Here both conventional multiple cell method [2] and new single cell method introduced by us, which is very effective in calculating above characteristics have been used.

1.2 Organization of the Thesis.

Emphasis in chapter two and three will be on a brief introduction to FDTD method including a survey of it to demonstrate range of its applications and possible areas for future research. In fourth chapter, basic problems confronted by researchers in FDTD method have been taken up. In chapters, five, six and seven briefs details of Radiation boundary conditions and detailed discussion of material boundary conditions including split and unsplit approaches have been taken up. In eighth chapter, the scheme introduced in the present thesis, which has made material boundary conditions material independent is presented with its use in microwave circuits and antenna problems in anisotropic media. In nineth chapter, frequency dependent characteristics of microstrip on an arbitrary anisotropic substrate have been worked out. A new single cell method to calculate these characteristics has been introduced. Though the main objective of the thesis has been design of an electromagnetic simulator for microwave circuits and radiators in anisotropic media but in due course of evolution of algorithm it turned out that it encompasses material which are isotropic, and lossy. It can also cover dispersive and nonlinear materials with few very straightforward modifications.

Chapter 2

FDTD Method: A Brief Survey

Introduction

There are three methods to predict electromagnetic effects in any geometry under consideration viz. Rigorous Analysis, Numerical Computation and Experimentation Of these methods, Numerical Computation is the newest and fastest growing approach Of the many approaches to electromagnetic computation, including MOM, FDTD, FEM, GTD, and Physical Optics, the FDTD technique is applicable to the widest range of the problems. As surveyed by K.L.Shlager and J.B.Schneider, there is sixty-fold increase in publications in 1996 as compared to 1985 and it is increasing day by day. The increase in publications is mainly due to various reasons. First can be attributed to increased computation facilities, which are growing cheaper very fast in terms of cost. Secondly as people are trying to encompass new problems of electromagnetics, they are recognizing new fundamental issues in FDTD and trying to address them.

To select right approach for the problem at hand it is essential to study briefly about the existing research in that particular field. We have also done the same when we started thesis work. For the sake of completeness to the introduction to FDTD, we are providing a list of fundamental issues in FDTD.

2.1 Fundamental Issues

Following topics have been broadly recognized as fundamental issues of importance in the field of FDTD.

2.1.1 Approaches

There are two approaches to FDTD.

(A). Separate field formalism and

(B). Total field formalism.

In first of these approaches the incident field is specified analytically through out the problem space and only the scattered field is determined. Here only scattered fields are

absorbed at the problem space outer boundaries. In the situations where incident fields are of much larger amplitude compared to scattered fields and only scattered fields are of importance, computing scattered fields only and absorbing them is advantageous from accuracy point of view.

In the second approach total field is computed only over an interior subsection of the computational domain, while scattered fields are calculated in the remaining (exterior) portion of the grid. Radiation boundary conditions are applied over these scattered fields. To obtain this division of the computational domain into scattered-field and total-field regions, the incident field is specified over the boundary between these two regions.

A comparison by Holland and Williams [3] demonstrated that, due to numerical dispersion, the total field is superior to scattered field approach. Secondly scattered field approach does not accommodate nonlinear media. However, for problems involving only linear medium and not containing shielded cavities, the scattered formulation is more desired approach.

2.1.2 Absorbing Boundary Conditions

These can be classified as

(A) Differential–Equation based and other non material ABCs

(B) Material ABCs.

Differential-Equation based ABCs are approximation of one way wave equation [38] and Material ABCs are made up of artificial lossy material, which surrounds the computing domain. Both of these ABCs have been handled in details in subsequent chapters.

2.1.3 Gridding

There are various types of gridding schemes in use depending upon the problem under consideration.

2.1.3.1 Orthogonal Grids

Cartesian gridding was the scheme proposed in original formulation but if any surface which varies smoothly, but not along the axes, then it has to be staircased. This approximation leads to significant errors in many problems. In addition, if any object under considerations has small-scale structure then in orthogonal gridding one has to use excessively fine gridding.

Therefore, it is natural that if any object is more naturally described in any other coordinate system other than Cartesian, it is always preferable to update equation for that particular system

2.1.3.2 Subgridding

Issue of fine structure is resolved by dividing problem space in sub-domains, which are gridded more finely than the rest of the problem. The key issue here is the coupling of the fine and coarse grids. Various interpolation techniques are used to define fields at the boundary of fine and coarse gridding. In addition to interpolation techniques, a discretised form of wave equation [4] is used to obtain fields on the boundary between the grids.

2.1.3.3   Subcellular Techniques

These techniques allow modeling of thin wires and similar objects without the use of excessively fine gridding [5]

2.1.3.4   Conformal Grids

In this approach, the fields are expressed in terms of their covariant components (flow along a coordinate direction) and contravariant components (flow through a constant coordinate surface) and an integral formulation is used to obtain the update equations. In a nonorthogonal system, these covariant and contravariant are not collinear and auxiliary equations must be obtained to express one form in terms of the other. [6]

2.1.4 Material Modeling

Various types of materials with complex geometries are to be handled by FDTD. To solve these several techniques have been reported.

2.1.4.1   Frequency Dispersive Material

One of the attractive features of the FDTD is that it is a wide band method and it will be incorrect if material parameters are assumed to be constant. To take care of them several schemes have been proposed.

2.1.4.2 Surface–Impedance Boundary Conditions

These formulations have shown to provide significant computational savings over a full FDTD model. Several of SIBC formulations have been presented by researchers

2.1.4.3 Thin Material Sheets

There are several schemes treating thin sheets of conducting and dielectric material but most of these treat only tangential components of the electric fields at air/dielectric boundary. A scheme suggested by Tirkas and Demarest [7] presented an FDTD model for thin dielectric sheets that treated not only the tangential components of electric fields at the air/sheet interface, but also the normal component of the field in the sheet. A comparison of the FDTD methods for modeling thin dielectric and conducting sheets was given by Maloney and smith [8]

2.1.4.4 Anisotropic Materials

Treatment of these materials forms the core of this thesis. There have been several proposed schemes modifying original Yee's algorithm for anisotropic materials but most of them focus upon the materials, which can be diagonalised. Recently, 1993 onwards, people have tried treatment of full tensor permeability and permittivity material in FDTD and our thesis tries to attempt extension of FDTD to these full tensor material and extension of PML to these problems. We have tried to use unsplit formulation of PML and though the treatment of these problems have been usually assumed to be quite memory intensive but we have tried a uniform algorithm through out the computing domain space and at the same time we have tried to conserve the memory requirement.

2.1.4.5 Nonlinear Materials

Mostly in optics to model optical devices, techniques have been developed to treat nonlinear materials with FDTD. Apart from above, wherever material properties are function of fields present in media, several publications have been reported to treat the problem. Few to name are, nonlinear effects of ferrites, instantaneous nonlinearity of permittivity, Dispersive nonlinear Fabry–Perot cavities, propagation of famtosecond pulses in Dispersive and nondispersive nonlinear media, Lorentz dispersion, Kerr nonlinearities and incorporation of both Kerr and dispersive nonlinear effects to obtain temporal and spatial optical solitons from simulation of the full-wave time-domain

Maxwell's equations. The list may be endless but it is indication of prowess of FDTD method.

2.1.5 Active and Passive Device Modeling

This field has recently drawn attention and gained wide popularity. Two approaches are used. In first analytical device models are used directly with the FDTD method. In second, lumped–element subgrid models are used in which device behavior is determined by other software. The second approach may be preferable in modeling of active devices with complicated equivalent circuit models.

2.1.6 Transformations

For complicated scatterers, time harmonic and pulsed illumination is used to determine the equivalent electric and magnetic currents on a virtual surface that completely encloses the scatterer. These currents are then transformed to the far field

2.1.7 Digital Signal-Processing Techniques

By using digital signal processing techniques in conjunction with the FDTD method relevant data such as frequency–domain scattering parameters can be extracted from FDTD simulations of the shorter duration than would otherwise be possible.

2.1.8 Techniques to Reduce Numerical Dispersion Errors

To reduce numerical dispersion errors many people suggested higher order approximations of space and time derivatives. But ,recently proposed techniques ,such as those employing wavelets, make a significant departure from traditional methods in order to reduce dispersion errors. One such technique, derived from theory of wavelets, is Multiresolution time domain (MRTD)[9]. To suppress spurious modes, researchers have used Daubechies wavelets.

2.1.9 Radiating Structures

Initially FDTD was used to model scattering from objects. However by including the feeding source within the grid , it is possible to model radiating structures. This has led to the use of FDTD to model antennas. Papers have been published on following

(A) Simple antennas like Cylindrical and conical monopoles, thinwire dipoles and thin wire Yagi antennas etc

(B) Horn Antennas

(C) Antennas for Pulse Radiation

(D) Microstrip antennas

(E) Dielectric Resonator Antennas

(F) Hand held Antennas

(G) Antenna Arrays

(H) Other Radiating surfaces like cavity backed antennas, Active antennas etc.

2.1.10 Microwave Devices and Guiding Structures

The FDTD has found wide applications in modeling microwave devices and guiding structures. In this area, several techniques to improve the efficiency of the FDTD have been developed. Such techniques include the compact two dimensional FDTD method for guided–wave structures, ABCs specifically developed for Guided wave problems, and the previously Discussed advanced schemes for gridding and reducing numerical dispersion.

To name a few areas, we are giving a list

(A) Waveguides, Feeds, Junctions, and Resonators

(B) Microstrip

(C) Vias , interconnects and transmission lines

(D) Algorithm improvements

There has been active research in reducing the computations needed to analyze three-dimensional guided–wave structures. These approaches utilize compact two-dimensional FDTD method, the MRTD method, and conformal FDTD methods. The compact two-dimensional FDTD method is based on introducing a phase shift along the direction of propagation, which reduces three dimensions to two dimensions

2.1.11 Discrete Scatterers

Research has mostly been confined to calculation of Radar cross section (RCS of scatterer). In addition to that, modeling of perfectly conducting or dielectric scatterers has been done.

2.1.12   Infinite and Periodic Structures

These include periodic guided wave structures, periodic phased array antenna, metallic strip-grating etc.

2.1.13   Ground Penetrating Radar

Prompt by the use of FDTD to study the scattering from a discrete object or the radiation from a source in the presence of a planar boundary, researchers have tried problems related to subsurface radars and ground penetrating radars.

2.1.14   Hybrid Techniques

The FDTD method has also been combined with other techniques where it would be difficult or infeasible to model the complete geometry in a single space lattice. A hybrid FDTD/method of moments approach [10] based upon schelkunoff's field-equivalence theorems to investigate coupling problems involving loaded cavities have been reported long back. Others are hybrid spectral/FDTD, Hybrid ray/FDTD, Hybrid FDTD/partial-eigen function-expansion method and hybrid FDTD asymptotic method etc.

A Web site http://www.eecs.wsu.edu/~schneidj/fdtd-bib.html presents listing of papers on FDTD. Here list is exhaustive and very useful for finding references on any FDTD related topics in which someone wishes to start his research career.

Chapter3

The FDTD Method

Introduction

In this chapter, we are going to review the basic Maxwell's equations and FDTD algorithm based on these equations We have focussed upon central differencing scheme, using the same to discretise Maxwell equations and construction of FDTD algorithm for full wave analysis of a most generalized problem. Also we have tried to include algorithm suitable from programming point of view.

3.1 Maxwell Equations

The Maxwell curl equations in Cartesian Coordinates are written as

$$\frac{\partial H_z}{\partial y} - \frac{\partial H_y}{\partial z} = \varepsilon \frac{\partial E_x}{\partial t} + \sigma E_x \qquad (3.1)$$

$$\frac{\partial H_x}{\partial z} - \frac{\partial H_z}{\partial x} = \varepsilon \frac{\partial E_y}{\partial t} + \sigma E_y \qquad (3.2)$$

$$\frac{\partial H_y}{\partial x} - \frac{\partial H_x}{\partial y} = \varepsilon \frac{\partial E_z}{\partial t} + \sigma E_z \qquad (3.3)$$

$$\frac{\partial E_z}{\partial y} - \frac{\partial E_y}{\partial z} = -\mu \frac{\partial H_x}{\partial t} - \rho H_x \qquad (3.4)$$

$$\frac{\partial E_x}{\partial z} - \frac{\partial E_z}{\partial x} = -\mu \frac{\partial H_y}{\partial t} - \rho H_y \qquad (3.5)$$

$$\frac{\partial E_y}{\partial x} - \frac{\partial E_x}{\partial y} = -\mu \frac{\partial H_z}{\partial t} - \rho H_z \qquad (3.6)$$

Where

Ex, Ey, Ez, Hx, Hy and Hz are the Cartesian components of electric and magnetic fields.

ε is electrical permittivity and μ is magnetic permeability.

ρ is magnetic resistivity and σ is electrical conductivity.

3.2 The Central Difference Scheme

Using following scheme of discretisation, above equations can be solved Central Differencing scheme has been used because it is second order accurate

$$(i, j, k) = (i\Delta x, j\Delta y, k\Delta z) \tag{3.7}$$

$$F^n(i, j, k) = F^n(i\Delta x, j\Delta y, k\Delta z, n\Delta t) \tag{3.8}$$

$$\frac{\partial F^n(i, j, k)}{\partial x} = \frac{F^n\left(i + \frac{1}{2}, j, k\right) - F^n\left(i - \frac{1}{2}, j, k\right)}{\Delta x} + order\left(\Delta x^2\right) \tag{3.9}$$

$$\frac{\partial F^n(i, j, k)}{\partial t} = \frac{F^{n+\frac{1}{2}}(i, j, k) - F^{n-\frac{1}{2}}(i, j, k)}{\Delta t} + order\left(\Delta t^2\right) \tag{3.10}$$

3.3 FDTD Algorithm for Full Wave Analysis

If we discretise Equation (3.4) as per above scheme, The resulting equation is

$$
\begin{aligned}
H_x^{n+\frac{1}{2}}\left(i, j + \frac{1}{2}, k + \frac{1}{2}\right) = &\frac{1 - \dfrac{\rho(i, j + \frac{1}{2}, k + \frac{1}{2})}{2\mu(i, j + \frac{1}{2}, k + \frac{1}{2})}}{1 + \dfrac{\rho(i, j + \frac{1}{2}, k + \frac{1}{2})}{2\mu(i, j + \frac{1}{2}, k + \frac{1}{2})}} * H_x^{n-\frac{1}{2}}\left(i, j + \frac{1}{2}, k + \frac{1}{2}\right) \\
&- \frac{\Delta t}{\mu(i, j + \frac{1}{2}, k + \frac{1}{2})} * \frac{1}{1 + \dfrac{\rho(i, j + \frac{1}{2}, k + \frac{1}{2})}{2\mu(i, j + \frac{1}{2}, k + \frac{1}{2})}} \\
&* \left[\begin{array}{l} \dfrac{1}{\Delta y}\left(E_z^n(i, j+1, k + \frac{1}{2}) - E_z^n(i, j, k + \frac{1}{2})\right) \\ - \dfrac{1}{\Delta z}\left(E_y^n(i, j + \frac{1}{2}, k+1) - E_y^n(i, j + \frac{1}{2}, k)\right) \end{array} \right]
\end{aligned} \tag{3.11}
$$

As evident from above equation, that dealing with half indices is problematic, as most of the programming languages do permit matrix indices to be integers only. If Yee's [1] original cell is modified as shown below then above problem can be easily circumvented. Here position of field components is kept same, only the way they are addressed is different. Here indices are associated with each cell and all fields components in this cell

different. Here indices are associated with each cell and all fields components in this cell have the same indices though their position is implied in the cell and is different from each other. This means in a cell, field components are still half space step apart from each other but their indices are same as shown below
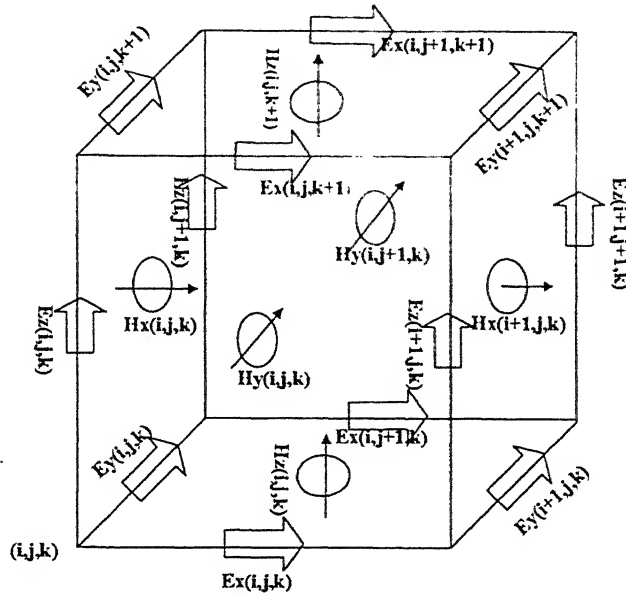
Figure3.1 YEE's cell

As is evident that above formulation makes programming an easy affair with no botheration of half indices. Above scheme of Yee is called 'leapfrog in time' scheme. Here first H is evaluated at time (N+1/2) from H at (N-1/2) and E at N. Then E components are evaluated at time (N+1) using H at (N+1/2) and E at N. Again N is increased By 1 and same procedure is repeated. This interleaves E and H temporally and results in a centered difference or ' leapfrog in time' approach. Following set of equations result by using above scheme. We are giving a complete set of equations for all six components

H Magnetic field, ρ Magnetic resistivity
E Electric field, σ Electrical conductivity
ε Permittivity, μ permeability
$\Delta x, \Delta y, \Delta z$ space steps, Δt time steps

$$(3.12)$$

16

$$H_x^{n+\frac{1}{2}}(i,j,k) = \frac{1 - \dfrac{\rho(i,j,k)}{2\mu(i,j,k)}}{1 + \dfrac{\rho(i,j,k)}{2\mu(i,j,k)}} * H_x^{n-\frac{1}{2}}(i,j,k)$$

$$- \frac{\Delta t}{\mu(i,j,k)} * \frac{1}{1 + \dfrac{\rho(i,j,k)}{2\mu(i,j,k)}}$$

$$* \left[\begin{array}{l} \dfrac{1}{\Delta y}\left(E_z^n(i,j+1,k) - E_z^n(i,j,k)\right) \\[2mm] -\dfrac{1}{\Delta z}\left(E_y^n(i,j,k+1) - E_y^n(i,j,k)\right) \end{array} \right] \qquad (3.13)$$

$$H_y^{n+\frac{1}{2}}(i,j,k) = \frac{1 - \dfrac{\rho(i,j,k)}{2\mu(i,j,k)}}{1 + \dfrac{\rho(i,j,k)}{2\mu(i,j,k)}} * H_y^{n-\frac{1}{2}}(i,j,k)$$

$$- \frac{\Delta t}{\mu(i,j,k)} * \frac{1}{1 + \dfrac{\rho(i,j,k)}{2\mu(i,j,k)}}$$

$$* \left[\begin{array}{l} \dfrac{1}{\Delta z}\left(E_x^n(i,j,k+1) - E_x^n(i,j,k)\right) \\[2mm] -\dfrac{1}{\Delta x}\left(E_z^n(i+1,j,k) - E_z^n(i,j,k)\right) \end{array} \right] \qquad (3.14)$$

$$H_z^{n+\frac{1}{2}}(i,j,k) = \frac{1 - \dfrac{\rho(i,j,k)}{2\mu(i,j,k)}}{1 + \dfrac{\rho(i,j,k)}{2\mu(i,j,k)}} * H_z^{n-\frac{1}{2}}(i,j,k)$$

$$- \frac{\Delta t}{\mu(i,j,k)} * \frac{1}{1 + \dfrac{\rho(i,j,k)}{2\mu(i,j,k)}}$$

$$* \left[\begin{array}{l} \dfrac{1}{\Delta x}\left(E_y^n(i+1,j,k) - E_y^n(i,j,k)\right) \\[2mm] -\dfrac{1}{\Delta y}\left(E_x^n(i,j+1,k) - E_x^n(i,j,k)\right) \end{array} \right] \qquad (3.15)$$

17

$$
E_x^{n+1}(i,j,k) = \frac{1 - \dfrac{\rho(i,j,k)}{2\varepsilon(i,j,k)}}{1 + \dfrac{\rho(i,j,k)}{2\varepsilon(i,j,k)}} * E_x^n(i,j,k)
$$

$$
- \frac{\Delta t}{\varepsilon(i,j,k)} * \frac{1}{1 + \dfrac{\rho(i,j,k)}{2\varepsilon(i,j,k)}}
$$

$$
* \left[\begin{array}{l} \dfrac{1}{\Delta y}\left(H_z^{n+\frac{1}{2}}(i,j,k) - H_z^{n+\frac{1}{2}}(i,j-1,k) \right) \\[2em] - \dfrac{1}{\Delta z}\left(H_y^{n+\frac{1}{2}}(i,j,k) - H_y^{n+\frac{1}{2}}(i,j,k-1) \right) \end{array} \right] \qquad (3.16)
$$

$$
E_y^{n+1}(i,j,k) = \frac{1 - \dfrac{\rho(i,j,k)}{2\varepsilon(i,j,k)}}{1 + \dfrac{\rho(i,j,k)}{2\varepsilon(i,j,k)}} * E_y^n(i,j,k)
$$

$$
- \frac{\Delta t}{\varepsilon(i,j,k)} * \frac{1}{1 + \dfrac{\rho(i,j,k)}{2\varepsilon(i,j,k)}}
$$

$$
* \left[\begin{array}{l} \dfrac{1}{\Delta z}\left(H_x^{n+\frac{1}{2}}(i,j,k) - H_x^{n+\frac{1}{2}}(i,j,k-1) \right) \\[2em] - \dfrac{1}{\Delta x}\left(H_z^{n+\frac{1}{2}}(i,j,k) - H_z^{n+\frac{1}{2}}(i,j-1,k) \right) \end{array} \right] \qquad (3.17)
$$

$$E_z^{n+1}(i,j,k) = \frac{1 - \dfrac{\rho(i,j,k)}{2\varepsilon(i,j,k)}}{1 + \dfrac{\rho(i,j,k)}{2\varepsilon(i,j,k)}} * E_z^{n}(i,j,k)$$

$$- \frac{\Delta t}{\varepsilon(i,j,k)} * \frac{1}{1 + \dfrac{\rho(i,j,k)}{2\varepsilon(i,j,k)}}$$

$$* \left[\begin{array}{c} \dfrac{1}{\Delta x}\left(H_y^{n+\frac{1}{2}}(i,j,k) - H_y^{n+\frac{1}{2}}(i-1,j,k) \right) \\[2mm] -\dfrac{1}{\Delta y}\left(H_x^{n+\frac{1}{2}}(i,j,k) - H_x^{n+\frac{1}{2}}(i,j-1,k) \right) \end{array} \right] \qquad (3.18)$$

3.4 FDTD Code Architecture

At this stage it is apt to consider FDTD code requirements and architecture of the program. Inefficiently written program may take large memory and execution time may become so large that testing and debugging may not be possible. Here we will consider FDTD code architecture for Perfectly Matched Layers .It may slightly differ from application to application but in general, it is applicable to almost all applications.

The code architecture is summarized as:

- Driver
- Problem space setup
- Test object definition
- E, H field algorithms
- Absorbing Boundary Conditions
- Data saver
- Data processing for the given problem
- Results display

3.4.1 Driver

- Calls problem setup subroutine and the test object definition subroutine
- Time steps over index N

- While looping over N, calls E, H subroutines and Absorbing Boundary Condition subroutines
- At appropriate time steps or at each step it calls data saver to store sampled data
- After completion of looping over index N routines for data processing are called, results are computed and displayed.

3.4.2 Problem Space setup

- Sets the problem space size

  Sets the number of cells in each dimension

  Sets the cell size (Δx, Δy, Δz)
- Calculates the Δt time step according to courant stability condition
- Calculates the constant multipliers

3.4.3 Test Object Definition

Cells or individual field components in the cells are flagged indicating their composition. This dictates how the E, H algorithm is to process the data: as perfect conductor, lossy dielectric, free space, or other more complicated material. It is usually convenient to set default material to free space; the array of flags can be read for a preprocessing check of the geometry and composition of the object.

3.4.4 E, H Field Algorithm

Calculate the response of a component from its own prior time value and that of the nearest–neighbor field quantities (Es around Hs and Hs around the Es) according to the type of material present at that component location:

> Free space
>
> Lossy dielectric
>
> Lossy magnetic
>
> Perfect conductor

3.4.5 Absorbing Boundary Conditions(ABCs)

These conditions truncate computing domain, ideally without causing any reflection of fields from the truncation boundary. Again depending upon ABCs, implementation may differ. ABCs can be split-up in several regions as face ABCs, Edge ABCs and Corner

ABCs [17]. For each region there will be a different algorithm and they will be computed one after another. In ABCs, equation constants may be different from working volume and they may be different in different ABC regions. So if they are treated one after another, code may be quite long though it may take less memory and computationally it may be fast. But obvious disadvantages are that it is quite time consuming to develop this kind of code and once code is completed it is a big headache to debug it due to the enormous size of code and a number of subroutines. In our opinion if sufficient memory is available than treat whole computing domain as made up of single ABC region and define value of elements of a constant multiplier matrices, depending upon the region they represent. This makes memory requirement large but code is uniform, very compact, easy to debug and execution time does not increase significantly. In fact there is no need for separate ABC algorithm. The E, H field algorithm takes care of ABCs.

3.4.6 Data Saver

Saves response data such as E and H field components, currents, or other quantities in the FDTD computation space in arrays at chosen time steps.

3.4.7 Data Processing and Result Display

This basically consists of calling library routines for Fourier transforms, various mathematical operations and graphic displays of the fields and writing results to a file for later reference.

A generalized flow chart for any FDTD code is given in figure (3.2).

```
┌─────────────────────────────────┐
│       DEFINE PARAMETERS         │
└─────────────────────────────────┘
                │
                ▼
┌─────────────────────────────────┐
│          BUILD OBJECT           │
└─────────────────────────────────┘
                │
                ▼
┌─────────────────────────────────┐
│         UPDATE H FIELD          │◄──────────┐
└─────────────────────────────────┘           │
                │                              │
                ▼                              │
┌─────────────────────────────────┐           │
│         UPDATE E FIELD          │           │
└─────────────────────────────────┘           │
                │                              │
                ▼                              │
┌─────────────────────────────────┐           │
│           APPLY ABCs            │           │
└─────────────────────────────────┘           │
                │                              │
                ▼                              │
┌─────────────────────────────────┐           │
│           SAVE DATA             │           │
└─────────────────────────────────┘           │
                │                              │
                ▼                              │
┌─────────────────────────────────┐           │
│           IF N<NMAX             │───────────┘
└─────────────────────────────────┘    ┌──────┐
                │          ┌──────┐     │  NO  │
                │          │ YES  │     └──────┘
                ▼          └──────┘
┌─────────────────────────────────┐
│  PROCESS DATA  & DISPLAY RESULTS │
└─────────────────────────────────┘
```
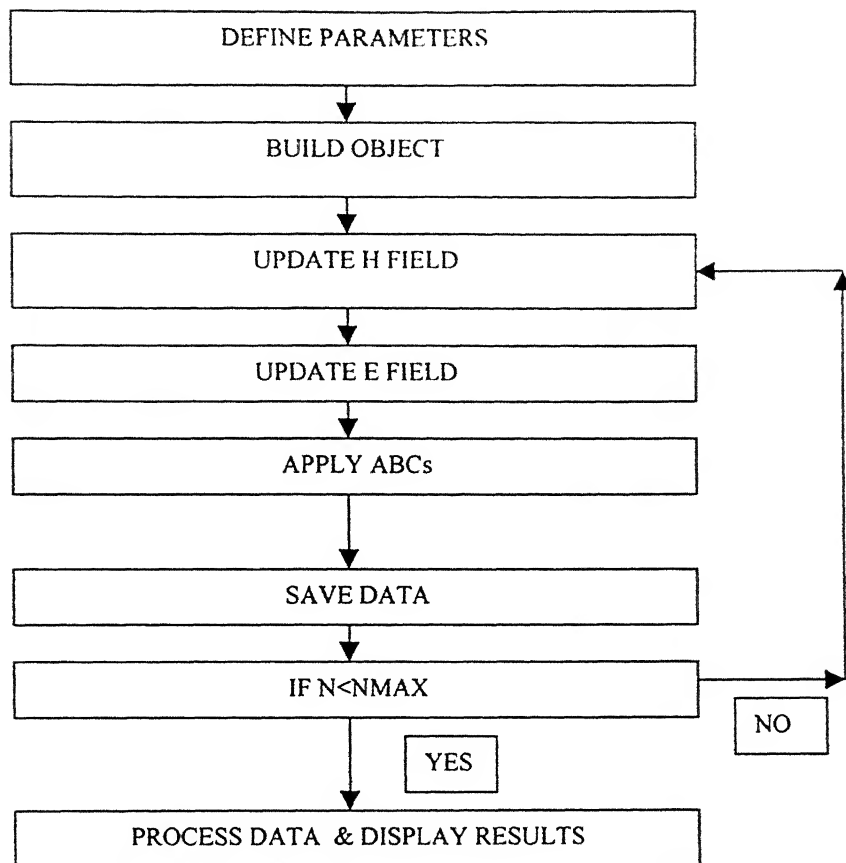
FDTD FLOW CHART

Figure (3.2).

Chapter 4

FDTD Fundamentals

Introduction

In this Chapter, the practical difficulties for implementation of FDTD method have been addressed. There are three main issues viz. Cell size, Time step size, and Source specification.

4.1 Cell Size

There are two basic factors, which affect cell size. As per the Nyquist sampling theorem, highest frequency in the signal must be sampled at least twice. So $\lambda = 2 \, \Delta x$ gives the maximum cell size which could be taken. For accurate results usually a smaller fraction of wavelength is taken .The limit varies depending upon the accuracy demand and usually it is $\lambda/10$ to $\lambda/20$ or even smaller. Such a high level of sampling is required because at any particular time step the FDTD grid is a discrete spatial sample of the field distribution. From the Nyquist sampling theorem, there must be at least two samples per spatial period (wavelength) in order for the spatial information to be adequately sampled. Because our sampling is not exact, and our smallest wavelength is not precisely known, more than two samples per wavelength are required. Another related consideration is grid dispersion error. Due to the approximation inherent in FDTD, waves of different frequencies will propagate at slightly different speeds through the grid. This difference in propagation speed also depends on the direction of propagation relative to the grid. For accurate and stable results, the grid dispersion error must be reduced to an acceptable level, which can be readily accomplished by reducing the cell size. By looking at Numerical Dispersion relation [40], it is quite evident that as spatial step reduces Numerical Dispersion relation reduces to Analytical Dispersion relation.

Another cell size consideration is that the important characteristics of the problem geometry must be accurately modeled. Normally if cell size is $\lambda/10$ to $\lambda/20$ or even

smaller then this requirement is usually met but in certain cases if it is not so, then finer gridding is required. This sometimes leads to a situation where grid size is excessively large and some times object can not be properly modeled by finer grid e.g. thin wires. In such cases Sub-cellular techniques [5] are used Many a times subgridding [4] comes handy. Depending upon nature of the problem gridding is done and size of computational domain is determined.

4.2 Time Step Size

Once the cell size is determined, The maximum size of the time step Δt immediately follows from the Courant condition [41]. The basis for the Courant condition is that in one time step any point on a plane wave must not pass through more than one cell. It is because during one time step FDTD can propagate the wave only from one cell to its nearest neighbors. In the direction perpendicular to lattice planes, wave propagates most rapidly. So with this we can say

$$v * \Delta t \leq \Delta x \qquad \text{for stability in one dimension} \qquad (4.1)$$

For three dimensional space

$$v \Delta t \leq \frac{1}{\sqrt{\dfrac{1}{\Delta x^2} + \dfrac{1}{\Delta y^2} + \dfrac{1}{\Delta z^2}}} \qquad (4.2)$$

When equality holds, the discretised wave most closely follows the actual wave propagation and grid dispersion errors are minimized. Smaller values of Δt does not give most accurate results. However exception to this occurs in case of conductive materials and nonlinear materials where time step size is smaller than what is required for equality.

4.3 Source Specification

The type of source to be used is dependent upon the problem under specification but there are several popular types of sources, which have emerged as experience has grown with FDTD method.

4.3.1 Compact Pulse

$$Source(t) = \frac{1}{320}\left(10 - 15\cos 2\pi t + 6\cos 4\pi t - \cos 6\pi t\right) \quad \text{for } t \leq 1\,\text{ns}$$

$$Source(t) = 0 \quad\quad\quad\quad\quad\quad\quad\quad \text{for } t > 1\,\text{ns} \quad (4.3)$$

Use of compact pulse is reserved for the applications where response over a wide band is not required and grid dispersion errors are to be kept to a minimum. Examples are testing or comparison of various Radiation Boundary Conditions. This compact pulse has very little high frequency contents and thus dispersion errors are hold to a minimum.

4.3.2 Gaussian Pulse

Here we take 'pw' as half width of the Gaussian pulse in seconds and the width is defined as the distance between the points where pulse reduces to 5 % of its maximum value. 'τ' is the location of the peak of the pulse in sec.

$$\tau = pw$$

$$alpha = \left(\frac{1}{0.25 * pw}\right)^2$$

$$Source(t) = e^{\left(-alpha*(t-\tau)^2\right)} \quad\quad (4.4)$$

Maximum frequency content of Gaussian pulse is approximately given by

$$f_{max} = \frac{1}{2 * pw} \quad\quad\quad (4.5)$$

This source is preferred for the applications where response over a wide band of frequencies is desired. Its Fourier transform is also Gaussian. Whenever space is filled up with penetrable material then spatial cell size is calculated keeping in mind the wavelength of the wave in that material. So accordingly cell size reduces by a factor of square root of dielectric constant which leads to reduction in value of time step almost by the same factor and if pulse width is specified in terms of time steps its width reduces to half in terms of time and frequency content goes double which in turn will lead to a lot of

grid dispersion error. So care should always be taken to specify pulse width always in seconds and this reduces chance for making any mistake in source excitation.

Another guideline for using the Gaussian pulse is to take its Fourier transform and look for a 20 dB down frequency. If at this frequency spatial step size is one tenth of the wavelength than we can have accurate results upto that frequency. As far as noise and stability are concerned, if we have appreciable energy in high frequency components then it could be a problem. But by taking tau sufficiently large this possibility of high frequency components in pulse is reduced. Also to put quantitatively, we have put another criterion that at wavelengths four times the minimum cell size, pulse amplitude should be down by 120 dB.

4.3.3 Sinusoidal Wave

Wherever response for a single frequency is required, sinusoidal source is used.

$$Source(t) = \sin(2 * \pi * f * t) \qquad (4.6)$$

One major issue in source consideration is the point of excitation and mode of excitation. Usually excitation in dominant mode is preferred but some times it is not known accurately. Reason for exciting in dominant mode is that, less number of other unwanted modes are generated. If it is not known accurately then closest approximation is done, so less number of other unwanted modes are generated and little distance is required for them to travel to die down and what propagates ultimately down the line is the dominant mode. Dominant mode leads to reduction in size of computing domain.

In addition, point of excitation is very important. In paper by Zhang et al. [2] the excitation was done on front wall of a computing domain inside of which, microstrip discontinuities were analyzed. They excited microstrip on the front wall by setting tangential electric field under the strip as gaussian pulse and rests of the points on plane were set to zero. This amounted to an electric wall condition, which induced a dc current or tangential magnetic field on the front surface and near by. When reflected pulse arrived they switched on an absorbing boundary condition. If boundary conditions are applied on this local magnetic field, errors accumulate and solution blows up. So after pulse left the plane and before it reflected back from discontinuity, boundary conditions

steps in side the computing domain to avoid inclusion of this local DC field. In summary this is a very complicated arrangement and size of computing domain also increases.

Another scheme used by sheen et al. [11] was to make source plane a magnetic wall with tangential electric field existing on it. Magnetic wall condition was imposed by them using image theory. They set H_{tan} outside the magnetic wall equal to $-H_{tan}$ inside the wall in terms of amplitude and, then remaining electric field components on the source wall were calculated using the finite–difference equations. This gave little distortion of the source.

A very novel and highly accurate scheme was proposed by Zhao et al. [27,28]. In this scheme source plane was put few cells inside the computing domain at near–end terminal as shown in figure (4.1) and plane wave source condition [41] was applied. Though the excitation was done beneath the microstrip but remaining points on the plane were calculated using normal FDTD algorithm and at excitation points following equation was applied to simulate plane wave source condition
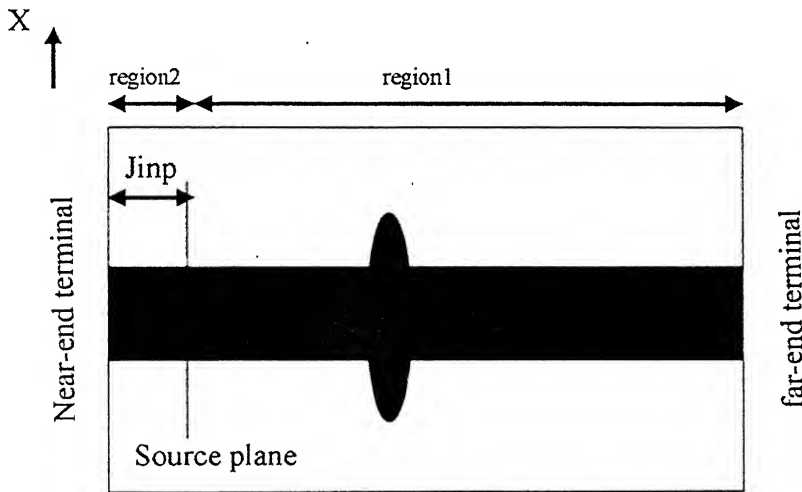
Figure 4.1 Advanced source excitation scheme

$$E_z^{n+1}(i,j_{inp},k) = E_z^n(i,j_{inp},k) + \frac{\Delta t}{\varepsilon\Delta x}\left(H_y^{n+\frac{1}{2}}(i+1,j_{inp},k) - H_y^{n+\frac{1}{2}}(i,j_{inp},k) \right)$$

$$- \frac{\Delta t}{\varepsilon\Delta y}\left(H_x^{n+\frac{1}{2}}(i,j_{inp}+1,k) - H_x^{n+\frac{1}{2}}(i,j_{inp},k) \right)$$

$$+ E_{z,inc}^n(i,j_{inp},k) \tag{4 7}$$

1.Above equation is for the points lying below the strip in the plane inp. For rest of the points in the inp plane simple FDTD equations are applied

2. Above equation assumes that all conductivities and resistivities are zero. For lossy materials the equation need to be modified accordingly.

Within the region 1, the EM fields, contain the incident wave (propagates in +y direction) and reflected wave from any discontinuity, if present. Where as the EM fields in region2, contain the incident wave (propagation in -Y direction) and the reflected wave. In region 2 the incident wave propagating in –Y direction and reflected waves are immediately absorbed on near end terminal plane, while the incident wave propagating in +Y direction is used to examine the discontinuous system itself.

It is also to be noted that while exciting in three dimension space, using a point source, above equation is not to be used. It has been observed that wave does not propagate. Only last term of incident source is to be used and rest of the terms are dropped in this case.

Chapter 5

Radiation Boundary Conditions

Introduction

There are two broad categories of the problems encountered in EM theory. In one type of problems, Initial and Boundary values are known whereas another category includes the problems where boundary conditions are not known. These problems are called open problems. When these problems are dealt by FDTD method the natural question is 'how to define computing domain'. As whole infinite space can not be taken as computing domain because of limitation of computer memory, we need to keep it limited. So computing domain is limited to a size where it can accommodate structure or geometry to be analyzed. Once computing domain is limited then obvious problem arises that at the boundary of this domain, how to apply FDTD equations, as central differencing schemes need, value of fields inside as well as outside of the boundary. Since we do not have values outside the boundary, we can not use simple FDTD equations here. Some new set of equations is required which simulate propagation of waves to infinity. These equations are expected to absorb whatever waves strike at boundary without giving any reflection. Since properties of waves arriving at the boundaries is not known before hand, designing of these absorbing equations, which are also called absorbing or radiation boundary conditions (ABCs or RBCs), is a difficult task.

Primary requirement of an ABC is that irrespective polarization, angle of incidence and frequency of incident waves, it must absorb all of them without any reflection. This reflection free boundary will permit the FDTD solution of the fields inside the computing domain to be true at all time steps. Though the ABCs described here have been *rendered obsolete because of the invention of Perfectly Matched Layers,* which provides performance that is much more superior. This material is still important from the point of view of academic interest and for implementing these ABCs where computer resources are extremely limited.

In this section, the theory and numerical implementation of one way wave equation ABCs, a very useful class of radiation conditions in Cartesian coordinates has been presented. One of them, the Mur's second order radiation boundary condition, is appropriate for effectively

truncating a two- or three- dimensional FDTD space lattice with an overall level of spurious reflections of 1%-5% for outer lattice planes located 10 - 20 space cells from a target surface

5.1 One Way Wave Equations

A partial differential equation, which permits wave propagation only in one direction, is called a "one way wave equation." Figure (5 1) below shows a finite, two-dimensional Cartesian domain, on which the time dependent wave equation is to be simulated. In the interior of Ω, a numerical scheme which models wave propagation in all direction is applied On $\partial\Omega$, the outer Boundary of Ω, only numerical wave motion that is outward from Ω is permitted. The boundary must permit outward propagating numerical wave analogs to exit Ω just as if the simulation were performed on a computational domain of infinite extent A scheme, which enacts a one way wave equation on $\partial\Omega$ for this purpose is called a Radiation Boundary Condition.
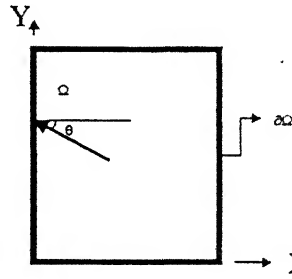
Fig 5.1 Numerical plane wave analog incident upon left grid boundary of a 2 d Cartesian computational Domain

5.2 Derivation By Wave Equation Factoring

The Derivation of a RBC whose purpose is to absorb numerical waves incident upon the outer boundary of a finite difference grid can be explained in terms of operator factoring. Consider a two dimensional wave equation in Cartesian coordinates

$$U_{xx} + U_{yy} - \frac{1}{c^2}U_{tt} = 0 \qquad (5.1)$$

This is a compact representation of following wave equation

$$\frac{\partial^2 U}{\partial x^2} + \frac{\partial^2 U}{\partial y^2} - \frac{1}{c^2}\frac{\partial^2 U}{\partial t^2} = 0 \qquad (5.2)$$

Where U is a scalar field component; the subscript xx, yy, and tt denote second partial derivatives with respect to x, y. and t, respectively; c is the wave phase velocity. The partial differential operator here is

$$L = D_x^2 + D_y^2 - \frac{1}{c^2} D_t^2 \quad (5.3)$$

Which uses the notation

$$D_x^2 = \frac{\partial^2}{\partial x^2}, D_y^2 = \frac{\partial^2}{\partial y^2}, D_z^2 = \frac{\partial^2}{\partial z^2} \quad (5.4)$$

The wave equation is then compactly written as

$$LU = 0 \quad (5.5)$$

The wave operator, L, can be factored in the following manner:

$$LU = L^+ L^- U = 0 \quad (5.6)$$

Where

$$L^- = D_x - \frac{D_t}{c}\sqrt{1 - S^2} \quad (5.7)$$

With

$$S = \frac{D_y}{(D_t \, c)} \quad (5.8)$$

The operator L^+, is similarly defined except for a "+"sign before the radical.

Enquist and Mazda [38] showed that at a grid boundary, say at x=0, the application of L^- to the wave function, U, will exactly absorb a plane wave propagating toward the boundary at an arbitrary angle, θ. Thus,

$$L^- U = 0 \quad (5.9)$$

If applied at x=0, functions as an exact analytical RBC which absorbs wave motion from the interior of the spatial domain, Ω. The operator, L^-, performs the same function for a plane wave propagating at an arbitrary angle towards the other x boundary in Figure (5.1) at $x = h$. The presence of the radical in equation (5.7) classifies L^- as a pseudo-differential operator that is non-local in both the space and time variable. This is an undesirable characteristic in that it prohibits the direct numerical implementation of (5.9) as a RBC. Approximation of the radical in (5.7) produces RBC's that can be implemented numerically and are useful in FDTD simulations with minimum reflections over a range of incident angles. The RBC, used in FDTD electromagnetic wave codes, is simply a two term Taylor series approximation to the radical in (5.7), given by

$$\sqrt{1 - S^2} \approx 1 - \frac{1}{2}S^2 \quad (5.10)$$

Substituting (5.10) in (5.7), we obtain

$$\left(D_x - \frac{D_t}{c} + \frac{c}{2}\frac{D_y^2}{D_t} \right) U = 0 \quad (5.11)$$

Multiplying (5.11) through by D_t, and identifying the differential operators as partial derivatives, we obtain the following analytical RBC which can be numerically implemented at the x = 0 grid boundary

$$U_{xt} - \frac{1}{c}U_{tt} + \frac{c}{2}U_{yy} = 0 \quad (5.12)$$

Equation (5.12) is a very good approximation to exact RBC of (5.9) for relatively small values of S, which satisfy the Taylor series approximation of (5.10). This is equivalent to saying that (5.12) presents a nearly reflection less grid truncation for numerical plane wave modes which strike the x=0 grid boundary at small values of the incident angle, θ. Analogous approximate, analytical RBC's can be derived for the other grid boundaries

$$U_{xt} + \frac{1}{c}U_{tt} - \frac{c}{2}U_{yy} = 0 \quad (5.13) \qquad \text{at } x = h$$

$$U_{yt} - \frac{1}{c}U_{tt} + \frac{c}{2}U_{xx} = 0 \qquad (5.14) \qquad \text{at } y = 0$$

$$U_{yt} + \frac{1}{c}U_{tt} - \frac{c}{2}U_{xx} = 0 \qquad (5.15) \qquad \text{at } y = h$$

For the FD-TD simulation of the vector Maxwell's equations, the RBC's of (5.12)–(5.15) are applied to individual Cartesian components of E or H that are located at, and tangential to, the grid boundaries.

The Derivation of RBC's for the three-dimensional case follows the above development closely. The wave equation, given by

$$U_{xx} + U_{yy} + U_{zz} - \frac{1}{c^2}U_{tt} = 0 \qquad (5.16)$$

has the associated partial differential operator

$$L = D_x^2 + D_y^2 + D_z^2 - \frac{1}{c^2}D_t^2 \qquad (5.17)$$

L can be factored in a manner of (5.6) to provide an exact radiation boundary, L⁻ having the same form as that of (5.7), but with S given by

$$S = \left[\left(\frac{D_y}{D_t\, c} \right)^2 + \left(\frac{D_z}{D_t\, c} \right)^2 \right]^{\frac{1}{2}} \qquad (5.18)$$

Again, L⁻, applied to the scalar wave function, U, at the grid boundary will exactly absorb a plane wave propagating toward the boundary at an arbitrary angle.

Using the Taylor series approximation of (5.7), we obtain an approximate RBC at x = 0 in differential-operator form

$$\left(D_x - \frac{D_t}{c} + \frac{c}{2}\frac{D_y^2}{D_t} + \frac{c}{2}\frac{D_z^2}{D_t} \right) U = 0 \qquad (5.19)$$

Multiplying (5.19) through by D_t, and identifying the differential operators as partial derivatives, we obtain the corresponding approximate, analytical RBC which can be numerically implemented at the x=0 lattice boundary

$$U_{xt} - \frac{1}{c}U_{tt} + \frac{c}{2}U_{yy} + \frac{c}{2}U_{zz} = 0 \qquad (5.20)$$

Equation (5.20) is a very good approximation of the exact RBC of (5.9) for relatively small values of S given by (5.18). This is equivalent to saying that (5.20) presents a nearly reflection less lattice truncation for numerical plane wave modes which strike the x = 0 lattice boundary close to broadside. Analogous approximate, analytical RBC's can be derived for the other lattice boundaries

$$U_{xt} + \frac{1}{c}U_{tt} - \frac{c}{2}U_{yy} - \frac{c}{2}U_{zz} = 0 \qquad (5.21) \qquad \text{at x = h}$$

$$U_{yt} - \frac{1}{c}U_{tt} + \frac{c}{2}U_{xx} + \frac{c}{2}U_{zz} = 0 \qquad (5.22) \qquad \text{at y = 0}$$

$$U_{yt} + \frac{1}{c}U_{tt} - \frac{c}{2}U_{xx} - \frac{c}{2}U_{zz} = 0 \qquad (5.23) \qquad \text{at y = h}$$

$$U_{zt} - \frac{1}{c}U_{tt} + \frac{c}{2}U_{xx} + \frac{c}{2}U_{yy} = 0 \qquad (5.24) \qquad \text{at z = 0}$$

$$U_{zt} + \frac{1}{c}U_{tt} - \frac{c}{2}U_{xx} - \frac{c}{2}U_{yy} = 0 \qquad (5.25) \qquad \text{at z = h}$$

For the FD-TD simulation of the vector Maxwell's equations, the RBC's of (5.20) – (5.25) are applied to individual Cartesian components of E or H that are located at, and tangential to, the grid boundaries.

Equations (5.12)-(5.15) for two dimensional grid, and equations (5.20)-(5.25), representing three-dimensional grid have been found to be very effective if differencing scheme suggested

by Mur [39] is used. Mur's Scheme has been shown to truncate lattice space with just 1% - 5% reflections for arbitrary targets.

5.3   Mur Differencing scheme

Consider the following Figure (5.2) used for illustrating Mur's RBC

W(0,j+1)   W(1,j+1)_____ Y=(j+1)∆y

W(0,j)   W(1/2,j)   W(1,j)   Y= j ∆y

W(0,j-1)   W(1,j-1) _____ Y=(j-1)∆y

X=0   X=∆X
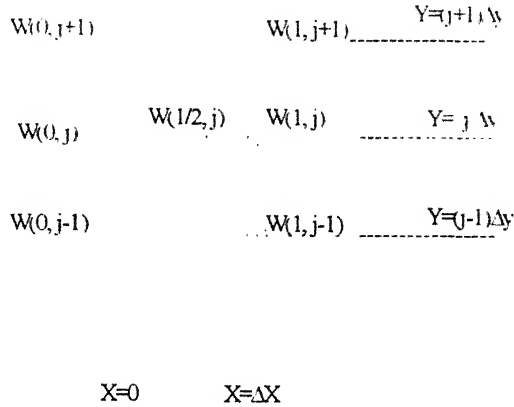
Fig5.2. Points near the x=0 Boundary used in Mur differencing
 Scheme

A Finite difference based scheme for 2-D RBC equations (5.12)-(5.15) and 3-D RBC equations (5.20)-(5.25) was introduced by Mur [39]. We are illustrating the scheme for 2-D grid case at x = 0. Mur applied equation (5.12) at point W (1/2,j) and used central Differencing to write partial derivatives. The mixed partial x and t derivatives on left-hand side of equation (5.12) are written out using central differences

$$
W_{xt}\Big|_{\frac{1}{2},j,n} = \frac{\dfrac{\partial W^{n+1}}{\partial x}\left(\dfrac{1}{2},j\right) - \dfrac{\partial W^{n-1}}{\partial x}\left(\dfrac{1}{2},j\right)}{2\Delta t}
$$

$$
= \frac{\left[\dfrac{W^{n+1}(1,j) - W^{n+1}(0,j)}{\Delta x}\right] - \left[\dfrac{W^{n-1}(1,j) - W^{n-1}(0,j)}{\Delta x}\right]}{2.\Delta t} \qquad (5.26)
$$

Next, partial t derivatives on the left hand side of (5.12) is written out as an average of time derivatives at the adjacent points (0,j) and (1,j)

$$
\begin{aligned}
W_{tt}\Big|_{\frac{1}{2},j,n} &= \frac{1}{2}\left[\frac{\partial^2 W^n}{\partial t^2}(0,j) + \frac{\partial^2 W^n}{\partial t^2}(1,j)\right] \\
&= \frac{1}{2}\left[\frac{W^{n+1}(0,j) - 2W^n(0,j) + W^{n-1}(0,j)}{\Delta t^2}\right. \\
&\quad \left. + \frac{W^{n+1}(1,j) - 2W^n(1,j) + W^{n-1}(1,j)}{\Delta t^2}\right]
\end{aligned}
\tag{5.27}
$$

And, the partial y derivative on the left hand side of (5.12) is written out as an average of y derivatives at the adjacent points (0,j) and (1,j)

$$
\begin{aligned}
W_{yy}\Big|_{\left(\frac{1}{2},j,n\right)} &= \frac{1}{2}\left[\frac{\partial^2 W^n}{\partial y^2}(0,j) + \frac{\partial^2 W^n}{\partial y^2}(1,j)\right] \\
&= \frac{1}{2}\left[\frac{W^n(0,j+1) - 2W^n(0,j) + W^n(0,j-1)}{\Delta y^2}\right. \\
&\quad \left. + \frac{W^n(1,j+1) - 2W^n(1,j) + W^n(1,j-1)}{\Delta y^2}\right]
\end{aligned}
\tag{5.28}
$$

Substituting the finite difference expressions of (5.26)-(5.28) and solving for $W^{n+1}(0,j)$, we obtain the following time-stepping algorithm for components of W along the x = 0 grid boundary which implements the Taylor's series of RBC of (5.12)

$$
\begin{aligned}
W^{n+1}(0,j) &= -W^{n-1}(1,j) + \frac{c\Delta t - \Delta x}{c\Delta t + \Delta x}\left[W^{n+1}(1,j) + W^{n-1}(0,j)\right] \\
&\quad + \frac{2\Delta x}{c\Delta t + \Delta x}\left[W^n(1,j) + W^n(0,j)\right] \\
&\quad + \frac{(c\Delta t)^2 \Delta x}{2\Delta y^2(c\Delta t + \Delta x)}\left[W^n(0,j+1) - 2W^n(0,j) + W^n(0,j-1)\right. \\
&\quad \left. + W^n(1,j+1) - 2W^n(1,j) + W^n(1,j-1)\right]
\end{aligned}
\tag{5.29}
$$

Analogous finite–difference expressions for the Mur RBC at each of the other grid boundaries x = h, y=0, and y = h, can be derived by proper substitutions into (5.13), (5.14),

and (5 15), respectively, in the same manner. More simply, these Mur RBC can be obtained by inspection from (5.26)–(5.29) using coordinate symmetry arguments.

RBC for 3-D case can be derived, if Figure (5.2) is now supposed to be representing individual Cartesian components of E and H located in lattice plane z = kΔz at x = 0 lattice boundary. Here, the Mur scheme involves implementing the partial derivatives of (5.20) as numerical central differences expanded about the auxiliary W component, W_n (1/2,j, k), located one half space cell from the grid boundary at (0,j, k). The partial derivatives, W_{xt}, W_{tt}, and W_{yy} are identical in form to (5.26), (5.27), and (5.28), respectively, and are evaluated in lattice plane z = kΔz. The partial derivative, Wzz, is expressed as an average of z derivatives at the adjacent points (0, j, k) and (1, j, k)

$$
\begin{aligned}
W_{zz}\Big|_{\frac{1}{2},j,k,n} &= \frac{1}{2}\left[\frac{\partial^2 W^n}{\partial z^2}(0,j,k) + \frac{\partial^2 W^n}{\partial z^2}(1,j,k)\right] \\
&= \frac{1}{2}\left[\frac{W^n(0,j,k+1) - 2W^n(0,j,k) + W^n(0,j,k-1)}{\Delta z^2}\right. \\
&\quad \left. + \frac{W^n(1,j,k+1) - 2W^n(1,j,k) + W^n(1,j,k-1)}{\Delta z^2}\right]
\end{aligned} \quad (5.30)
$$

Substituting these finite–difference expressions into (5.20) and solving for W^{n+1}(0, j, k), we obtain the following time stepping algorithm for components of W along the x=0 lattice boundary which implements the Taylor series RBC of (5.20).

$$
\begin{aligned}
W^{n+1}(0,j,k) &= -W^{n-1}(1,j,k) + \frac{c\Delta t - \Delta x}{c\Delta t + \Delta x}\left[W^{n+1}(1,j,k) + W^{n-1}(0,j,k)\right] \\
&+ \frac{2\Delta x}{c\Delta t + \Delta x}\left[W^n(1,j,k) + W^n(0,j,k)\right] \\
&+ \frac{(c\Delta t)^2 \Delta x}{2\Delta y^2(c\Delta t + \Delta x)}\left[W^n(0,j+1,k) - 2W^n(0,j,k) + W^n(0,j-1,k)\right. \\
&\quad \left. + W^n(1,j+1,k) - 2W^n(1,j,k) + W^n(1,j-1,k)\right] \\
&+ \frac{(c\Delta t)^2 \Delta x}{2\Delta z^2(c\Delta t + \Delta x)}\left[W^n(0,j,k+1) - 2W^n(0,j,k) + W^n(0,j,k-1)\right. \\
&\quad \left. + W^n(1,j,k+1) - 2W^n(1,j,k) + W^n(1,j,k-1)\right]
\end{aligned} \quad (5.31)
$$

Analogous finite difference expressions for the Mur RBC at each of the other lattice boundaries, x = h, y = 0, y = h, z = 0, and z = h, can be derived by substituting into (5.21)-

(5.25) Respectively, in the same manner More simply, these Mur RBC's can be obtained by inspection from (5.26)–(5 28) and (5 30) using coordinate symmetry arguments

5.4 Special Corner RBC

Upon inspecting (5.29) and (5.31), it is clear that the Mur's finite difference scheme for the two terms Taylor series RBC's cannot be implemented for the field components located at grid corners. It is due to the fact that some of the necessary field data used in the Mur expressions at these points are outside of the grid and not available It is necessary to implement a special corner radiation boundary condition at these points which (1) utilizes available field data in the grid; (2) yields acceptably low levels of reflection of outgoing numerical wave modes; and (3) numerically stable.

Figure (5.3) illustrates the two–dimensional grid geometry for a simple and stable special corner RBC used successfully for a variety of two and three-dimensional FDTD simulations.
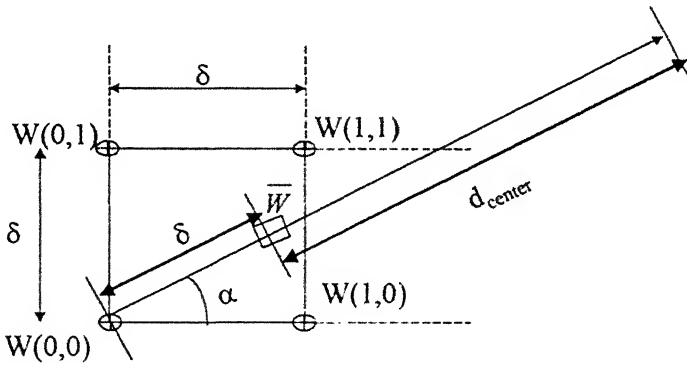
Figure 5.3: Points near the x=0,y=0 grid corner used in the special corner radiation boundary condition (square grid case).

Here basic assumption is that wave propagates along a radial line from the center of a domain. So field at corner point W (0,0), is taken to be just the time retarded value of an interior field, $\overline{W}$, located along a radial line connecting the corner point to the center of the grid. Also it is assumed that $c\Delta t = \partial/2$ is maintained, so that if, $\overline{W}$ is located exactly one cell width, δ, inward along the radial line, The time retardation of the outgoing numerical wave in

propagating from $\overline{W}$ to W (0,0) is exactly two time steps. Over all, the special corner RBC is given by

$$W^{n+1} = f_{radial} \overline{W}^{n-1} \qquad (5.32)$$

Where f_{radial} is the attenuation factor for the radially outgoing wave .In two dimensions from figure (5.3)

$$f_{radial} = \left(\frac{d_{centre}}{d_{centre} + 1} \right)^2 \qquad (5.33)$$

$$
\begin{aligned}
\overline{W}^{n-1} = &\ (1 - \sin\alpha)(1 - \cos\alpha) W^{n-1}(0,0) \\
&+ (1 - \sin\alpha)\cos\alpha\, W^{n-1}(1,0) \\
&+ \sin\alpha(1 - \cos\alpha) W^{n-1}(0,1) \\
&+ \sin\alpha\cos\alpha\, W^{n-1}(1,1) \qquad (5.34)
\end{aligned}
$$

Where d_{center} is the radial distance, in cell-widths, from $\overline{W}$ to the center of the grid, and α is the azimuthal angle of the radial line at W (0,0). Note that the value of $\overline{W}^{n-1}$ is determined by simple linear interpolation of the four surrounding field values including W (0,0) at time step n-1. Extension to three dimension is straight forward, yielding for W^{n+1} (0,0,k)

$$f_{radial} = \left(\frac{d_{centre}}{d_{centre} + 1} \right) \qquad (5.35)$$

$$
\begin{aligned}
\overline{W}^{n-1} = &\ (1 - \sin\beta)(1 - \cos\beta \sin\alpha)(1 - \cos\beta \cos\alpha)\overline{W}^{n-1}(0,0,k) \\
&+ (1 - \sin\beta)(1 - \cos\beta \sin\alpha)\cos\beta \cos\alpha\,\overline{W}^{n-1}(1,0,k) \\
&+ (1 - \sin\beta)\cos\beta \sin\alpha(1 - \cos\beta \cos\alpha)\overline{W}^{n-1}(0,1,k) \\
&+ (1 - \sin\beta)\cos^2\beta \sin\alpha \cos\alpha\,\overline{W}^{n-1}(1,1,k) \\
&+ \sin\beta(1 - \cos\beta \sin\alpha)(1 - \cos\beta \cos\alpha)\overline{W}^{n-1}(0,0,k+1) \\
&+ \sin\beta(1 - \cos\beta \sin\alpha)\cos\beta \cos\alpha\,\overline{W}^{n-1}(1,0,k+1) \\
&+ \sin\beta \cos\beta \sin\alpha(1 - \cos\beta \cos\alpha)\overline{W}^{n-1}(0,1,k+1) \\
&+ \sin\beta \cos^2\beta \sin\alpha \cos\alpha\,\overline{W}^{n-1}(1,1,k+1) \qquad (5.36)
\end{aligned}
$$

β is the azimuthal angle of the radial line at W (0,0,k) Note that the value of $\overline{W}^{n-1}$ is determined by simple linear interpolation of the eight surrounding field values, including W(0,0,k), at time step n-1. Other corners can also be worked out in a similar manner or simply by inspection equations can be written using coordinate symmetry argument

Another corner RBC, which also works well, is given as below

$$W^{n+1}(0,0) = W^{n}(0,1) + \frac{v * delt - del}{v * delt + del}\left(W^{n+1}(0,1) - W^{n}(0,0)\right) \qquad (5.37)$$

We have worked with both corner RBC and results are not very different

5.5   Generalized and Higher–Order RBC's

Trefethen and Halpern [42] proposed a generalization of the two terms Taylor series approximation to the radical in equation (5.7), considering the use of the rational function approximation

$$\sqrt{1 - S^2} = r(S) = \frac{p_m(S)}{q_n(S)} \qquad (5.38)$$

On the interval [-1,1], where p_m and q_n are the polynomials in S of degree m and n, respectively; and r (S) is said to be of type (m, n). With $S = c\, D_y / D_t$, the [-1,1] approximation interval on S is equivalent to approximation of the exact one way wave equation of equation (5.9) along the x = 0 grid boundary for the range of incident wave angles $\theta = -90°$ to $\theta = 90°$

For example, by specifying r (S) as a general (2,0) approximant, the radical is approximated by an interpolating polynomial of the form

$$\sqrt{1 - S^2} \approx p_o + p_2 S^2 \qquad (5.39)$$

Resulting in the general second–order, approximate, analytical RBC,

$$U_{xt} - \frac{p_o}{c} U_{tt} - p_2 c U_{yy} = 0 \qquad (5.40)$$

The choice of the coefficients, p_o and p_2, is determined by the method of interpolation that is used. Standard techniques such as Pade`, least-square, or Chebyshev approximation are

applied with the goal of interpolating the radical optimally over the [-1,1] range of S, there by producing an approximate RBC whose performance is good over a wide range of incident wave angles. Mur's two term Taylor series approximation of (5.9) is now seen in a more general sense as a pade' (2,0) interpolation i.e. with coefficient s $p_0 = 1$ and $p2 = -1/2$ in (5.40). Higher order approximation to the radical in equation (5.7) gives better ABCs. for example, the use of the general type (2,2) rational function

$$\sqrt{1 - S^2} \approx \frac{p_o + p_2 S^2}{q_o + q_2 S^2} \qquad (5.41)$$

Gives the general third–order, approximate, analytical RBC

$$q_o U_{xtt} + q_2 c^2 U_{xyy} - \frac{p_o}{c} U_{ttt} - p_2 c U_{tyy} = 0 \qquad (5.42)$$

Appropriate selection of the p and q coefficients in (5.42) produces various families of RBC's as suggested in [42]. The only problem is that as higher order approximations are used, discretized equations become quite large. Third order equations may contain as many as 50 terms or more at each of the grid truncation boundary. These also require increased storage. Since the invention of Perfectly Matched Layers, this third and higher order RBC's have become obsolete. Only Mur's RBC is used because of its simplicity and that too, in situation where demand on accuracy is not very high.

5.6   Numerical Experimentation with MUR's RBC

We had planned to use Mur's RBC when we started with the thesis work as till that time we were not aware of PML or its MIPML variant. That time we had developed code SOABC for second order Mur RBC for use later in project. Our results were in excellent confirmation with results produced by Berenger in his paper [13]. We have performed test used in [13]. We have considered the same 100*50 cell domain, with the same space and time increments, respectively 1.5 cm and 25 picosec. The domain was surrounded by MUR RBC. Our computation was done for both TE and TM case .In TE case excitation was done at magnetic point and for TM case excitation was done at electric point. Excitation was done using a compact pulse

41

$$H_z(50,20) = \frac{1}{320}\left(10 - 15\cos 2\pi t + 6\cos 4\pi t - \cos 6\pi t\right)$$

$$H_z(50,20) = 0 \quad if \ t > 1 \, ns \tag{5.43}$$

A reference solution was computed using a large domain of 400*400, allowing a boundary free solution during a 500 time steps. Denoting H_z (i,j) the field in the test domain and H_{zr} (i,j),its counterpart in reference domain ,two kinds of results are presented and compared with those of Berenger[13].

First the reflected field along a boundary (j = 1), at the time step 100, normalized to the peak value of the field at point (50, 1)

$$R(i) = \left[H_z(i,1) - H_{zr}(i,1)\right] / H_{zr}(50,1)_{max} \tag{5.44}$$

And, second, the L^2 norm of the error on the 100*50 domain as a function of time,

$$L^2 = \sum_{i=1}^{100}\sum_{j=1}^{50}\left[H_z(i,j) - H_{zr}(i,j)\right]^2 \tag{5.45}$$

As evident from our results in figure (5.4a) that reflection is of the order of 1% -4% and our results are in excellent agreement with those of Berenger in figure (5.4b).

Here we would like to highlight the reasons for adapting to Perfectly Matched Layers. Zhang et al. [2] found that the Fourier transform of the time domain results is very sensitive to numerical errors, notably those resulting from imperfect treatment of the Absorbing boundary conditions used to truncate the numerical computation of an open structure. Thus, even though the time domain results may be reasonably accurate, The frequency –domain results obtained from their Fourier transform may not be acceptable as useful data.

Even Zhang et al. [2] used a new super absorption technique for their research. This prompted us to look for other Radiation Boundary Conditions. We experimented with Perfectly Matched Layers and found its performance extremely superior compared to whatever RBCs discussed here. Details of PML and its Variant MIPML [32], using which we have developed simulator MIPML, have been taken up in next chapter.
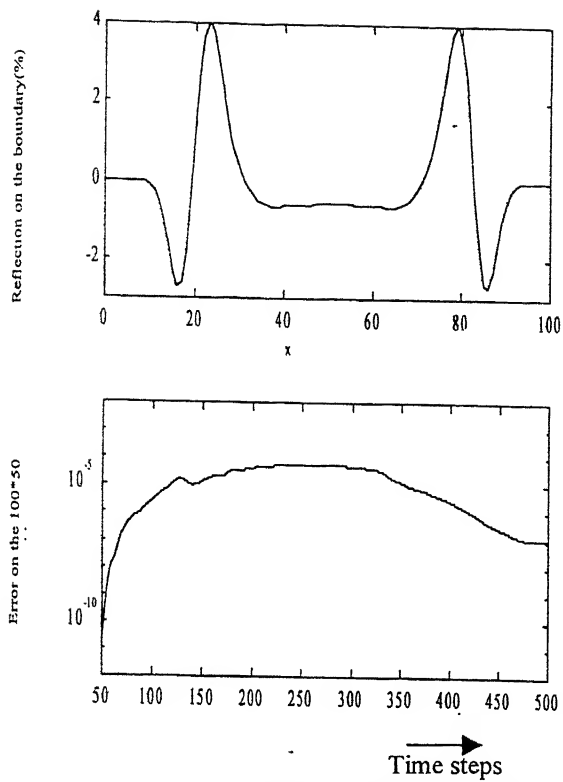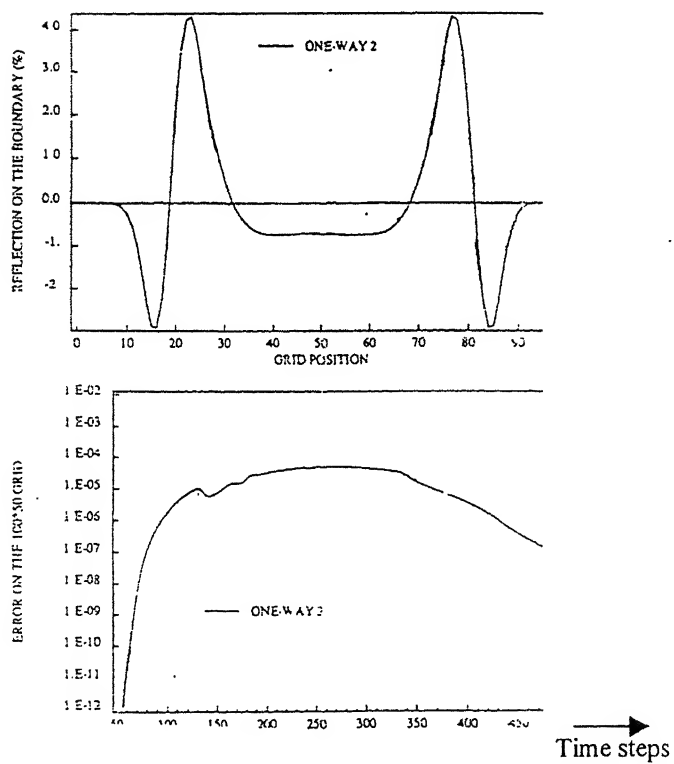
Figure 5.4a Results produced by Program SOABC.

Figure 5.4b Results Published by Berenger

Chapter 6
Perfectly Matched Layers

Introduction

One of the basic considerations in any open boundary problem in FDTD is the reflection less truncation of the computing domain and also reducing size of the computing domain by placing it as close as possible to the scatterer under analysis. One of the earlier techniques [3], consisted of surrounding working domain with an absorbing material whose impedance was matched to the working domain. But this had the basic assumption that the waves are incident normally upon the interface of the working domain and absorbing material for reflection less transmission. So the absorbing layer had to be place quite far from the scatterer to make outgoing waves nearly normal incident. Another technique, which was discussed in previous chapter and has been very popular so far, is approximation of one way wave equation initially exhibited for acoustic wave by Enquist and Mazda [38]. Mur [39] and various researchers with higher order approximations applied this one way wave equation for creating useful ABCs. Though accuracy was reasonably good in time domain but for better accuracy in frequency domain, results in time domain needed to be further improved for some applications. Here, in most of the ABCs based upon approximation of one way equations, absorbing boundary needed to be placed away from the object for normal incident. Also second or higher order absorbing boundary conditions, which account for oblique incident, do not work for inhomogeneous structures because these have been defined for uniform space.

Perfectly Matched Layers [13] do over come all above stated problems and accuracy is better than any other ABC by −100dB. It is Virtually reflection free for all angles of incidence, polarization and over ultra-wide frequency range [26].

6.1 Theory of Perfectly Matched Layers

Maxwell Equations for TE to z case for a medium as shown in figure 6.1 having permeability as μ and permitivity as ε are given by

$$\varepsilon \frac{\partial E_x}{\partial t} + \sigma E_x = \frac{\partial H_z}{\partial y}$$

$$\varepsilon \frac{\partial E_y}{\partial t} + \sigma E_y = \frac{\partial H_z}{\partial x}$$

$$\mu \frac{\partial H_z}{\partial t} + \rho H_z = \frac{\partial E_x}{\partial y} - \frac{\partial E_y}{\partial x} \qquad (6.1)$$

If

$$\frac{\sigma}{\varepsilon} = \frac{\rho}{\mu} \qquad (6.2)$$
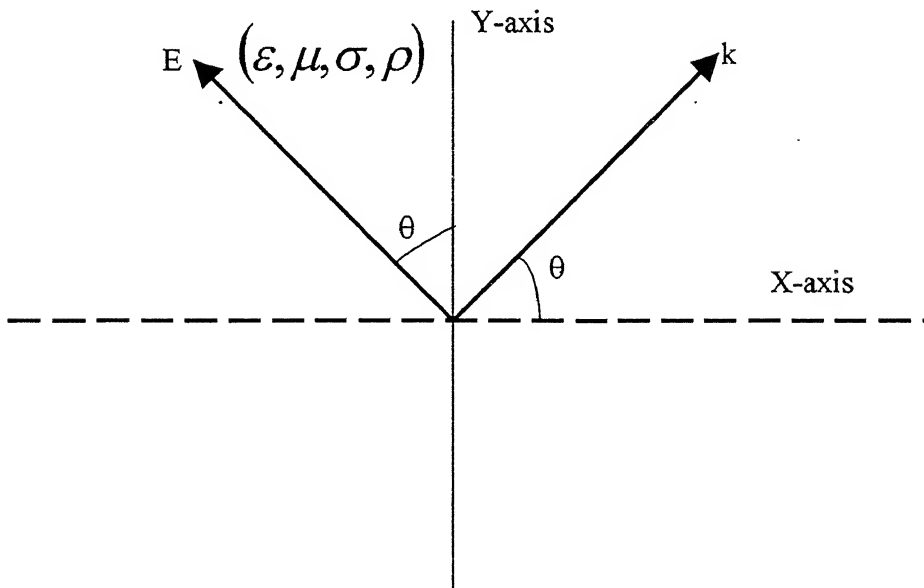
Figure6.1 E field and propagation vector k in a medium

Then impedance of above medium becomes equal to the impedance of the medium with same permittivity and permeability but with no loss terms i.e. ρ and σ both are equal to zero. Impedance can be determined by first solving above equations to arrive at wave equation, which gives value of propagation constant and then putting value of it in above equations to find ratio of E_x/H_z or E_y/H_z, which gives the value of impedance. Hence

$$\nabla^2 E + \omega^2 \mu\varepsilon \left(1 + \frac{\rho}{j\omega\varepsilon}\right)\left(1 + \frac{\rho}{j\omega\mu}\right) E = 0 \qquad (6.3)$$

$$k^2 = \omega^2 \mu\varepsilon \left(1 + \frac{\sigma}{j\omega\varepsilon}\right)\left(1 + \frac{\rho}{j\omega\mu}\right) \qquad (6.4)$$

And solution of above equation is of the form given by equation (6.5) below, in a medium shown above in figure 6.1

$$E = \left(E_0 \cos\theta \ u_y - E_0 \sin\theta \ u_x\right) e^{-j(k1x+k2y)} \qquad (6.5)$$

After substituting above in equation (6.1) we get

$$H_x = H_y = 0$$

$$(j\omega\mu + \rho)H_z = \frac{\partial\left(-E_0 \sin\theta \ e^{-j(k1x+k2y)}\right)}{\partial y} - \frac{\partial\left(-E_0 \cos\theta \ e^{-j(k1x+k2y)}\right)}{\partial x}$$

Using

$$k1 = k\cos\theta, k2 = k\sin\theta \qquad (6.6\,a)$$

We get

$$H_z = \left(\frac{jk}{\rho + j\omega\mu}\right) E_0 e^{-j(k1x+k2y)} \qquad (6.6\,b)$$

$$E = E_0 e^{-j(k1x+k2y)}$$

$$\frac{E}{H_z} = 1 \Big/ \left(\frac{jk}{\rho + j\omega\mu}\right)$$

Substitute value of k in above equation

$$\frac{E}{H_z} = \sqrt{(\rho + j\omega\mu)/(\sigma + j\omega\varepsilon)} \qquad (6.7)$$

Hence

$$Z = \sqrt{(j\omega\mu + \rho)/(j\omega\varepsilon + \sigma)} \qquad (6.8)$$

If equation (6.2) is put in above Z reduces to

$$Z = \sqrt{\mu/\varepsilon} \qquad (6.9)$$

Which is for the lossless medium.

This proves that above medium ($\sigma,\rho,\varepsilon,\mu$) is matched to the inner medium ($0,0,\varepsilon,\mu$).

Now lets first derive snell's law and reflection coefficient for the interface of these two mediums, shown in figure 6.2
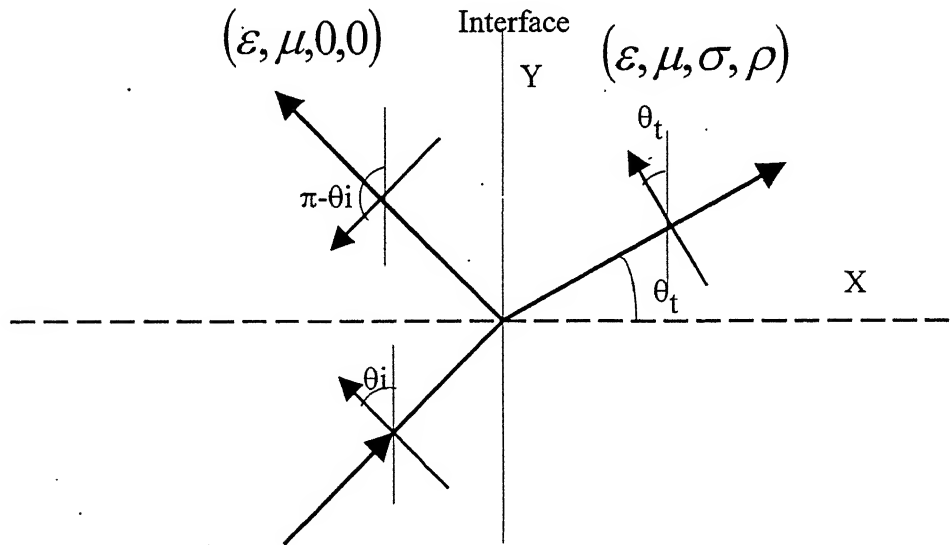
Figure 6.2 Propagation of wave from working medium to absorbing medium

Matching tangential components at interface x=0 we can write

$$E_i \cos\theta_i \; e^{-j(k1\sin\theta_i y)} - E_r \cos\theta_r \; e^{-j(k1\sin\theta_r y)} = E_t \cos\theta_t \; e^{-j(k2\sin\theta_t y)} \quad (6.10)$$

Define

$$\Gamma = -\frac{E_r}{E_i}, T = \frac{E_r}{E_i} \qquad (6.11a)$$

$$E_i \cos\theta_i \; e^{-j(k1\sin\theta_i y)} + \Gamma E_i \cos\theta_r \; e^{-j(k1\sin\theta_r y)} = TE_i \cos\theta_t \; e^{-j(k2\sin\theta_t y)} \qquad (6.11b)$$

Above is possible when

$k1\sin\theta_i = k1\sin\theta_r = k2\sin\theta_t$

This gives the snell's law

$$\frac{\sin\theta_i}{\sin\theta_t} = \frac{k2}{k1} \qquad (6.12)$$

For a matched medium defined by equation (6.2), above law becomes

$$\frac{\sin\theta_i}{\sin\theta_t} = \sqrt{\left(1 + \frac{\sigma}{j\omega\varepsilon}\right)\left(1 + \frac{\rho}{j\omega\mu}\right)} \qquad (6.13)$$

Hence

$$\theta_i \neq \theta_t \qquad (6.14)$$

For a matched medium incident angle is not equal to transmitted angle.

Also from equation (6.11b)

$$(1+\Gamma)\cos\theta_i = T\cos\theta_t \qquad (6.15)$$

Since Hz is parallel to Y-Z plane.

$H_{zi} + H_{zr} = H_{zt}$

$\frac{1}{z1}(E_{zi} + E_{zr}) = \frac{1}{z2}E_{zt}$

$\frac{1}{z1}(E_{zi} - \Gamma E_{zi}) = \frac{1}{z2}TE_{zi}$

$$\frac{1}{z1}(1-\Gamma) = \frac{1}{z2}T \qquad (6.16)$$

From equations (6.15) and (6.16)

$$\Gamma = \frac{Z2\cos\theta_t - Z1\cos\theta_i}{Z2\cos\theta_t + Z1\cos\theta_i} \qquad (6.17)$$

For a matched medium though Z1 may be equal to Z2 but $\theta_i \neq \theta_t$ hence reflection coefficient is not equal to zero.

For this reason as mentioned above, in PML, splitting of the fields is done. By splitting the field components reflection coefficient can be made zero along with impedance matching. In equation (6.1) Hz varies with x and y both. So it is splitted in two components, one of these vary with x-direction only and the other one varies in y-direction only. X-travelling waves are absorbed by the conductivities ρ_x (magnetic) and σ_x (electric). Similarly y travelling waves are absorbed by conductivity subscripted y i.e. the ρ_y and σ_y.

If both couples of conductivity are matched then medium is reflection less if it surrounds a medium with same permeability and permittivity but zero conductivity and resistivity. Referring to figure (6.1), we can write Maxwell equations and various fields components in a medium with anisotropic conductivity, as following.

$$\varepsilon \frac{\partial E_x}{\partial t} + \sigma_y E_x = j\omega\varepsilon(1 + \frac{\sigma}{j\omega\varepsilon})E_x = \frac{\partial(H_{zx} + H_{zy})}{\partial y} \qquad (6.18a)$$

$$\varepsilon \frac{\partial E_y}{\partial t} + \sigma_x E_y = -\frac{\partial(H_{zx} + H_{zy})}{\partial x} \qquad (6.18b)$$

$$\mu \frac{\partial H_{zx}}{\partial t} + \rho_x H_{zx} = -\frac{\partial E_y}{\partial x} \qquad (6.18c)$$

$$\mu \frac{\partial H_{zy}}{\partial t} + \rho_y H_{zy} = +\frac{\partial E_x}{\partial y} \qquad (6.18d)$$

$$E_x = -E_o \sin\theta \, e^{-j\omega(t - \alpha x - \beta y)} \qquad (6.18e)$$

$$E_y = -E_o \cos\theta \, e^{-j\omega(t - \alpha x - \beta y)} \qquad (6.18f)$$

$$H_{zx} = -H_{ox} e^{-j\omega(t - \alpha x - \beta y)} \qquad (6.18g)$$

$$H_{zy} = -H_{oy} e^{-j\omega(t - \alpha x - \beta y)} \qquad (6.18h)$$

Write equation (6.18 a)-(6.18d) in frequency domain and solve them for α and β, after putting values of fields from equation (6.18 e)-(6.18h) in them. We get following expressions

$$\alpha = \sqrt{\varepsilon\mu} * \left(1 + \frac{\sigma_x}{j\omega\varepsilon}\right) * \frac{\cos\theta}{G} = \frac{1}{v} * \left(1 + \frac{\sigma_x}{j\omega\varepsilon}\right) * \frac{\cos\theta}{G} \qquad (6.19a)$$

$$\beta = \sqrt{\varepsilon\mu} * \left(1 + \frac{\sigma_y}{j\omega\varepsilon}\right) * \frac{\sin\theta}{G} = \frac{1}{v} * \left(1 + \frac{\sigma_y}{j\omega\varepsilon}\right) * \frac{\sin\theta}{G} \qquad (6.19b)$$

Where

$$G = \sqrt{w_x \cos^2\theta + w_y \sin^2\theta} \qquad (6.19c)$$

$$w_x = \frac{1 + \dfrac{\sigma_x}{j\omega\varepsilon}}{1 + \dfrac{\rho_x}{j\omega\mu}} \qquad (6.19d)$$

$$w_y = \frac{1 + \dfrac{\sigma_y}{j\omega\varepsilon}}{1 + \dfrac{\rho_y}{j\omega\mu}} \qquad (6.19e)$$

So a general equation for any field component becomes

$$\psi = \psi_o e^{-j\omega\left(t - \frac{(x\cos\theta + y\sin\theta)}{cG}\right)} e^{-\left(\frac{\sigma_x}{\varepsilon}\right)\frac{\cos\theta}{cG}x} e^{-\left(\frac{\sigma_y}{\varepsilon}\right)\frac{\sin\theta}{cG}y} \qquad (6.20)$$

Above is the solution for propagating waves in PML and it is evident that decay along the direction of propagation is due to artificial conductivity introduced.

6.2 Propagation between Two Perfectly Matched Layers

Doing the analysis similar to done above we can find the snell's law and reflection factor for the wave propagation between two perfectly matched mediums and these are as following

$$\left(1 + \frac{\sigma_{y1}}{j\omega\varepsilon}\right)\frac{\sin\theta_i}{G1} = \left(1 + \frac{\sigma_{y2}}{j\omega\varepsilon}\right)\frac{\sin\theta_t}{G2} \qquad (6.21a)$$

$$\Gamma = \frac{Z2\cos\theta_t - Z1\cos\theta_i}{Z2\cos\theta_t + Z1\cos\theta_i} \qquad (6.21b)$$

$$\Gamma = \frac{G2\cos\theta_t - G1\cos\theta_i}{G2\cos\theta_t + G1\cos\theta_i} \qquad (6.21c)$$

Where G2 and G1 are defined through equation (6.19c)

If

$$\sigma_{y1} = \sigma_{y2} \qquad (6.22)$$

And both the mediums follow perfectly matched condition of equation (6.2) then

For all frequencies and angle of incidents

$$\theta_i = \theta_t \qquad (6.23a)$$
$$\Gamma = 0 \qquad (6.23b)$$

6.3 Practical Conclusions of Theory of PML

As a summary of this PML we can say that propagation between two PMLs, whose conductivities follow matching condition of equation (6.2), will be reflection less at

1. The interface normal to X-axis if $\sigma_{y1} = \sigma_{y2}$

2. The interface normal to Y-axis if $\sigma_{x1} = \sigma_{x2}$

3. Above still holds good if equal conductivities are zero , which is the case with vacuum and a perfectly matched layer e.g. vacuum is (0,0,0,0) and medium is $(0,0,\sigma y,\rho y)$ at the interface normal to Y-axis or medium1 is $(\sigma x,\rho x,0,0)$ and medium2 is $(\sigma x,\rho x,\sigma y,\rho y)$ at the interface normal to Y-axis.

6.4 PML for FDTD

Though theoretically there should be no reflection if above conditions are satisfied but unfortunately there is numerical reflection if conductivity is changed abruptly. So smooth transition of conductivity is done over several cells thus minimizing numerical reflections and last PML is terminated with PEC though not compulsory. In equation (6.20) above last two exponential are responsible for amplitude decay and one of them is unity so equation (6.20) reduces to following at distance d

$$\psi(d) = \psi(0)e^{-\sigma d \frac{\cos\theta}{\varepsilon c.}} \qquad (6.24)$$

It reflects back from perfectly conducting layer and travels a distance d again hence reflection coefficient is

$$r_p = e^{-\sigma \frac{2d}{\varepsilon c} \cos\theta} \qquad (6.25)$$

Since so far we assumed σ constant with respect to d which is not the case with numerical computation where σ varies with distance x. So above becomes

$$r_p = e^{-2\frac{\cos\theta}{\varepsilon c}\int_0^d \sigma(x)dx}$$
(6.26)

Where d is the total thickness of the PML.

With selection of following profile for variation of σ

$$\sigma(x) = \sigma_m \left(\frac{x}{d}\right)^n$$
(6.27a)

$$r_p = e^{-\frac{2}{(n+1)}.\sigma_m.d.\frac{\cos\theta}{\varepsilon c}}$$
(6.27b)

Now it is quite straightforward to discretize equations (6.18a-6.18d)

6.5 Short Comings of PML

At this stage it is worth considering equation for evanescent waves. Consider following diagram showing propagation of a wave in medium 2
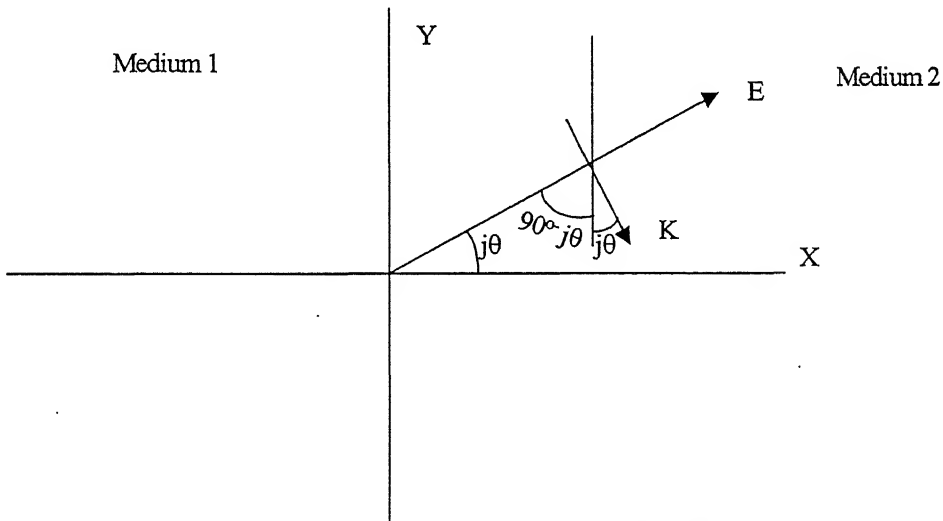

Figure 6.3 Propagation of evanescent wave in medium2

If E is an evanescent wave then angle θ is imaginary. Here in direction x propagation constant is real and in y direction it is imaginary. Field components in the form of matrix can be expressed as following

$$[E_x \ E_y \ H_{zx} \ H_{zy}] = [E_o \cosh\theta \quad jE_o \sinh\theta \quad H_{zxo} \quad H_{zyo}] e^{j\omega(t-\alpha x - \beta y)} \qquad (6.28a)$$

Putting above equations in equation (6.18a-6.18d)

$$(\sigma_y + j\omega\varepsilon)E_o \cosh\theta = -j\omega\beta(H_{zxo} + H_{zyo})$$

$$j(\sigma_x + j\omega\varepsilon)E_o \sinh\theta = j\omega\alpha(H_{zxo} + H_{zyo})$$

$$(\rho_y + j\omega\mu)H_{zyo} = -j\omega\beta E_o \cosh\theta \ , \ (\rho_x + j\omega\mu)H_{zxo} = -\omega\alpha E_o \sinh\theta$$

Solving above we get

$$\alpha = -\left(\frac{1}{cG}\right)\left(j + \frac{\sigma_x}{\omega\varepsilon}\right)\sinh\theta \qquad (6.28b)$$

$$\beta = +\left(\frac{1}{cG}\right)\left(1 - j\frac{\sigma_y}{\omega\varepsilon}\right)\cosh\theta \qquad (6.28c)$$

Where

$$G^2 = W_y \cosh^2\theta - W_x \sinh^2\theta$$

$$W_x = \frac{\mu}{\varepsilon}\left(\frac{\sigma_x + j\omega\varepsilon}{\rho_x + j\omega\mu}\right)$$

$$W_y = \frac{\mu}{\varepsilon}\left(\frac{\sigma_y + j\omega\varepsilon}{\rho_y + j\omega\mu}\right)$$

When values of α and β are put in equation (6.28a), above gives the field variation for all components. It can be easily seen that equation (6.28b) which express propagation along x direction, evanescent waves have natural attenuation which does not contain σx and it is not accelerated in PML.

6.6 Numerical Experiments

We have repeated the experiment done by us in chapter 5 with Mur's second order approximation of one way wave equation as Absorbing Boundary Condition but this time with split formulation of PML proposed by Berenger [13]. This Experiment has been picked up from Berenger's original paper [13] and our results using program 'PMLTE', developed by us, are in excellent confirmation with Berenger. We have also repeated experiment done by Katz et al. [25] on the same software and results are identical. Reflection coefficients of the order of –100dB or high is quite normal which is –60dB

better than what Mur's ABC could achieve at its best. If Thickness of PML is increased with optimum profile then any value of reflection coefficient is possible. In the program Developed by us we have used exponential differencing scheme as [13] and [25] both claimed it is a necessity because of sharp variations in the fields in PML regions. But it is not necessary to use exponential differencing as it produces same results as central differencing scheme does [15]. In our all experiments in subsequent chapters we have used central differencing and found it very effective and attractive because it is simple compared to exponential differencing. Our results and Those of Berenger and Katz have been enclosed for comparison.

Also it is very evident that this material absorbing boundary condition is consisting of non-Maxwellian material and requires splitting of the fields. It leads to more computer memory than expected from any Maxwellian formulation. Also as most of the time people work with Maxwellian formulations of the fields it is a bit difficult to understand this different formulation. For these reasons we have opted for unsplit formulation.

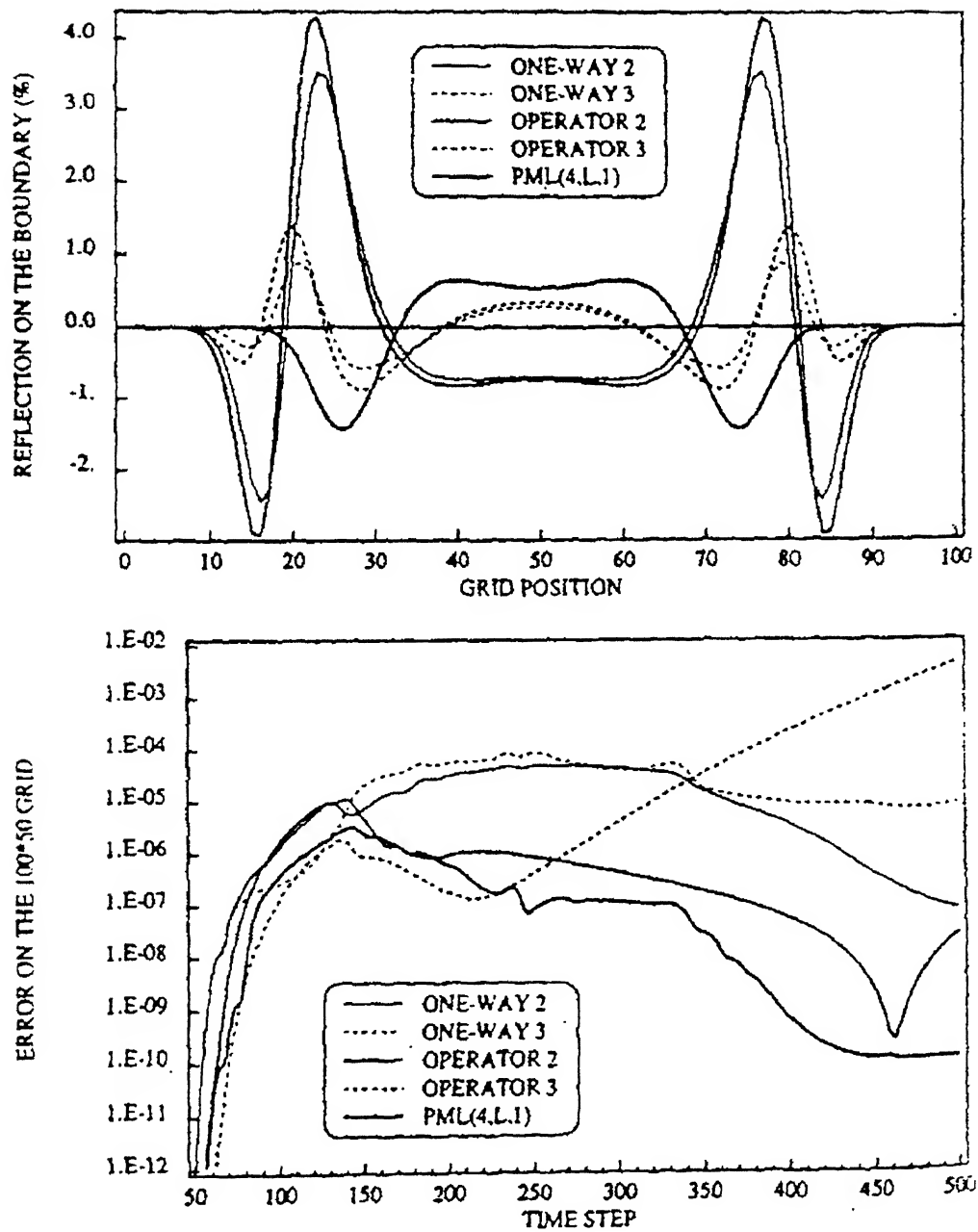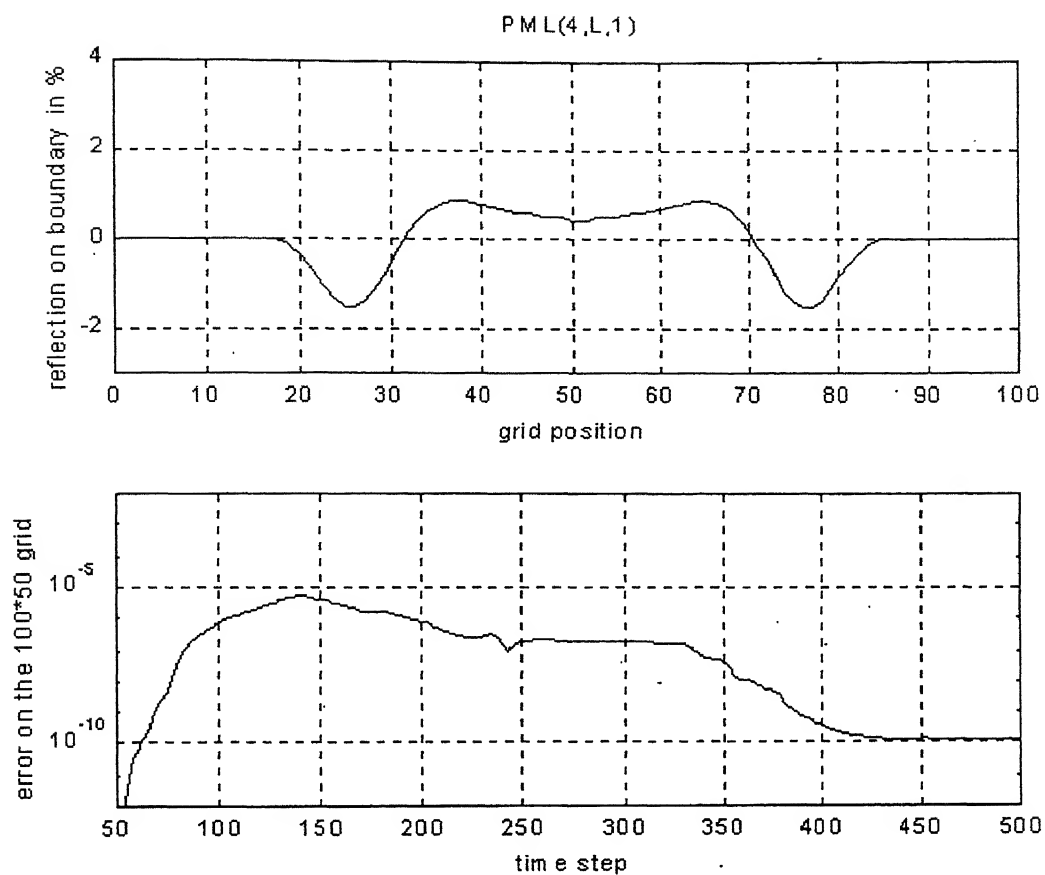Figure 6.4 Berenger's result for PML (4,L, 1)

Figure6.5 results produced by program 'PMLTE' for the same
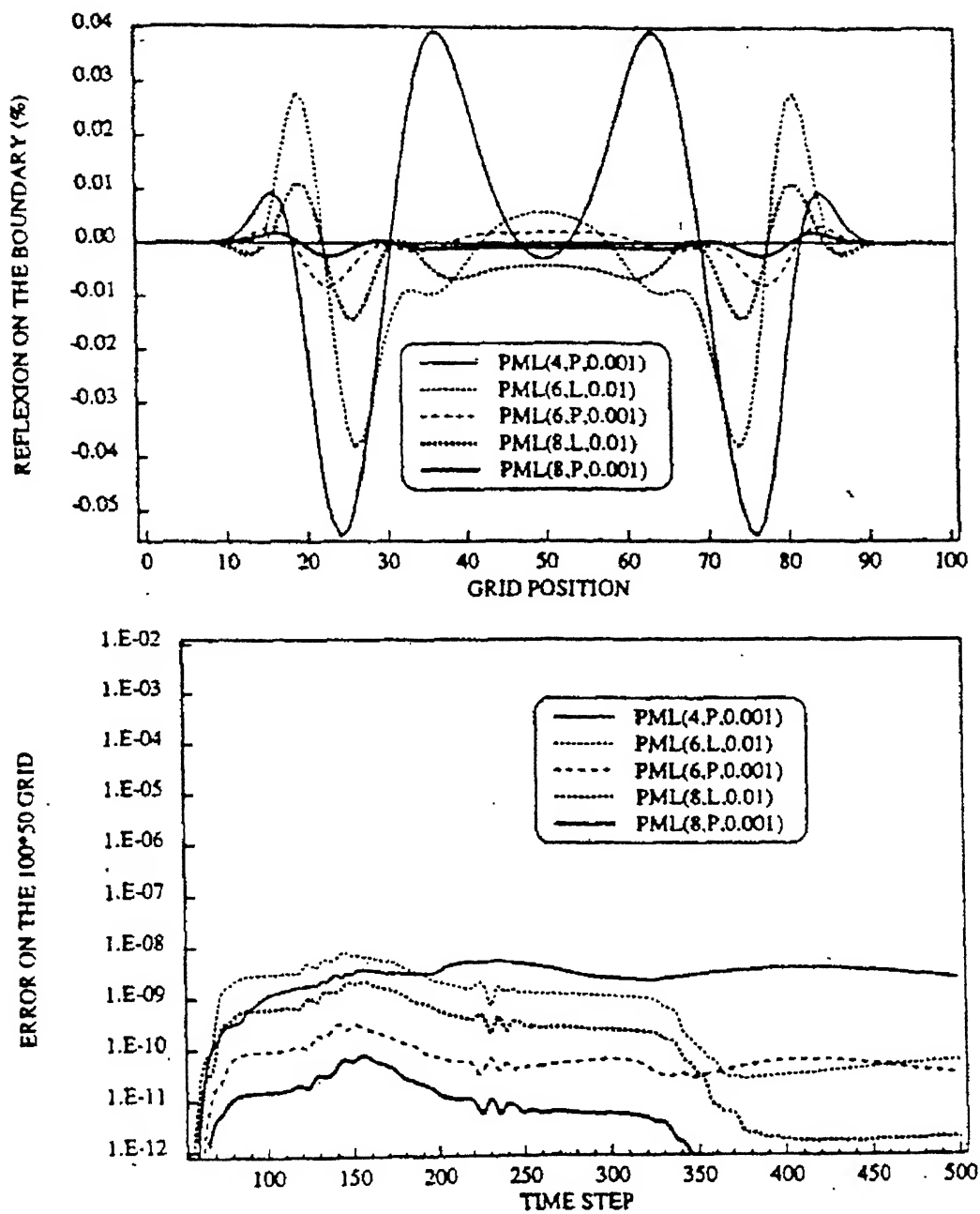
PML parameters as in Figure6.4

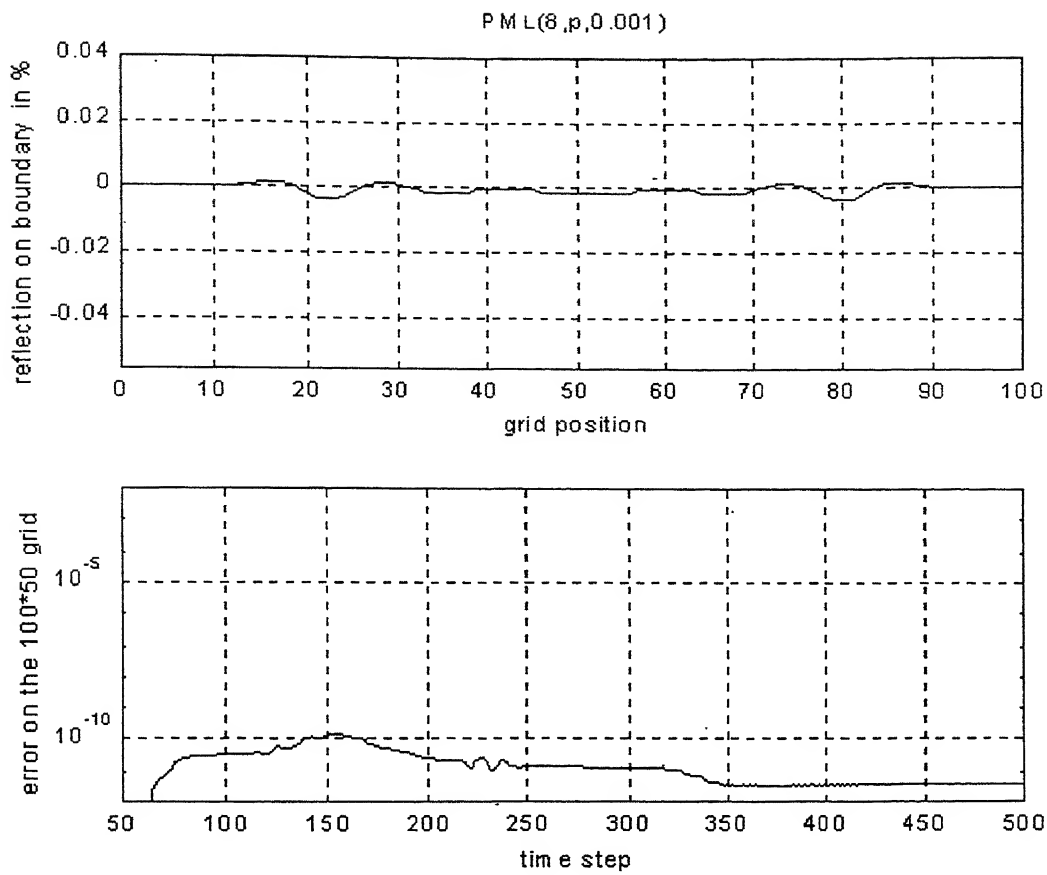Figure6.6 Results produced by Berenger for Various PML

Figure 6.7 Results produced by program 'PMLTE' for PML (8,p, 0.001%)
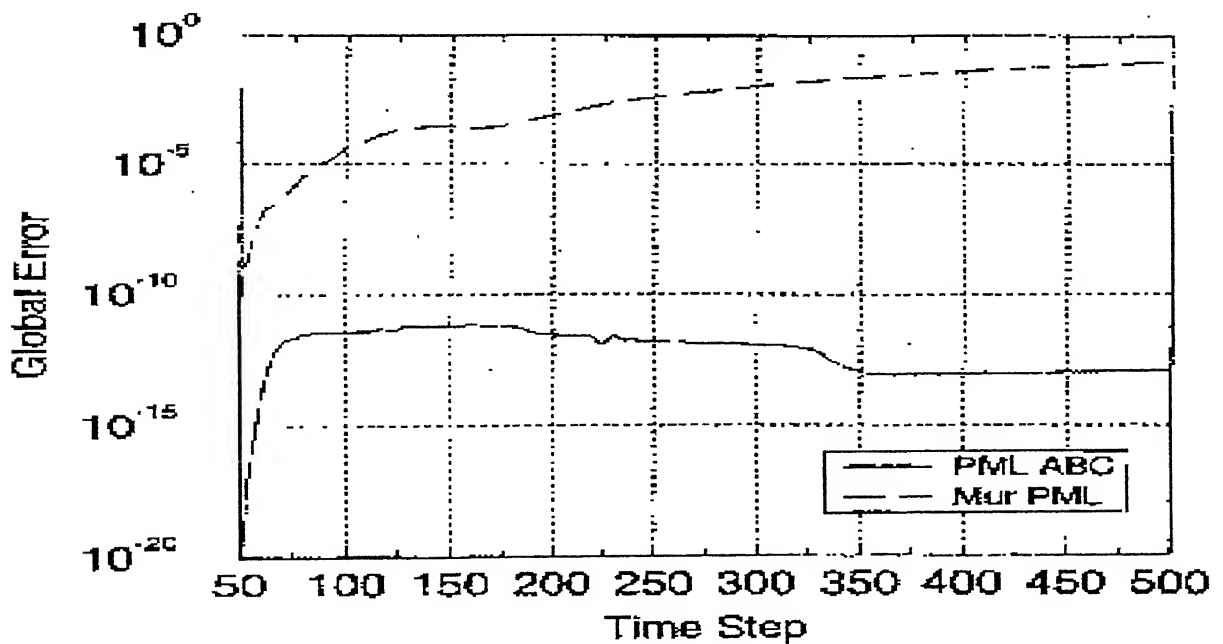
Figure 6.8 Results produced by Katz et al. for PML (16, p, 0.001%)
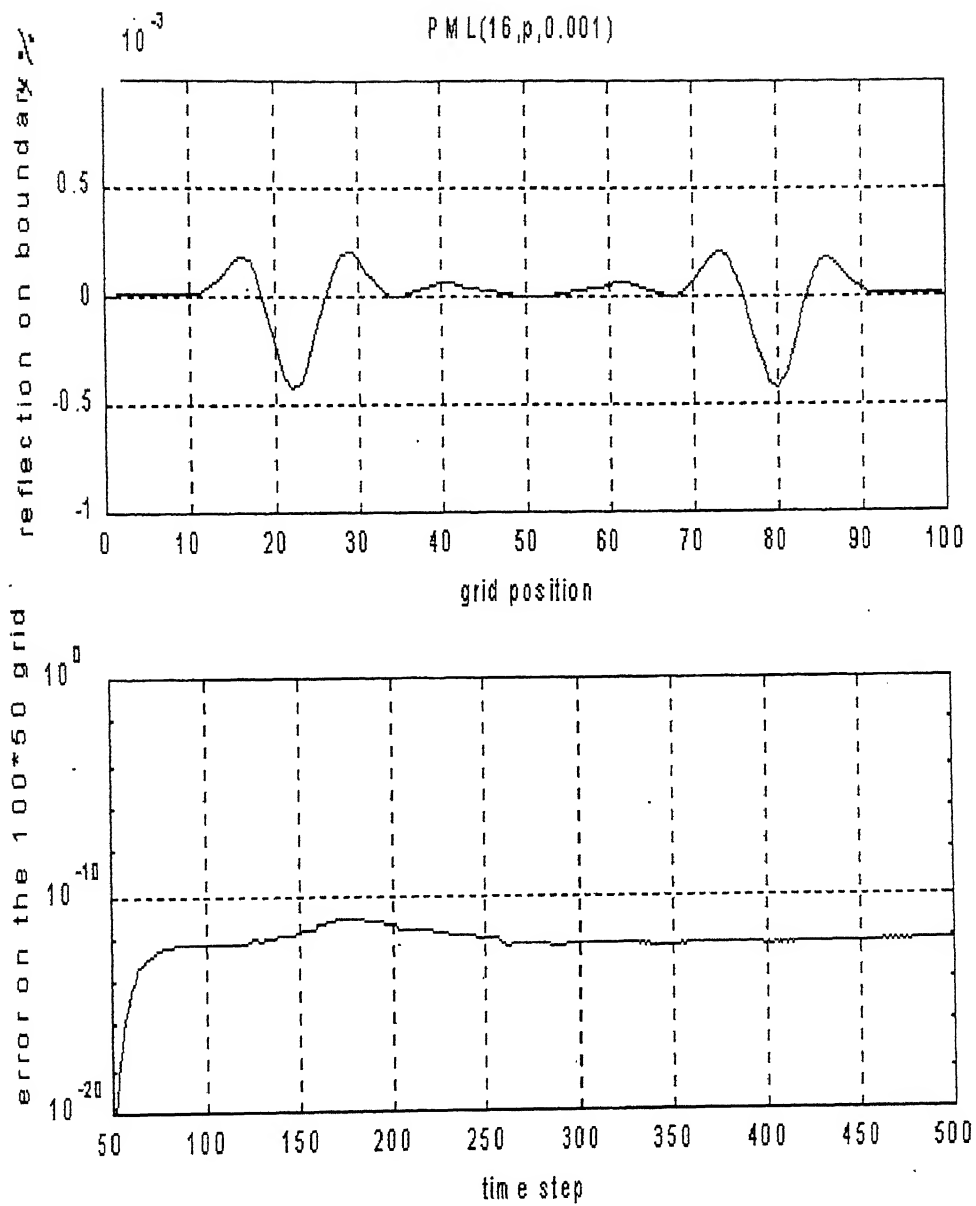
Figure 6.9 Results produced by program 'PMLTE' for PML (16,p, 0.001)

Chapter 7

Unsplit Formulation of Perfectly Matched Layers

Introduction

In previous chapter, we introduced concept of Perfectly Matched Layers as Absorbing boundary condition. Field equations were non-Maxwellian in the perfectly matched layers and fields were to be splited up. From practical considerations of computing, it amounted to more memory requirements. Secondly splitting of fields introduced a sort of uneasiness because of habit of dealing with Maxwellian formulations. Following the work of Berenger [13], Chew and Weedon [18] introduced a complex stretched – coordinate formulation (cscf) of the PML, which was more compact. The principal advantage of cscf is the ease of mathematically manipulating the PML equations and providing a pathway to map PML in other coordinate systems such as Cylindrical and spherical coordinates.

Following Chew and Weedon's work, Sacks et al. [19] introduced an anisotropic perfectly matched layer formulation in which medium conductivities were tensors and no transformation was required. This medium followed more familiar Maxwell equations for fields and thus it was termed as UPML (Unsplit PML) as no splitting of the fields was required.

Here we will give brief introduction of cscf, then we will present UPML and various forms of it to take care of lossy and dispersive mediums. In this chapter, we will confine to UPML for isotropic medium in rectangular coordinates, as this is the basis for our Material Independent Perfectly Matched Layers (MIPML). However, it is quite straightforward to extend the same to other coordinate systems. S.D. Gedney has given details of UPML.[20,21]

7.1 A Stretched Coordinate Formulation

Here to present Berenger's equation [13] in non-split form, a coordinate mapping into complex space is introduced which is given as

$$\tilde{x} \to \int_0^x s_x(x')dx' \quad, \tilde{y} \to \int_0^y s_y(y')dy' \quad, \tilde{z} \to \int_0^z s_z(z')dz' \qquad (7.1)$$

Where it is assumed that PML parameters, $s_i = 1 + \sigma/j\omega\varepsilon$, are continuous function along the axial directions. The partial derivatives in stretched coordinates are

$$\frac{\partial}{\partial\tilde{x}} = \frac{1}{s_x}\frac{\partial}{\partial x} \quad, \frac{\partial}{\partial\tilde{y}} = \frac{1}{s_y}\frac{\partial}{\partial y} \quad, \frac{\partial}{\partial\tilde{z}} = \frac{1}{s_z}\frac{\partial}{\partial z} \qquad (7.2)$$

Thus the ∇ operator in complex space is defined as:

$$\tilde{\nabla} = \hat{x}\frac{\partial}{\partial\tilde{x}} + \hat{y}\frac{\partial}{\partial\tilde{y}} + \hat{z}\frac{\partial}{\partial\tilde{z}} = \hat{x}\frac{1}{s_x}\frac{\partial}{\partial x} + \hat{y}\frac{1}{s_y}\frac{\partial}{\partial y} + \frac{1}{s_z}\hat{z}\frac{\partial}{\partial z} \qquad (7.3)$$

Maxwell's equation in the complex coordinate stretched space are then expressed as

$$-j\omega\mu\vec{H} = \tilde{\nabla} \times \vec{E}$$

$$= \hat{x}\left(\frac{1}{s_y}\frac{\partial}{\partial y}E_z - \frac{1}{s_z}\frac{\partial}{\partial z}E_y\right) + \hat{y}\left(\frac{1}{s_z}\frac{\partial}{\partial z}E_x - \frac{1}{s_x}\frac{\partial}{\partial x}E_z\right) + \hat{z}\left(\frac{1}{s_x}\frac{\partial}{\partial x}E_y - \frac{1}{s_y}\frac{\partial}{\partial y}E_x\right)$$

$$(7.4a)$$

$$j\omega\varepsilon\vec{E} = \tilde{\nabla} \times \vec{H}$$

$$= \hat{x}\left(\frac{1}{s_y}\frac{\partial}{\partial y}H_z - \frac{1}{s_z}\frac{\partial}{\partial z}H_y\right) + \hat{y}\left(\frac{1}{s_z}\frac{\partial}{\partial z}H_x - \frac{1}{s_x}\frac{\partial}{\partial x}H_z\right) + \hat{z}\left(\frac{1}{s_x}\frac{\partial}{\partial x}H_y - \frac{1}{s_y}\frac{\partial}{\partial y}H_x\right)$$

$$(7.4b)$$

Above can be easily derived from equations (6.18a–6.18d).

Inserting E from equation (7.5c) into equation (7.5d) will give following wave equation

$$\beta \times (\frac{1}{\omega \varepsilon s} \overline{=} \beta) \times H = -\omega \mu \overline{s} H$$

$$\beta \times \frac{1}{s} \beta \times H = -\omega \omega \mu \varepsilon \overline{s} H = -k^2 \overline{s} H$$

$$\beta \times (\overline{s}^{-1} \beta) \times H + k^2 \overline{s} H = 0 \qquad (7.6)$$

$$k^2 = \omega^2 \varepsilon \mu$$

Setting determinant of above matrix to zero

$$\det \left(\begin{bmatrix} 0 & 0 & \beta_y^a \\ 0 & 0 & -\beta_x^a \\ -\beta_y^a & \beta_x^a & .0 \end{bmatrix} \begin{bmatrix} s_x^{-1} & 0 & 0 \\ 0 & s_y^{-1} & 0 \\ 0 & 0 & s_z^{-1} \end{bmatrix} \begin{bmatrix} 0 & 0 & \beta_y^a \\ 0 & 0 & -\beta_x^a \\ -\beta_y^a & \beta_x^a & 0 \end{bmatrix} + \begin{bmatrix} k^2 s_x & 0 & 0 \\ 0 & k^2 s_y & 0 \\ 0 & 0 & k^2 s_z \end{bmatrix} \right) = 0$$

$$\det \left(\begin{bmatrix} 0 & 0 & \beta_y^a \\ 0 & 0 & -\beta_x^a \\ -\beta_y^a & \beta_x^a & 0 \end{bmatrix} \begin{bmatrix} 0 & 0 & \beta_y^a s_x^{-1} \\ 0 & 0 & -\beta_x^a s_y^{-1} \\ -\beta_y^a s_z^{-1} & \beta_x^a s_z^{-1} & 0 \end{bmatrix} + \begin{bmatrix} k^2 s_x & 0 & 0 \\ 0 & k^2 s_y & 0 \\ 0 & 0 & k^2 s_z \end{bmatrix} \right) = 0$$

$$\begin{vmatrix} k^2 s_x - (\beta_y^a)^2 s_z^{-1} & \beta_x^a \beta_y^a s_z^{-1} & 0 \\ \beta_x^a \beta_y^a s_z^{-1} & k^2 s_y - (\beta_x^a)^2 s_z^{-1} & 0 \\ 0 & 0 & k^2 s_z - (\beta_y^a)^2 s_x^{-1} - (\beta_x^a)^2 s_y^{-1} \end{vmatrix} = 0$$

$$(k^2 s_z - (\beta_y^a)^2 s_x^{-1} - (\beta_x^a)^2 s_y^{-1})((k^2 s_x - (\beta_y^a)^2 s_z^{-1})(k^2 s_y - (\beta_x^a)^2 s_z^{-1}) - (\beta_x^a \beta_y^a s_z^{-1})^2) = 0$$

$$k^2 - (\beta_y^a)^2 s_x^{-1} s_z^{-1} - (\beta_x^a)^2 s_y^{-1} s_z^{-1} = 0$$

Upon solving, further

$$\beta_x^a = \sqrt{k^2 s_y s_z - (\beta_y^a)^2 s_x^{-1} s_y} \qquad (7.7)$$

Now let us consider fields within working volume with total wave (incident and reflected both) as following

$$H_1 = \hat{z} H_o (1 + \Gamma e^{2j\beta_x^i x}) e^{-j(\beta_x^i x + \beta_y^i y)}$$

$$E_1 = \frac{1}{j\omega\varepsilon} \begin{bmatrix} 0 & -\dfrac{\partial}{\partial z} & \dfrac{\partial}{\partial y} \\ \dfrac{\partial}{\partial z} & 0 & -\dfrac{\partial}{\partial x} \\ -\dfrac{\partial}{\partial y} & \dfrac{\partial}{\partial x} & 0 \end{bmatrix} \begin{bmatrix} 0 \\ 0 \\ H_o(1 + \Gamma e^{2j\beta_x^i x}) e^{-j(\beta_x^i x + \beta_y^i y)} \end{bmatrix} .$$

$$E_1 = \frac{1}{\omega\varepsilon} \begin{bmatrix} -\beta_y^i H_o (1 + \Gamma e^{2j\beta_x^i x}) e^{-j(\beta_x^i x + \beta_y^i y)} \\ \beta_x^i H_o (1 - \Gamma e^{2j\beta_x^i x}) e^{-j(\beta_x^i x + \beta_y^i y)} \\ 0 \end{bmatrix} \qquad (7.8)$$

Now consider PML medium with following transmitted magnetic field.

$$H_2 = \hat{z} H_o \, \tau \, e^{-j(\beta_x^a x + \beta_y^a y)}$$

$$E_2 = \frac{1}{j\omega\varepsilon s} \begin{bmatrix} 0 & -\dfrac{\partial}{\partial z} & \dfrac{\partial}{\partial y} \\ \dfrac{\partial}{\partial z} & 0 & -\dfrac{\partial}{\partial x} \\ -\dfrac{\partial}{\partial y} & \dfrac{\partial}{\partial x} & 0 \end{bmatrix} \begin{bmatrix} 0 \\ 0 \\ \hat{z} H_o \, \tau \, e^{-j(\beta_x^a x + \beta_y^a y)} \end{bmatrix}$$

$$E_2 = \frac{1}{j\omega\varepsilon} \begin{bmatrix} s_x^{-1} & 0 & 0 \\ 0 & s_y^{-1} & 0 \\ 0 & 0 & s_z^{-1} \end{bmatrix} \begin{bmatrix} 0 & -\dfrac{\partial}{\partial z} & \dfrac{\partial}{\partial y} \\ \dfrac{\partial}{\partial z} & 0 & -\dfrac{\partial}{\partial x} \\ -\dfrac{\partial}{\partial y} & \dfrac{\partial}{\partial x} & 0 \end{bmatrix} \begin{bmatrix} 0 \\ 0 \\ H_o\, \tau\, e^{-j(\beta_x^a x + \beta_y^a y)} \end{bmatrix}$$

$$E_2 = \frac{1}{j\omega\varepsilon} \begin{bmatrix} s_x^{-1} & 0 & 0 \\ 0 & s_y^{-1} & 0 \\ 0 & 0 & s_z^{-1} \end{bmatrix} \begin{bmatrix} -\beta_y^a H_o\, \tau\, e^{-j(\beta_x^a x + \beta_y^a y)} \\ \beta_x^a H_o\, \tau\, e^{-j(\beta_x^a x + \beta_y^a y)} \\ 0 \end{bmatrix}$$

$$E_2 = \frac{1}{j\omega\varepsilon} \begin{bmatrix} -s_x^{-1}\beta_y^a H_o\, \tau\, e^{-j(\beta_x^a x + \beta_y^a y)} \\ s_y^{-1}\beta_x^a H_o\, \tau\, e^{-j(\beta_x^a x + \beta_y^a y)} \\ 0 \end{bmatrix} \tag{7.9}$$

Setting

$$E1_y = E2_y$$

From equation (7.8) and (7.9), at interface, existing at x=0 gives

$$\beta_x^i H_o (1 - \Gamma e^{2j\beta_x^i x}) e^{-j(\beta_x^i x + \beta_y^i y)} = s_y^{-1} \beta_x^a H_o\, \tau\, e^{-j(\beta_x^a x + \beta_y^a y)}$$

Putting x=0 and canceling common terms on both the sides, we get

$$\beta_x^i (1 - \Gamma) e^{-j\beta_y^i y} = s_y^{-1} \beta_x^a\, \tau\, e^{-j\beta_y^a y}$$

Where

$$\tau = (1 + \Gamma)$$

Above equation is true only if following conditions are met

(a) $\beta'_y y = \beta^a_y y$ (7.10)

(b) $\dfrac{(1+\Gamma)}{(1-\Gamma)} = \dfrac{\beta'_x}{s_y^{-1}\beta^a_x}$

$\Gamma = \dfrac{\beta'_x - s_y^{-1}\beta^a_x}{\beta'_x + s_y^{-1}\beta^a_x}$ (7.11a)

$\Gamma = 0$ only if $\beta^i_x = s_y^{-1}\beta^a_x$ (7.11b)

Consider equation (7.7), which is given below again

$$\beta^a_x = \sqrt{k^2 s_y s_z - (\beta^a_y)^2 s_x^{-1} s_y}$$

If following condition is satisfied

$s_x^{-1} = s_y = s_z$ (7.11c)

Then above equation (7.7) reduces to

$$\beta^a_x = s_y \sqrt{k^2 - (\beta^a_y)^2}$$

Which can be written as following, using equation (7.10) and dispersion relation for isotropic media

$$\beta^a_x = s_y \sqrt{k^2 - (\beta^i_y)^2} = s_y \beta^i_x$$

Which is same as equation (7.11b)

Consequently ,$\Gamma = 0$ for all β^a_x .

the condition for reflection less transmission for TMz case is same as equation (7.11c)

If a plane wave is incident on a half space with interface at x=constant plane and composed of a uniaxial medium with permittivity and permeability tensors

$$\overline{\overline{\varepsilon}} = \varepsilon \begin{bmatrix} \varepsilon_1 & 0 & 0 \\ 0 & \varepsilon_2 & 0 \\ 0 & 0 & \varepsilon_3 \end{bmatrix} \begin{bmatrix} s_x^{-1} & 0 & 0 \\ 0 & s_x & 0 \\ 0 & 0 & s_x \end{bmatrix} \qquad (7.12a)$$

And

$$\overline{\overline{\mu}} = \mu \begin{bmatrix} \mu_1 & 0 & 0 \\ 0 & \mu_2 & 0 \\ 0 & 0 & \mu_3 \end{bmatrix} \begin{bmatrix} s_x^{-1} & 0 & 0 \\ 0 & s_x & 0 \\ 0 & 0 & s_x \end{bmatrix} \qquad (7.12b)$$

Then the plane wave is purely transmitted into the uniaxial medium irrespective of polarization, frequency and angle of incident.

In UPML,Ex is discontinuous across the x=constant boundary ,while Dx=εsx^{-1}Ex is continuous.In berengers medium both Ex and Dx are continuous.These two mediums have different gauss's laws.

In corner regions following similar kind of analysis the general tensor is determined to be

$$\overline{\overline{\varepsilon}} = \varepsilon \begin{bmatrix} \varepsilon_1 & 0 & 0 \\ 0 & \varepsilon_2 & 0 \\ 0 & 0 & \varepsilon_3 \end{bmatrix} \begin{bmatrix} \dfrac{s_y s_z}{s_x} & 0 & 0 \\ 0 & \dfrac{s_x s_z}{s_y} & 0 \\ 0 & 0 & \dfrac{s_y s_x}{s_z} \end{bmatrix} \qquad (7.13a)$$

$$\overline{\overline{\mu}} = \mu \begin{bmatrix} \mu_1 & 0 & 0 \\ 0 & \mu_2 & 0 \\ 0 & 0 & \mu_3 \end{bmatrix} \begin{bmatrix} \dfrac{s_y s_z}{s_x} & 0 & 0 \\ 0 & \dfrac{s_x s_z}{s_y} & 0 \\ 0 & 0 & \dfrac{s_y s_x}{s_z} \end{bmatrix} \qquad (7.13b)$$

In working volume $s_i = 1$ where i=x,y,z and in regions outside the working volume $s_i > 1$ where i is the axis along which wave is propagating . In this region parameters for other perpendicular directions are $s_{perpendicular\,to\,i} = 1$ .In corner region all $s_i > 1$.

For inhomogeneous mediums also it can be demonstrated that UPML does its job.

7.3 Theoretical Performance of The PML

If boundary is assumed to be PEC wall, power reflects back into the interior FDTD region.The reflection coefficient for isotropic working medium is computed using a simple transmission line analysis and has an amplitude of

$$R(\theta) = e^{(-2\sigma\eta\varepsilon_r d\cos\theta)} \qquad (7.14)$$

Where θ is the angle of incidence ,d is the thickness of the PML slab ,η is the characteristic impedance of the reference material ,and σ is the conductivity of the PML .

In this discussion,we have assumed propagating waves but in case of evanscent waves there is no acceleration to attenuation. So if

$$S_x = \kappa_x + \frac{\sigma_x}{j\omega\varepsilon_0} \qquad (7.15)$$

then we have

$$\gamma_x^a = s_x\gamma_x^i = \left(\kappa_x\alpha_x^i + \frac{\beta_x^i\sigma_x}{\omega\varepsilon_o}\right) + j\left(\kappa_x\beta_x^i - \frac{\alpha_x^i\sigma_x}{\omega\varepsilon_o}\right) \qquad (7.16)$$

$\kappa_x > 1$ will increase decay rate of the evanescent waves.

7.4 The Discrete Space

In discrete space spatial scaling of conductivity profile for magnetic and electric fields is done. Usually most successful are polynomial and geometric scaling .polynomial scaling is simply

$$\sigma(x) = \left(\frac{x}{d}\right)^m \sigma_{max} \qquad (7.17a)$$

$$R(\theta) = e^{\left(-2\eta\varepsilon_r\sigma_{max}\,d\cos\theta\,/\,(m+1)\right)} \qquad (7.17b)$$

If real part of s is greater than one then it can also be spatially scaled using polynomial scalling. To this end we let

$$\mathcal{K}(x) = 1 + \left(\mathcal{K}_{max} - 1\right)\left(\frac{x}{d}\right)^m \qquad (7.17c)$$

For geometric scaling ,the PML conductivity profile is defined as

$$\sigma(x) = \sigma_o\left(g^{\frac{1}{\Delta x}}\right)^x \qquad (7.18a)$$

Reflection coefficient for geometric scaling can be evaluated by integration over PML as for polynomial scaling and it is

$$R(\theta) = e^{-\frac{2\eta\sigma_0\Delta x\left(g^N-1\right)\cos\theta}{\ln g}} \qquad (7.18b)$$

similarly if $\kappa > 1$,it can be geometrically scaled as

$$\mathcal{K}(x) = \left(q^{\frac{1}{\Delta x}}\right)^x \qquad (7.18c)$$

Here σ_o is determined from R(0) which is predetermined along with g and d.

$$\sigma_o = \frac{-\ln[R(0)]\ln(g)}{2\eta\varepsilon_r\Delta x\left(g^N-1\right)} \qquad (7.18d)$$

7.5 Descritization Error

Design of effective UPML requires balancing of theoretical reflection error and Discretization error. If σ_{max} is small, then maximum reflection is due to its PEC backing. To avoid it and some times with the intention of keeping reflection coefficient small, σ_{max} is chosen to be large. But because of FDTD approximation, then Discretization error is

too large. Total reflection error could be several order of magnitudes higher than predicted theoretically by σ_{max} and R (0) relation.

The largest Discretization error occurs at interface. Thus, it is desirable to keep step discontinuity at interface to be kept to a minimum. For the same reason, spatial scaling of conductivity is done but if further rise of conductivity after the interface is too rapid then Reflections from layers near interface are significant.

With extensive experimentation, it has been found that optimum value of σ_{max} is

$$\sigma_{opt} = \frac{m+1}{150\pi\sqrt{\varepsilon_r}\Delta x} \qquad (7.19)$$

This expression has proven quite robust for many applications. Above value may prove quite large when PML terminates elongated structures or sources with large duration. For the latter case, large reflection errors can occur in late time. It can be proven with following

From equation (6.11a) we get

$$\Gamma_o = \left(1 - \sqrt{\frac{s_x^*(0)}{s_x(0)}}\right) \Bigg/ \left(1 + \sqrt{\frac{s_x^*(0)}{s_x(0)}}\right) \qquad (7.20a)$$

In discrete space magnetic tensor and electric tensors are staggered by one half of a cell. Therefore at interface we have $s_x^* = 1$. Thus above equation reduces to

$$\Gamma_o = -\left(1 - \sqrt{s_x(0)}\right) \Bigg/ \left(1 + \sqrt{s_x(0)}\right) \qquad (7.20b)$$

By putting value of s_x in above we get

$$\Gamma_o = \frac{\sqrt{\omega - [j\sigma_x(0)/\varepsilon_o]} - \sqrt{\omega}}{\sqrt{\omega - [j\sigma_x(0)/\varepsilon_o]} + \sqrt{\omega}}$$

If $\omega \gg \sigma_x(0)/\varepsilon_o$, then $\Gamma = 0$. If $\omega \ll \sigma_x(0)/\varepsilon_o$ then $\Gamma = 1$. Therefore all low frequency components will reflect back. A cutoff frequency is defined

$$f_c = \sigma_x(0)/2\pi\varepsilon_o \qquad\qquad (7.20c)$$
$$t_c = 1/fc \qquad\qquad (7.20d)$$

From above two equations it is clear that time exposure of PML can be increased by decreasing $\sigma_x(0)$, which mean this, will reduce $R(\theta)$. So optimal value of σmax will be smaller than given by equation (7.19)

To circumvent this complex frequency shifted tensor is used as a choice for s tensor. This will be explained in coming sections.

7.6   Efficient Implementation of UPML in FDTD

For derivation of the finite difference time domain expressions, starting with the UPML equations, Ampere's law is expressed as

$$
\begin{bmatrix} \dfrac{\partial H_z}{\partial y} - \dfrac{\partial H_y}{\partial z} \\[2mm] \dfrac{\partial H_x}{\partial z} - \dfrac{\partial H_z}{\partial x} \\[2mm] \dfrac{\partial H_y}{\partial x} - \dfrac{\partial H_x}{\partial y} \end{bmatrix} = j\omega\varepsilon_o \begin{bmatrix} \varepsilon_1 & 0 & 0 \\ 0 & \varepsilon_2 & 0 \\ 0 & 0 & \varepsilon_3 \end{bmatrix} \begin{bmatrix} \dfrac{s_y s_z}{s_x} & 0 & 0 \\[2mm] 0 & \dfrac{s_x s_z}{s_y} & 0 \\[2mm] 0 & 0 & \dfrac{s_x s_y}{s_z} \end{bmatrix} \begin{bmatrix} E_x \\ E_y \\ E_z \end{bmatrix} \qquad (7.21a)
$$

$\varepsilon_{i=1,2,3}$ are relative dielectric constant and $s_{i=x,y,z} = \kappa_i + \dfrac{\sigma_i}{j\omega\varepsilon_o}$

If transformation is done from frequency domain to time domain convolution of electric field with tensor will result which is computationally quite expensive. To circumvent it, following transformation is done.

$$Dx = \varepsilon_o \varepsilon_1 \frac{s_z}{s_x} E_x \quad Dy = \varepsilon_o \varepsilon_2 \frac{s_x}{s_y} E_y \quad Dz = \varepsilon_o \varepsilon_3 \frac{s_y}{s_z} E_z \tag{7.21b1}$$

$$\begin{bmatrix} \dfrac{\partial H_z}{\partial y} - \dfrac{\partial H_y}{\partial z} \\[2mm] \dfrac{\partial H_x}{\partial z} - \dfrac{\partial H_z}{\partial x} \\[2mm] \dfrac{\partial H_y}{\partial x} - \dfrac{\partial H_x}{\partial y} \end{bmatrix} = j\omega \begin{bmatrix} s_y & 0 & 0 \\ 0 & s_z & 0 \\ 0 & 0 & s_x \end{bmatrix} \begin{bmatrix} D_x \\ D_y \\ D_z \end{bmatrix} \tag{7.21b}$$

Now putting values of s in the equation we get

$$\begin{bmatrix} \dfrac{\partial H_z}{\partial y} - \dfrac{\partial H_y}{\partial z} \\[2mm] \dfrac{\partial H_x}{\partial z} - \dfrac{\partial H_z}{\partial x} \\[2mm] \dfrac{\partial H_y}{\partial x} - \dfrac{\partial H_x}{\partial y} \end{bmatrix} = \begin{bmatrix} j\omega\kappa_y + \dfrac{\sigma_y}{\varepsilon_o} & 0 & 0 \\[2mm] 0 & j\omega\kappa_z + \dfrac{\sigma_z}{\varepsilon_o} & 0 \\[2mm] 0 & 0 & j\omega\kappa_x + \dfrac{\sigma_x}{\varepsilon_o} \end{bmatrix} \begin{bmatrix} D_x \\ D_y \\ D_z \end{bmatrix}$$

$$\begin{bmatrix} \dfrac{\partial H_z}{\partial y} - \dfrac{\partial H_y}{\partial z} \\[2mm] \dfrac{\partial H_x}{\partial z} - \dfrac{\partial H_z}{\partial x} \\[2mm] \dfrac{\partial H_y}{\partial x} - \dfrac{\partial H_x}{\partial y} \end{bmatrix} = \begin{bmatrix} j\omega\kappa_y & 0 & 0 \\ 0 & j\omega\kappa_z & 0 \\ 0 & 0 & j\omega\kappa_x \end{bmatrix} \begin{bmatrix} D_x \\ D_y \\ D_z \end{bmatrix} + \begin{bmatrix} \dfrac{\sigma_y}{\varepsilon_o} & 0 & 0 \\[2mm] 0 & \dfrac{\sigma_z}{\varepsilon_o} & 0 \\[2mm] 0 & 0 & \dfrac{\sigma_x}{\varepsilon_o} \end{bmatrix} \begin{bmatrix} D_x \\ D_y \\ D_z \end{bmatrix}$$

$$\begin{bmatrix} \dfrac{\partial H_z}{\partial y} - \dfrac{\partial H_y}{\partial z} \\[2mm] \dfrac{\partial H_x}{\partial z} - \dfrac{\partial H_z}{\partial x} \\[2mm] \dfrac{\partial H_y}{\partial x} - \dfrac{\partial H_x}{\partial y} \end{bmatrix} = \frac{\partial}{\partial t}\begin{bmatrix} \kappa_y & 0 & 0 \\ 0 & \kappa_z & 0 \\ 0 & 0 & \kappa_x \end{bmatrix} \begin{bmatrix} D_x \\ D_y \\ D_z \end{bmatrix} + \begin{bmatrix} \dfrac{\sigma_y}{\varepsilon_o} & 0 & 0 \\[2mm] 0 & \dfrac{\sigma_z}{\varepsilon_o} & 0 \\[2mm] 0 & 0 & \dfrac{\sigma_x}{\varepsilon_o} \end{bmatrix} \begin{bmatrix} D_x \\ D_y \\ D_z \end{bmatrix}$$

Now above can be converted to standard FDTD equations. Consider transformation equation (7.21b1) after substituting expressions for s_i.

$$\left(\kappa_x + \frac{\sigma_x}{j\omega\varepsilon_o}\right)D_x = \varepsilon_o\varepsilon_r\left(\kappa_z + \frac{\sigma_z}{j\omega\varepsilon_o}\right)E_x$$

Multiplying both the sides by $j\omega$ and transforming into the time domain leads to

$$\left(\frac{\partial}{\partial t}(\kappa_x D_x) + \frac{\sigma_x}{\varepsilon_o}D_x\right) = \varepsilon_o\varepsilon_r\left(\frac{\partial}{\partial t}(\kappa_z E_x) + \frac{\sigma_z}{\varepsilon_o}E_x\right) \qquad (7.21c)$$

Similar equations can be written for other field components.

7.7 The Complex Frequency Shifted Tensor

In equation (7.20) we demonstrated that one of the limitations of using (7.21a) is that, signals of long duration suffer from large reflections off the PML interface. This effect is circumvented by using the CFS tensor. We let

$$s_i = \kappa_i + \frac{\alpha_i}{\alpha_i + j\omega\varepsilon_o} \quad ,i = x,y,z \qquad (7.22)$$

To derive time dependent formulation for ampere's law from equations (7.21a) and equations (7.22), consider for example a x-normal boundary ($s_z = s_y = 1$). Now introducing following variables:

$$D_x = \varepsilon_o\varepsilon_r\frac{1}{s_x}E_x, D_y = \varepsilon_o\varepsilon_r\ s_x E_y, D_z = \varepsilon_o\varepsilon_r\ s_x E_z \qquad (7.23a)$$

Then equation (7.21a) can be written in time dependent form

$$\frac{\partial}{\partial t}\overline{D} = \nabla\times\overline{H} \qquad (7.23b)$$

From equation (7.22) and equation (7.23a) expressions for Ex and Ey can be written as

$$\varepsilon_r \varepsilon_o \left(\alpha_x E_x + \varepsilon_o \frac{\partial}{\partial t} E_x \right) = (\kappa_x \alpha_x + \sigma_x) D_x + \kappa_x \varepsilon_o \frac{\partial}{\partial t} D_x \qquad (7.24a)$$

$$\varepsilon_r \varepsilon_o (\kappa_x \alpha_x + \sigma_x) E_y + \kappa_x \varepsilon_o \frac{\partial}{\partial t} E_y = \left(\alpha_x D_y + \varepsilon_o \frac{\partial}{\partial t} D_y \right) \qquad (7.24b)$$

Similar expression can be derived for Ez.

Putting values of s_i from equation (7.22) into equation (7.21a) we can drive electric field Ex, Ey and Ez as mentioned below in the corner regions. The constitutive relations are

$$Dx = \varepsilon_o \varepsilon_r \frac{1}{s_x} E_x$$

$$P_{x1} = s_y D_x$$

$$P_{x2} = s_y P_{x1}$$

Thus from ampere's law

$$\frac{\partial}{\partial t} P_{x2} = \frac{\partial}{\partial y} H_z - \frac{\partial}{\partial z} H_y$$

$$(\kappa_z \alpha_z + \sigma_z) P_{x1} + \kappa_z \varepsilon_o \frac{\partial}{\partial t} P_{x1} = \left(\alpha_z P_{x2} + \varepsilon_o \frac{\partial}{\partial t} P_{x2} \right)$$

$$(\kappa_y \alpha_y + \sigma_y) D_x + \kappa_y \varepsilon_o \frac{\partial}{\partial t} D_x = \left(\alpha_y P_{x1} + \varepsilon_o \frac{\partial}{\partial t} P_{x1} \right)$$

$$\varepsilon_r \varepsilon_o \left(\alpha_x E_x + \varepsilon_o \frac{\partial}{\partial t} E_x \right) = (\kappa_x \alpha_x + \sigma_x) D_x + \kappa_x \varepsilon_o \frac{\partial}{\partial t} D_x$$

We see that this method requires the introduction of three auxiliary expressions and variables compared to one required by the previous method. This results in an increase in computer time and memory. So this formulation should be reserved for special cases.

7.8   PML Termination for Conductive Media

Ampere's law in the conductive media

$$
\begin{bmatrix}
\dfrac{\partial H_z}{\partial y} - \dfrac{\partial H_y}{\partial z} \\[2mm]
\dfrac{\partial H_x}{\partial z} - \dfrac{\partial H_z}{\partial x} \\[2mm]
\dfrac{\partial H_y}{\partial x} - \dfrac{\partial H_x}{\partial y}
\end{bmatrix}
= j\omega\varepsilon_o
\begin{bmatrix}
\varepsilon_1 + \dfrac{\sigma}{j\omega\varepsilon_1} & 0 & 0 \\[2mm]
0 & \varepsilon_2 + \dfrac{\sigma}{j\omega\varepsilon_2} & 0 \\[2mm]
0 & 0 & \varepsilon_3 + \dfrac{\sigma}{j\omega\varepsilon_3}
\end{bmatrix}
\begin{bmatrix}
\dfrac{s_y s_z}{s_x} & 0 & 0 \\[2mm]
0 & \dfrac{s_x s_z}{s_y} & 0 \\[2mm]
0 & 0 & \dfrac{s_x s_y}{s_z}
\end{bmatrix}
\begin{bmatrix}
E_x \\[2mm] E_y \\[2mm] E_z
\end{bmatrix}
$$

$\varepsilon_{i=1,2,3}$ are relative dielectric constant and $s_{i=x,y,z} = \kappa_i + \dfrac{\sigma_i}{j\omega\varepsilon_o}$

$$
P_x = \frac{s_z}{s_x} E_x, \quad P_y = \frac{s_x}{s_y} E_y, \quad P_z = \frac{s_y}{s_z} E_z
$$

$$
P_x' = s_y P_x, \quad P_y' = s_z P_y, \quad P_z' = s_x P_z
$$

$$
\begin{bmatrix}
\dfrac{\partial H_z}{\partial y} - \dfrac{\partial H_y}{\partial z} \\[2mm]
\dfrac{\partial H_x}{\partial z} - \dfrac{\partial H_z}{\partial x} \\[2mm]
\dfrac{\partial H_y}{\partial x} - \dfrac{\partial H_x}{\partial y}
\end{bmatrix}
= j\omega\varepsilon_o
\begin{bmatrix}
\varepsilon_1 + \dfrac{\sigma}{j\omega\varepsilon_o} & 0 & 0 \\[2mm]
0 & \varepsilon_2 + \dfrac{\sigma}{j\omega\varepsilon_o} & 0 \\[2mm]
0 & 0 & \varepsilon_3 + \dfrac{\sigma}{j\omega\varepsilon_o}
\end{bmatrix}
\begin{bmatrix}
P_x' \\[2mm] P_y' \\[2mm] P_z'
\end{bmatrix}
$$

$$
\begin{bmatrix}
\dfrac{\partial H_z}{\partial y} - \dfrac{\partial H_y}{\partial z} \\[2mm]
\dfrac{\partial H_x}{\partial z} - \dfrac{\partial H_z}{\partial x} \\[2mm]
\dfrac{\partial H_y}{\partial x} - \dfrac{\partial H_x}{\partial y}
\end{bmatrix}
= \frac{\partial}{\partial t}
\begin{bmatrix}
\varepsilon_o \varepsilon_1 P_x' \\[2mm]
\varepsilon_o \varepsilon_2 P_y' \\[2mm]
\varepsilon_o \varepsilon_3 P_z'
\end{bmatrix}
+ \sigma
\begin{bmatrix}
P_x' \\[2mm] P_y' \\[2mm] P_z'
\end{bmatrix}
$$

$$
\frac{\partial}{\partial t}
\begin{bmatrix}
P_x' \\[2mm] P_y' \\[2mm] P_z'
\end{bmatrix}
= \frac{\partial}{\partial t}
\begin{bmatrix}
\kappa_y & 0 & 0 \\
0 & \kappa_z & 0 \\
0 & 0 & \kappa_x
\end{bmatrix}
\begin{bmatrix}
P_x \\[2mm] P_y \\[2mm] P_z
\end{bmatrix}
+
\begin{bmatrix}
\dfrac{\sigma_y}{\varepsilon_o} & 0 & 0 \\[2mm]
0 & \dfrac{\sigma_z}{\varepsilon_o} & 0 \\[2mm]
0 & 0 & \dfrac{\sigma_x}{\varepsilon_o}
\end{bmatrix}
\begin{bmatrix}
P_x \\[2mm] P_y \\[2mm] P_z
\end{bmatrix}
$$

$$
\frac{\partial}{\partial t}\left(\kappa_x P_x\right) + \frac{\sigma_x}{\varepsilon_o} P_x = \frac{\partial}{\partial t}\left(\kappa_z E_x\right) + \frac{\sigma_z}{\varepsilon_o} E_x \tag{7.26}
$$

Similarly by replacing x with y and z, we can write equation for y and z component respectively.

Chapter 8
Material Independent Perfectly Matched Layers

Introduction

PML technique originally developed by Berenger [13] has been extended for absorbing Evanescent waves and lossy materials [16]. A review of PML in chapter 6 with numerical experimentation and a review of UPML covering absorption of evanescent waves and lossy materials in chapter 7 have been presented. Obviously, to further enhance the capability of existing PML technique, extending it to cover anisotropic materials, merits attention. It was proven [31] that under certain circumstances no PML condition can be derived even for the simple case when only the arbitrary anisotropic dielectric is considered. However it was realized by us and Zhao [32] that above difficulties [31] can be overcome by using flux D and B instead of E and H. *Use of flux instead of field quantities makes it material independent. and extends PML to arbitrary anisotropic material.* Though the proof published by Zhao et al. [22] was given for arbitrary dielectric medium 2-D, the proof developed independently by us is for a material, which is arbitrary anisotropic in permeability and permittivity both. Our proof is applicable to split formulations in 2-D like [22]. For two-dimensional case our proof clearly demonstrates that there is no need to use D and B as said in [24]. Use of E and H equally works. In 3-D, use of D and B instead of E and H makes PML equations simple. It also makes matching conditions independent of permittivity and permeability tensors, so they are simplified and make algorithm independent of medium. In fact we have demonstrated very clearly that UPML equations are inherently Material Independent if material properties are not included in Maxwell equations by properly transforming fields and calculating them indirectly through the transforming equations.

8.1   PML in Two Dimensional Anisotropic Space

Expressing Maxwell equations as

$$j\omega D = \nabla \times H \qquad (8.1a)$$

$$-j\omega B = \nabla \times E \qquad (8.1b)$$

$$D = \bar{\bar{\varepsilon}}^{-1} E \qquad (8.1c)$$

$$B = \bar{\bar{\mu}}^{-1} H \qquad (8.1d)$$

$$\begin{bmatrix} H_x \\ H_y \\ H_z \end{bmatrix} = \begin{bmatrix} H_{ox}e^{-j(\beta_x x + \beta_y y + \beta_z z)} \\ H_{oy}e^{-j(\beta_x x + \beta_y y + \beta_z z)} \\ H_{oz}e^{-j(\beta_x x + \beta_y y + \beta_z z)} \end{bmatrix} \qquad (8.1e)$$

Putting above in Maxwell equations will yield

$$-\omega D = \beta \times H \qquad (8.2a)$$

$$\omega B = \beta \times E \qquad (8.2b)$$

By assuming permeability and permittivity tensors as following

$$[\bar{\mu}] = \begin{bmatrix} \mu_{xx} & \mu_{xy} & \mu_{xz} \\ \mu_{xy} & \mu_{yy} & \mu_{yz} \\ \mu_{xz} & \mu_{yz} & \mu_{zz} \end{bmatrix} = \begin{bmatrix} \mu_{xx} & \mu_{xy} & 0 \\ \mu_{xy} & \mu_{yy} & 0 \\ 0 & 0 & \mu_{zz} \end{bmatrix} \qquad (8.3a)$$

$$[\bar{\varepsilon}] = \begin{bmatrix} \varepsilon_{xx} & \varepsilon_{xy} & \varepsilon_{xz} \\ \varepsilon_{xy} & \varepsilon_{yy} & \varepsilon_{yz} \\ \varepsilon_{xz} & \varepsilon_{yz} & \varepsilon_{zz} \end{bmatrix} = \begin{bmatrix} \varepsilon_{xx} & \varepsilon_{xy} & 0 \\ \varepsilon_{xy} & \varepsilon_{yy} & 0 \\ 0 & 0 & \varepsilon_{zz} \end{bmatrix} \qquad (8.3b)$$

Then

$$[\bar{\mu}]^{-1} = \begin{bmatrix} X_{xx} & X_{xy} & 0 \\ X_{xy} & X_{yy} & 0 \\ 0 & 0 & X_{zz} \end{bmatrix} \qquad (8.4a)$$

$$[\bar{\varepsilon}]^{-1} = \begin{bmatrix} A_{xx} & A_{xy} & 0 \\ A_{xy} & A_{yy} & 0 \\ 0 & 0 & A_{zz} \end{bmatrix} \qquad (8.4b)$$

Let

$$[\nabla \times] = \begin{bmatrix} 0 & -\dfrac{\partial}{\partial z} & \dfrac{\partial}{\partial y} \\ \dfrac{\partial}{\partial z} & 0 & -\dfrac{\partial}{\partial x} \\ -\dfrac{\partial}{\partial y} & \dfrac{\partial}{\partial x} & 0 \end{bmatrix} \qquad (8.5)$$

$$[\beta \times] = \begin{bmatrix} 0 & -\beta_z & \beta_y \\ \beta_z & 0 & -\beta_x \\ -\beta_y & \beta_x & 0 \end{bmatrix} \qquad (8.6)$$

Taking a two dimensional X-Y plane at z=0 where

$$\frac{\partial}{\partial z} = 0 \qquad (8.7a)$$

and

$$[\beta \times] = \begin{bmatrix} 0 & 0 & \beta_y \\ 0 & 0 & -\beta_x \\ -\beta_y & \beta_x & 0 \end{bmatrix} \qquad (8.7b)$$

In working medium

$$
\begin{bmatrix} E_x \\ E_y \\ E_z \end{bmatrix} = -\frac{1}{\omega}
\begin{bmatrix} A_{xx} & A_{xy} & 0 \\ A_{xy} & A_{yy} & 0 \\ 0 & 0 & A_{zz} \end{bmatrix}
\begin{bmatrix} 0 & 0 & \beta_y^i \\ 0 & 0 & -\beta_x^i \\ -\beta_y^i & \beta_x^i & 0 \end{bmatrix}
\begin{bmatrix} H_x \\ H_y \\ H_{oz}(1+\Gamma e^{2j\beta_x^i x})e^{\left(-j(\beta_x^i x + \beta_y^i y)\right)} \end{bmatrix}
$$

(8.8a)

at $x = 0$

$$
\begin{bmatrix} E_x \\ E_y \\ E_z \end{bmatrix} = \frac{1}{\omega}
\begin{bmatrix} (-A_{xx}\beta_y^i(1+\Gamma) + A_{xy}\beta_x^i(1-\Gamma))H_{oz}e^{\left(-j\beta_y^i y\right)} \\ (-A_{xy}\beta_y^i(1+\Gamma) + A_{yy}\beta_x^i(1-\Gamma))H_{oz}e^{\left(-j\beta_y^i y\right)} \\ A_{zz}(\beta_y^i H_y - \beta_x^i H_x) \end{bmatrix}
$$

(8.8b)

In perfectly matched medium. .

$$
-\omega\bar{\varepsilon}E = \beta^S \times H
$$

$$
\begin{bmatrix} E_x \\ E_y \\ E_z \end{bmatrix} = -\frac{1}{\omega}
\begin{bmatrix} A_{xx} & A_{xy} & 0 \\ A_{xy} & A_{yy} & 0 \\ 0 & 0 & A_{zz} \end{bmatrix}
\begin{bmatrix} 0 & 0 & \beta_y^a s_y^{-1} \\ 0 & 0 & -\beta_x^a s_x^{-1} \\ -\beta_y^a s_y^{-1} & \beta_x^a s_x^{-1} & 0 \end{bmatrix}
\begin{bmatrix} H_x \\ H_y \\ H_{oz}\tau e^{\left(-j(\beta_x^a x + \beta_y^a y)\right)} \end{bmatrix}
$$

(8.9a)

at $x = 0$

$$
\begin{bmatrix} E_x \\ E_y \\ E_z \end{bmatrix} =
\begin{bmatrix} (-A_{xx}\beta_y^a s_y^{-1}(1+\Gamma) + A_{xy}\beta_x^a s_x^{-1}(1+\Gamma))H_{oz}e^{\left(-j\beta_y^a y\right)} \\ (-A_{xy}\beta_y^a s_y^{-1}(1+\Gamma) + A_{yy}\beta_x^a s_x^{-1}(1+\Gamma))H_{oz}e^{\left(-j\beta_y^a y\right)} \\ (\beta_y^a s_y^{-1}H_x - \beta_{xx}^a s_x^{-1}H_y)A_{zz} \end{bmatrix}
$$

(8.9b)

In above equations value of propagation constant matrix is taken from equations (7.4) which are for Berenger's split formulation. Matching tangential y components gives:

Phase matching

$$
\beta_y^i = \beta_y^a
$$ (8.10)

Amplitude matching

$$-A_{xy}\beta_y^i(1+\Gamma)+A_{yy}\beta_x^i(1-\Gamma)=-A_{xy}\beta_y^a s_y^{-1}(1+\Gamma)+A_{yy}\beta_x^a s_x^{-1}(1+\Gamma)$$

$$(A_{xy}\beta_y^i-A_{xy}\beta_y^a s_y^{-1}+A_{yy}\beta_x^a s_x^{-1})(1+\Gamma)=A_{yy}\beta_x^i(1-\Gamma)$$

$$\frac{(1+\Gamma)}{(1-\Gamma)}=\frac{A_{yy}\beta_x^i}{A_{xy}\beta_y^i-A_{xy}\beta_y^a s_y^{-1}+A_{yy}\beta_x^a s_x^{-1}} \qquad (8.11)$$

By putting phase matching condition in above

$$\Gamma=\frac{A_{yy}\left(\beta_x^i-\beta_x^a s_x^{-1}\right)-A_{xy}\beta_y^i\left(1-s_y^{-1}\right)}{A_{yy}\left(\beta_x^i+\beta_x^a s_x^{-1}\right)+A_{xy}\beta_y^i\left(1-s_y^{-1}\right)} \qquad (8.12)$$

If

$$s_y^{-1}=1 \qquad (8.13)$$

Then

$$\Gamma=\frac{A_{yy}\left(\beta_x^i-\beta_x^a s_x^{-1}\right)}{A_{yy}\left(\beta_x^i+\beta_x^a s_x^{-1}\right)} \qquad (8.14a)$$

$$\Gamma=0 \text{ if}\left(\beta_x^i=\beta_x^a s_x^{-1}\right) \qquad (8.14b)$$

$$\Gamma=0 \text{ if}\left(\beta_x^i s_x=\beta_x^a\right) \qquad (8.14c)$$

If

$$s_x=1+\frac{\sigma}{j\omega} \qquad (8.15)$$

Then

$$E_x = (-A_{xx}\beta_y^a s_y^{-1} + A_{xy}\beta_x^a s_x^{-1})H_{oz}e^{\left(-j\beta_x^a x - j\beta_y^a y\right)}$$ (8.16a)

$$E_x = (-A_{xx}\beta_y^i s_y^{-1} + A_{xy}\left(1+\frac{\sigma}{j\omega}\right)\beta_x^i s_x^{-1})H_{oz}e^{\left(-j\left(1+\frac{\sigma}{j\omega}\right)\beta_x^i x - j\beta_y^i y\right)}$$ (8.16b)

$$E_x = (-A_{xx}\beta_y^i s_y^{-1} + A_{xy}\left(1+\frac{\sigma}{j\omega}\right)\beta_x^i s_x^{-1})H_{oz}e^{\left(-j\beta_x^i x - j\beta_y^i y\right)}e^{-\frac{\sigma}{\omega}\beta_x^i x}$$ (8.16c)

$$E_x = (-A_{xx}\beta_y^i s_y^{-1} + A_{xy}\left(1+\frac{\sigma}{j\omega}\right)\beta_x^i s_x^{-1})H_{oz}e^{\left(-j\beta_x^i x - j\beta_y^i y\right)}e^{-\frac{\sigma}{v}\cos\theta x}$$ (8.16d)

Where

$$v = \frac{\beta_x^i}{\omega}$$ (8.17)

Here we see that wave attenuates in x direction in PML. Though the splitting of fields is not evident from derivation but it comes into picture with equation (8.13) and expression for propagation constant matrix in equation (8.9).

8.1   PML in 3-D for Anisotropic Medium

Here we will discuss some fundamental issues related to wave propagation in anisotropic media in 3-D space. In anisotropic medium Ex is dependent on Dx, Dy and Dz. It is the case with Ey and Ez. Similar statement can be made for magnetic field and flux components. This implies that in an anisotropic medium it is not possible to have TE or TM modes propagating. We have only Hybrid modes propagating. So any PML designed should be proved for Hybrid modes i.e. it should be able to absorb Hybrid modes without any reflection. All the derivations so far done have been for TE and TM modes in isotropic medium and curl equations in PML for isotropic medium are

$$\nabla \times \overline{E} = -j\omega\,\mu\,\overline{s}\,\overline{H}$$ (8.18a)

$$\nabla \times \overline{H} = -j\omega\,\varepsilon\,\overline{s}\,\overline{E}$$ (8.18b)

Which strongly suggests that *PML should be able to match any medium with the same matching conditions*. But in anisotropic medium we do not have propagating TE and TM modes so it is not possible to prove UPML conditions separately for propagating TE and TM modes, and then assume that it will hold good for all propagating hybrid modes also. This has been the practice for isotropic medium but can not be used for anisotropic medium. We have tried to prove that UPML absorbs hybrid waves incident upon from anisotropic medium by numerical simulation. Prior to that we will demonstrate that UPML is essentially Material Independent and with the use of proper transformations it can in fact match any medium. Let us assume that Maxwell's curl Equations, in PML for anisotropic medium, are

$$\nabla \times E = -\bar{s}\frac{\partial B}{\partial t} \qquad (8.19a)$$

$$\nabla \times H = -\bar{s}\frac{\partial D}{\partial t} \qquad (8.19b)$$

Here

$$\bar{s} = \begin{bmatrix} \dfrac{s_y s_z}{s_x} & 0 & 0 \\ 0 & \dfrac{s_x s_z}{s_y} & 0 \\ 0 & 0 & \dfrac{s_x s_y}{s_z} \end{bmatrix} \qquad (8.20)$$

$$s_x = \kappa + \frac{\sigma_x}{j\omega}$$

$$s_y = \kappa + \frac{\sigma_y}{j\omega}$$

$$s_z = \kappa + \frac{\sigma_z}{j\omega}$$

$$\kappa \geq 1$$

Kappa can be taken greater than one for absorbing evanescent waves. Also if medium is lossy, it can be taken greater than one to match it [21]. Its optimum value can be determined experimentally.

From equation (8.19b) and (8.20)

$$
\begin{bmatrix}
\dfrac{\partial H_z}{\partial y} - \dfrac{\partial H_y}{\partial z} \\[2mm]
\dfrac{\partial H_x}{\partial z} - \dfrac{\partial H_z}{\partial x} \\[2mm]
\dfrac{\partial H_y}{\partial x} - \dfrac{\partial H_x}{\partial y}
\end{bmatrix}
= j\omega
\begin{bmatrix}
\dfrac{s_y s_z}{s_x} & 0 & 0 \\[3mm]
0 & \dfrac{s_x s_z}{s_y} & 0 \\[3mm]
0 & 0 & \dfrac{s_x s_y}{s_z}
\end{bmatrix}
\begin{bmatrix}
D_x \\[2mm]
D_y \\[2mm]
D_z
\end{bmatrix}
\qquad (8.21)
$$

Before proceeding further we would like to bring out the special features of UPML equations. From equation (7.21c) after discretising we can write [20]

$$
D_x\Big|_{i+\frac{1}{2},j,k}^{n+\frac{1}{2}} = A.D_x\Big|_{i+\frac{1}{2},j,k}^{n+\frac{1}{2}} + B.\left[\frac{H_z\big|_{i+\frac{1}{2},j+\frac{1}{2},k}^{n} - H_z\big|_{i+\frac{1}{2},j-\frac{1}{2},k}^{n}}{\Delta y} - \right.
$$

$$
\left. \frac{H_y\big|_{i+\frac{1}{2},j,k+\frac{1}{2}}^{n} - H_y\big|_{i+\frac{1}{2},j,k-\frac{1}{2}}^{n}}{\Delta z} \right] \qquad (8.22a)
$$

$$
E_x\Big|_{i+\frac{1}{2},j,k}^{n+\frac{1}{2}} = C.E_x\Big|_{i+\frac{1}{2},j,k}^{n-\frac{1}{2}} + \frac{1}{\varepsilon_0 \varepsilon_r}\left[D..D_x\Big|_{i+\frac{1}{2},j,k}^{n+\frac{1}{2}} - E.D_x\Big|_{i+\frac{1}{2},j,k}^{n-\frac{1}{2}} \right] \qquad (8.22b)
$$

$$
A = \frac{\dfrac{\kappa_y}{\Delta t} - \dfrac{\sigma_y}{2\varepsilon_0}}{\dfrac{\kappa_y}{\Delta t} + \dfrac{\sigma_y}{2\varepsilon_0}}
\quad
B = \frac{1}{\dfrac{\kappa_y}{\Delta t} + \dfrac{\sigma_y}{2\varepsilon_0}}
\quad
C = \frac{\dfrac{\kappa_z}{\Delta t} - \dfrac{\sigma_z}{2\varepsilon_0}}{\dfrac{\kappa_z}{\Delta t} + \dfrac{\sigma_z}{2\varepsilon_0}}
\quad
D = \frac{\dfrac{\kappa_x}{\Delta t} + \dfrac{\sigma_x}{2\varepsilon_0}}{\dfrac{\kappa_z}{\Delta t} + \dfrac{\sigma_z}{2\varepsilon_0}}
\quad
E = \frac{\dfrac{\kappa_x}{\Delta t} - \dfrac{\sigma_x}{2\varepsilon_0}}{\dfrac{\kappa_z}{\Delta t} + \dfrac{\sigma_z}{2\varepsilon_0}}
$$

Referring to equation (7.17b) and taking θ=0 and ε_r=1 in this, we can write

$$\sigma_{max} = -\frac{c\varepsilon_o(m+1)\ln[R(0)]}{2d} \qquad (8.23a)$$

$$\sigma(x) = -\left(\frac{x}{d}\right)^m \cdot \frac{c\varepsilon_o(m+1)\ln[R(0)]}{2d} \qquad (8.23b)$$

If equation (8.23b) is put in expressions for A, B, C, D and E they become independent of ε_o. So we can say A, B, C, D and E are independent of medium properties. If relative effective dielectric constant is not equal to one then it can be taken care by removing it and increasing value of m, reflection factor and d by the same factor. Which means that if any equation is of the same form that of equation (7.5) it can be matched by UPML. Here equations (8.19) are of the same form that of equation (7.5) with permitivity and permeability included in B and D.

8.3 FDTD Equations for MIPML

From equation (8.16d), amplitude of a wave can be written as below in a generalized form

$$\psi(x) = \psi(0)e^{-\frac{\sigma}{v}\cos\theta \; x} \qquad (8.24)$$

Where interface of anisotropic medium and PML has been taken as reference. As is the usual practice either a PEC or PMC wall terminates a PML. Above mentioned wave travels from interface to PEC and reflects back and enters anisotropic media. So for a layer of thickness of d reflection factor can be defined as

$$R(\theta) = e^{(-2.\sigma.d\cos\theta\,/\,c)} \qquad (8.25a)$$

Again to minimize numerical reflections conductivity is gradually increased, with profile defined as below

$$\sigma(x) = \sigma_m \left(\frac{x}{d}\right)^m \qquad (8.25b)$$

And Reflection factor is given as

$$R(\theta) = e^{-2\left(\frac{\cos\theta}{c}\right)\int_0^d \sigma(x)dx} \qquad (8.25c)$$

Put equation (8.25b) for conductivity profile in equation (8.25c) and reflection factor becomes

$$R(\theta) = e^{-\left(\frac{2}{(n+1)}\right)\left(\frac{\sigma_m d}{c}\right)\cos\theta} \qquad (8.25d)$$

Conductivity is given by

$$\sigma_{max} = -\frac{c.(m+1)\ln[R(0)]}{2d} \qquad (8.26a)$$

$$\sigma(x) = -\left(\frac{x}{d}\right)^m \cdot \frac{c.(m+1)\ln[R(0)]}{2d} \qquad (8.26b)$$

Here v has been replace by c. Though v is not equal to c but by appropriately choosing m and d the ratio between v and c is taken care of.

Putting in equation (8.21), following transformation

$$s_x D_x b = s_z D_x \qquad (8.27a)$$
$$s_y D_y b = s_x D_y \qquad (8.27b)$$
$$s_z D_z b = s_y D_z \qquad (8.27c)$$

We get following equation

$$\begin{bmatrix} \dfrac{\partial H_z}{\partial y} - \dfrac{\partial H_y}{\partial z} \\[2mm] \dfrac{\partial H_x}{\partial z} - \dfrac{\partial H_z}{\partial x} \\[2mm] \dfrac{\partial H_y}{\partial x} - \dfrac{\partial H_x}{\partial y} \end{bmatrix} = j\omega \begin{bmatrix} s_1 & 0 & 0 \\ 0 & s_z & 0 \\ 0 & 0 & s_x \end{bmatrix} \begin{bmatrix} D_x b \\ D_y b \\ D_z b \end{bmatrix} \qquad (8.28)$$

Discretising equation (8.27) and equation (8.28) we get

$$D_x b \Big|_{i+\frac{1}{2},j,k}^{n+\frac{1}{2}} = A.D_x b \Big|_{i+\frac{1}{2},j,k}^{n+\frac{1}{2}} + B.\left[\frac{H_z \Big|_{i+\frac{1}{2},j+\frac{1}{2},k}^{n} - H_z \Big|_{i+\frac{1}{2},j-\frac{1}{2},k}^{n}}{\Delta y} - \right.$$

$$\left. \frac{H_y \Big|_{i+\frac{1}{2},j,k+\frac{1}{2}}^{n} - H_y \Big|_{i+\frac{1}{2},j,k-\frac{1}{2}}^{n}}{\Delta z} \right] \qquad (8.29a)$$

$$D_x \Big|_{i+\frac{1}{2},j,k}^{n+\frac{1}{2}} = C.D_x \Big|_{i+\frac{1}{2},j,k}^{n-\frac{1}{2}} + \left[D..D_x b \Big|_{i+\frac{1}{2},j,k}^{n+\frac{1}{2}} - E.D_x b \Big|_{i+\frac{1}{2},j,k}^{n-\frac{1}{2}} \right] \qquad (8.29b)$$

$$A = \frac{\dfrac{\kappa_y}{\Delta t} - \dfrac{\sigma_y}{2}}{\dfrac{\kappa_y}{\Delta t} + \dfrac{\sigma_y}{2}} \quad B = \frac{1}{\dfrac{\kappa_y}{\Delta t} + \dfrac{\sigma_y}{2}} \quad C = \frac{\dfrac{\kappa_z}{\Delta t} - \dfrac{\sigma_z}{2}}{\dfrac{\kappa_z}{\Delta t} + \dfrac{\sigma_z}{2}} \quad D = \frac{\dfrac{\kappa_x}{\Delta t} + \dfrac{\sigma_x}{2}}{\dfrac{\kappa_z}{\Delta t} + \dfrac{\sigma_z}{2}} \quad E = \frac{\dfrac{\kappa_x}{\Delta t} - \dfrac{\sigma_x}{2}}{\dfrac{\kappa_z}{\Delta t} + \dfrac{\sigma_z}{2}}$$

As discussed earlier we see that equations are identical to equations 8.21b and 8.21c. Also A, B, C, D and E are same as they were for UPML.

Similar equations can be derived for D_y, D_z, B_x, B_y and B_z. Here first components of B are calculated using the equations similar to equation (8.28) and equation (8.29). Then from B, Magnetic field H is calculated. From this value of H, flux density D is calculated which gives the E. This value of E is used to calculate B. Whole sequence is repeated for required number of time steps.

8.4 Calculation of Field Components in MIPML

In MIPML we calculate field components from flux densities. This is calculated as per following equations.

$$\begin{bmatrix} E_x \\ E_y \\ E_z \end{bmatrix} = \begin{bmatrix} \varepsilon_{xx} & \varepsilon_{xy} & \varepsilon_{xz} \\ \varepsilon_{xy} & \varepsilon_{yy} & \varepsilon_{yz} \\ \varepsilon_{xz} & \varepsilon_{yz} & \varepsilon_{zz} \end{bmatrix}^{-1} \begin{bmatrix} D_x \\ D_y \\ D_z \end{bmatrix}$$

$$\begin{bmatrix} H_x \\ H_y \\ H_z \end{bmatrix} = \begin{bmatrix} \mu_{xx} & \mu_{xy} & \mu_{xz} \\ \mu_{xy} & \mu_{yy} & \mu_{yz} \\ \mu_{xz} & \mu_{yz} & \mu_{zz} \end{bmatrix}^{-1} \begin{bmatrix} B_x \\ B_y \\ B_z \end{bmatrix}$$

$$[\overline{\mu}]^{-1} = \begin{bmatrix} X_{xx} & X_{xy} & X_{xz} \\ X_{xy} & X_{yy} & X_{yz} \\ X_{xz} & X_{yz} & X_{zz} \end{bmatrix}$$

$$[\overline{\varepsilon}]^{-1} = \begin{bmatrix} A_{xx} & A_{xy} & A_{xz} \\ A_{xy} & A_{yy} & A_{yz} \\ A_{xz} & A_{yz} & A_{zz} \end{bmatrix}$$

$$\begin{bmatrix} E_x \\ E_y \\ E_z \end{bmatrix} = \begin{bmatrix} A_{xx} & A_{xy} & A_{xz} \\ A_{xy} & A_{yy} & A_{yz} \\ A_{xz} & A_{yz} & A_{zz} \end{bmatrix} \begin{bmatrix} D_x \\ D_y \\ D_z \end{bmatrix}$$

$$E_x\Big|_{i+\frac{1}{2},j,k}^{n} = A_{xx} D_x\Big|_{i+\frac{1}{2},j,k}^{n} + A_{xy} D_y\Big|_{i+\frac{1}{2},j,k}^{n} + A_{xz} D_z\Big|_{i+\frac{1}{2},j,k}^{n} \qquad (8.30)$$

8.5 Extension to Arbitrary Anisotropic Dielectric Cases

The basic 3-D FDTD cell for MIPML is shown in Figure (8.1). It is inherent in FDTD that D_y and D_z do not exist at the same point where D_x exists. Therefore in equation (8.30) D_y and D_z are to be calculated at point (i+1/2,j, k). This is done by averaging D_y and D_z around the point (i+1/2,j, k). Here averaging does not cause much of error as it is also second order accurate [20]. The averaging referred here is done in space on D and equation (8.30) can be written as following

$$E_x^n\left(i+\frac{1}{2},j,k\right) = A_{xx}D_x^n\left(i+\frac{1}{2},j,k\right) + \frac{A_{xy}}{4}\left(D_y^n\left(i,j-\frac{1}{2},k\right)+D_y^n\left(i,j+\frac{1}{2},k\right)+\right.$$

$$\left.D_y^n\left(i+1,j-\frac{1}{2},k\right)+D_y^n\left(i+1,j+\frac{1}{2},k\right)\right)+\frac{A_{xz}}{4}\left(D_z^n\left(i,j,k-\frac{1}{2}\right)+D_z^n\left(i,j,k+\frac{1}{2}\right)\right.$$

$$\left.D_z^n\left(i+1,j,k-\frac{1}{2}\right)+D_z^n\left(i+1,j,k+\frac{1}{2}\right)\right) \qquad (8.31)$$

By inspection equations can be written for remaining 5 field components.
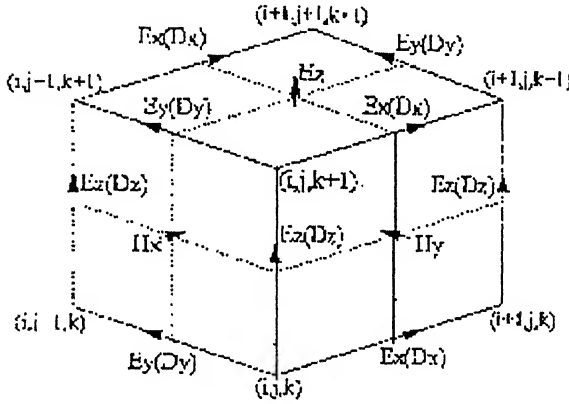
Figure 8.1 Basic MIPML CELL

8.6 Treatment of Perfect Electric Conductors

On the surface of PECs, the tangential electric field, E_t, must be zero, and the implementation of such a condition is straightforward in the FDTD updating formulation. However, from equation (8.21a) one can easily see that in the MIPML algorithm the PEC conditions $E_t=0$ cannot be kept because E is updated from D. Therefore in order to make sure that the PEC condition is correctly imposed for E_t, the values of the tangential electric displacement D_t on the surface of the PEC have to be calculated or justified. In following discussion, Different calculation procedures for D_t are adapted for the cases, first, when PEC is inside the mesh domain and, secondly, when it is at the boundary of the domain and exposed to incident waves coming directly on to it with no PML present. Both of these cases are present in microstrip problems. Here it is to be noted when waves come to PEC after passing through PML then D can be taken, as zero as it has been

attenuated to a very small value and such an assumption does not introduce any significant error.

8.6.1 If PEC is Located Inside The Mesh Domain

If such a PEC is located inside the mesh domain, say at $k = k_o$, then Dx and Dy can be calculated by imposing following conditions in equation (8.30) and similar equations.

$$E_x^n = 0, \quad E_y^n = 0 \tag{8.32}$$

$$D_x^n\left(i+\frac{1}{2},j,k_o\right) = -\frac{A_{xy}}{4A_{xx}}\left(D_y^n\left(i,j-\frac{1}{2},k_o\right)+D_y^n\left(i,j+\frac{1}{2},k_o\right)+\right.$$

$$\left. D_y^n\left(i+1,j-\frac{1}{2},k_o\right)+D_y^n\left(i+1,j+\frac{1}{2},k_o\right)\right)-\frac{A_{xz}}{4A_{xx}}\left(D_z^n\left(i,j,k_o-\frac{1}{2}\right)\right.$$

$$\left.+D_z^n\left(i,j,k_o+\frac{1}{2}\right)+D_z^n\left(i+1,j,k_o-\frac{1}{2}\right)+D_z^n\left(i+1,j,k_o+\frac{1}{2}\right)\right) \tag{8.33}$$

Similar equation can be written for D_y.

8.6.2 PEC at Domain Truncation

At the domain truncation ($k = 0$), equation (8.33) can not be used as many of the points lie outside the domain. Using equations given below, we can first calculate D_x, D_y and D_z flux at $k = 0$ and put in equation (8.33). Though above equation requires only D_y and D_z, D_x is required in the corresponding equation for D_y. Equations for D_x, D_y and D_z fields on $k=0$ plane are

$$D_x^n\left(i+\frac{1}{2},j,0\right) = 2D_x^n\left(i+\frac{1}{2},j,1\right)-D_x^n\left(i+\frac{1}{2},j,2\right) \tag{8.34a}$$

$$D_y^n\left(i,j+\frac{1}{2},0\right) = 2D_y^n\left(i,j+\frac{1}{2},1\right)-D_y^n\left(i,j+\frac{1}{2},2\right) \tag{8.34b}$$

$$D_z^n(i,j,0) = \frac{3}{2}D_z^n\left(i,j,\frac{1}{2}\right)-\frac{1}{2}D_z^n\left(i,j,\frac{3}{2}\right) \tag{8.34c}$$

Put above equations in equation (8.33) to get following equation whose each point is known to us

$$D_x^n(i+0.5, j, 0) = -\frac{A_{xy}}{4A_{xx}} * (2D_y^n(i, j-0.5, 1) - D_y^n(i, j-0.5, 2)$$

$$+ 2D_y^n(i, j+0.5, 1) - D_y^n(i, j+0.5, 2)$$

$$+ 2D_y^n(i+1, j-0.5, 1) - D_y^n(i+1, j-0.5, 2)$$

$$+ 2D_y^n(i+1, j+0.5, 2) - D_y^n(i+1, j+0.5, 2))$$

$$- \frac{A_{xy}}{4A_{xx}} * (3D_z^n(i, j, 0.5) - D_z^n(i, j, 1.5)$$

$$+ 3D_z^n(i+1, j, 0.5) - D_z^n(i+1, j, 1.5)) \qquad (8.35)$$

Similar equation can be written for D_y. While writing code for any of these PECs in any plane it is always suggested to make space diagram to avoid any mistake. One sample diagram is given below. Similar diagrams can be constructed for other components in various PECs located in various domain-truncating planes.
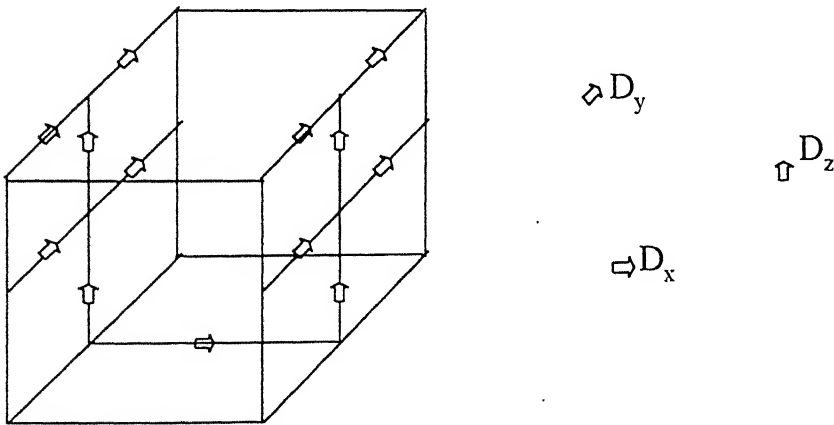
Figure8.2 components required for calculating Dx on PEC z = 0

Though condition of tangential electric components equal to zero at PEC is implicitly imposed through above formulation but it is always recommended that it should be applied on PEC wherever required.

8.7 Numerical Experiment

To validate numerically theory of UPML for arbitrary anisotropic medium we have done two experiments.

For first experiment we will compare our data with Zhao[23]. For second experiment Mr. Zhao, Nokia Research center, Helsinki, Finland, provided us data from his paper "An Efficient FDTD Algorithm for the analysis of Microstrip Patch antennas printed on a general anisotropic substrate", which is written using split formulation.

Both reference results have been obtained from split formulations. Our results have been obtained with unsplit formulation. In first experiment we have taken a domain uniformly filled with arbitrary anisotropic material with following specifications.

Sr. No	Parameter	Value
1.	Number of cells (including PML)in	
1.1	X-direction	40
1.2	Y-direction	40
1.3	Z-direction	41
2.	Cell in PML in each direction	8
3.	Number of time steps	51
4.	Step size	
4.1	X-direction	1.3 CMS
4.2	Y-direction	1.3 CMS
4.3	Z-direction	1.3 CMS
5.	Time step	25 e-12 sec
6.	parallel Axis permittivity	3
7.	Perpendicular axis permittivity	2
8.	parallel Axis permeability	3
9.	Perpendicular axis permeability	2
10.	Optical axis angle with crystal X-axis	30
11.	Reflection factor	0.0001
12.	Conductivity profile index	3

13.	Number of cells in reference domain, in	
13.1	X-direction	110
13.2	Y-direction	110
13.3	Z-direction	111
14.	Type of excitation(Dz)	compact pulse
15.	Point of excitation in both of the domains	center

In figure (8.3) reflection factor has been plotted. Figure (8.4) shows the results of [23]. Curve 2 is to be compared with our results. We find our results are excellent and comparable to those with split formulation. Here we would like to mention that due to limitations of computer memory our computing domain data is different from what has been taken in [23].

Reflection factor has been plotted on the interface (11:31,11,20) with MIPML, parallel to X-axis. Our MIPML performs better than –75 dB.

In second experiment we work out characteristics of a Patch antenna printed on a anisotropic dielectric substrate with material parameter as given below in table. This problem has been taken for two reasons, first to demonstrate that our simulator is capable of taking up any planar geometry and secondly results for this geometry are available to us.

Figure (8.5) shows the patch antenna geometry. Using the technique discussed above, this line–fed microstrip patch antenna printed on a general uniaxial anisotropic dielectric substrate is studied. The optical axis lies in the xz-plane. Following table gives description of the problem.

r. No	Parameter	Value
	Number of cells (including PML)in	
.1	X-direction	58
.2	Y-direction	80
.3	Z-direction	22
..	Number of cells in PML in	
..1	X-direction[PML left of the interface PML right of the interface]	8 8
..2	Y-direction[PML left of the interface PML right of the interface]	8 8
..3	Z-direction[PML left of the interface PML right of the interface]	0 8
..	Number of time steps	8000
4.	Step size	
4.1	X-direction	3.891e-004
4.2	Y-direction	0.4e-004
4.3	Z-direction	0.1985e-004
5.	Time step	0.4e-12
6.	parallel Axis permittivity	2.31
7.	Perpendicular axis permittivity	2.19
8.	parallel Axis permeability	1
9.	Perpendicular axis permeability	1
10.	Optical axis angle with crystal X-axis	$45°$
11.	Reflection factor	0.001%
12.	Conductivity profile index	4
13.	Excitation at two cells from interface with MIPML	Gaussian pulse
14.	Half width(T)	15 picosecs.
15.	Time delay	3.1 T
16.	Distance of reference port from patch edge	10 cells

The rectangular patch is $32\Delta x \times 40\Delta y$; the microstrip feeding port is $6 \Delta x \times 27 \Delta y$ and substrate thickness is $4 \Delta z$.

igure (8.6) shows incident and reflected waveforms with respect to time. Incident ~aveform is achieved by assuming no discontinuity i.e. no patch and reflected wave form ; achieved when patch antenna is present. Figure (8.7) shows the results supplied by Mr. .hao. Figure (8.8) shows the S_{11} of the patch antenna and figure (8.9) shows the results f Mr. Zhao. It seen that there is hardly any difference. This proves that simulator eveloped by us works correctly for arbitrary anisotropic media.

.8 Conclusions

\ code 'MIPML' has been developed for analyzing microwave circuits by extending nsplit formulations to arbitrary anisotropic materials. This simulator for designing and eveloping microwave circuits uses material absorbing boundary condition in which onductivities are independent of material characteristics. We have clearly demonstrated hat all the parameters used in UPML formulation equations are indeed material ndependent and UPML for isotropic materials can easily be used for all kind of naterials. Only parameters, s_i, need to be defined properly. Further due to this special eature of MIPML, it can also be used to absorb waves propagating in material consisting »f loss, dispersion, nonlinearly with slight modifications. We have also analyzed a planar liscontinuity of patch antenna type and found our results matching with those of other esearchers. This proves that software MIPML is correctly designed for analyzing any :ind of geometry on arbitrary anisotropic substrates and It can be used for the study of nicrostrip dispersion characteristics on anisotropic substrates with high accuracy.

Ref.Fac. along MIPML Interface in anisotropic media

.00e+1

.00e+1

.00e+1

.00e+2

.10e+2

.20e+2

.30e+2

10   15   20   25   30   35

X axis
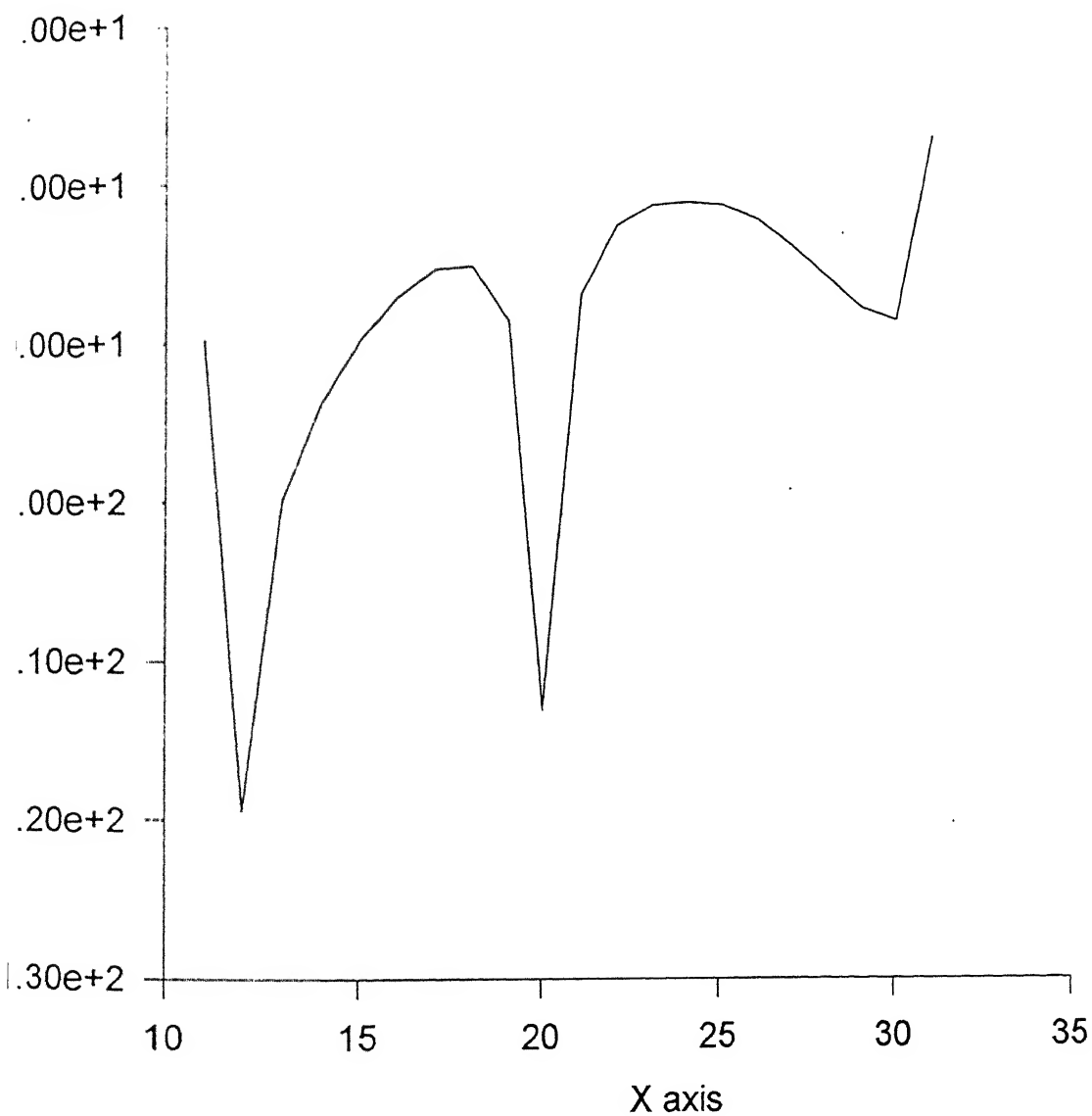
Figure 8.3 Reflection factor by Simulator MIPML
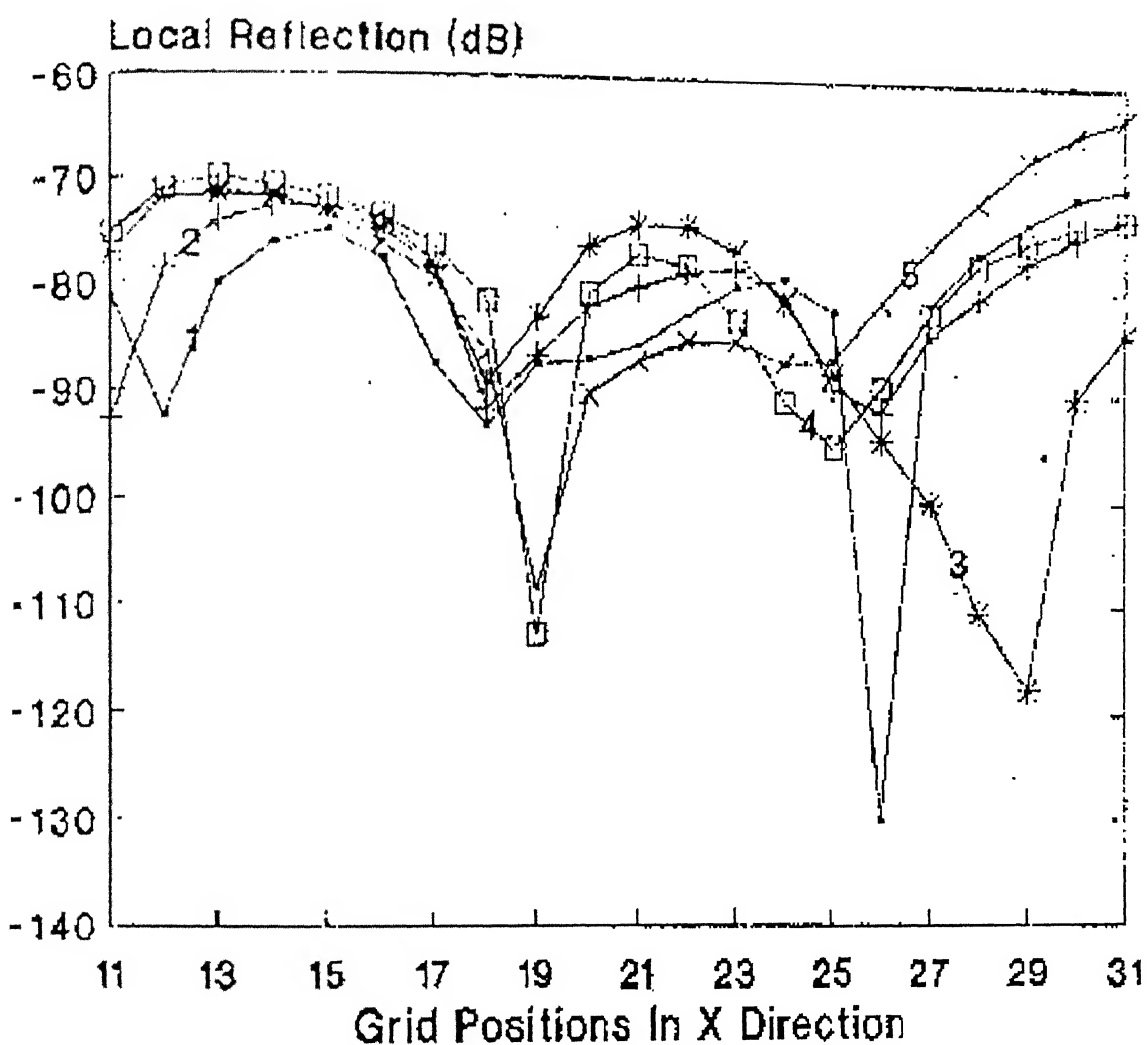
Normalized local reflections for the E_{ζ}-field component of the waves
ng the line (X, 11, 20.5), where curves 1–5 are for $\theta = 0, \pi/6, \pi/4, \pi/3$.
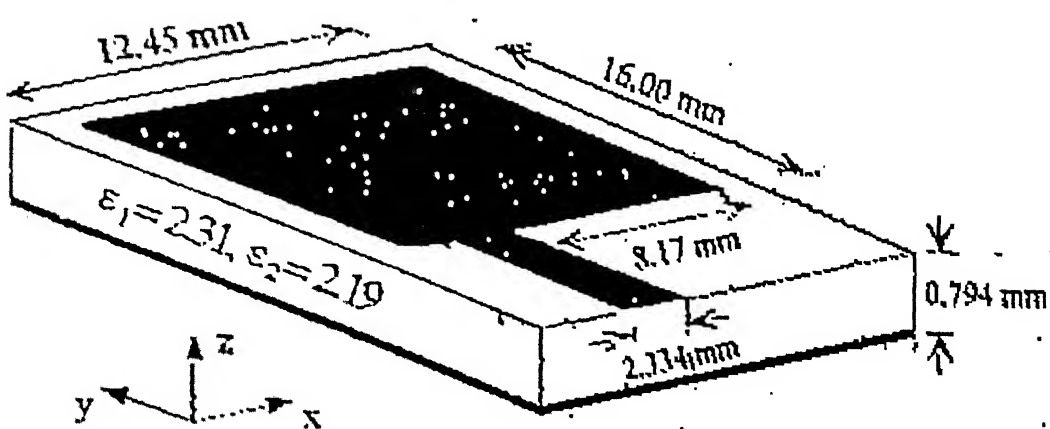2, respectively.

Figure 8.4

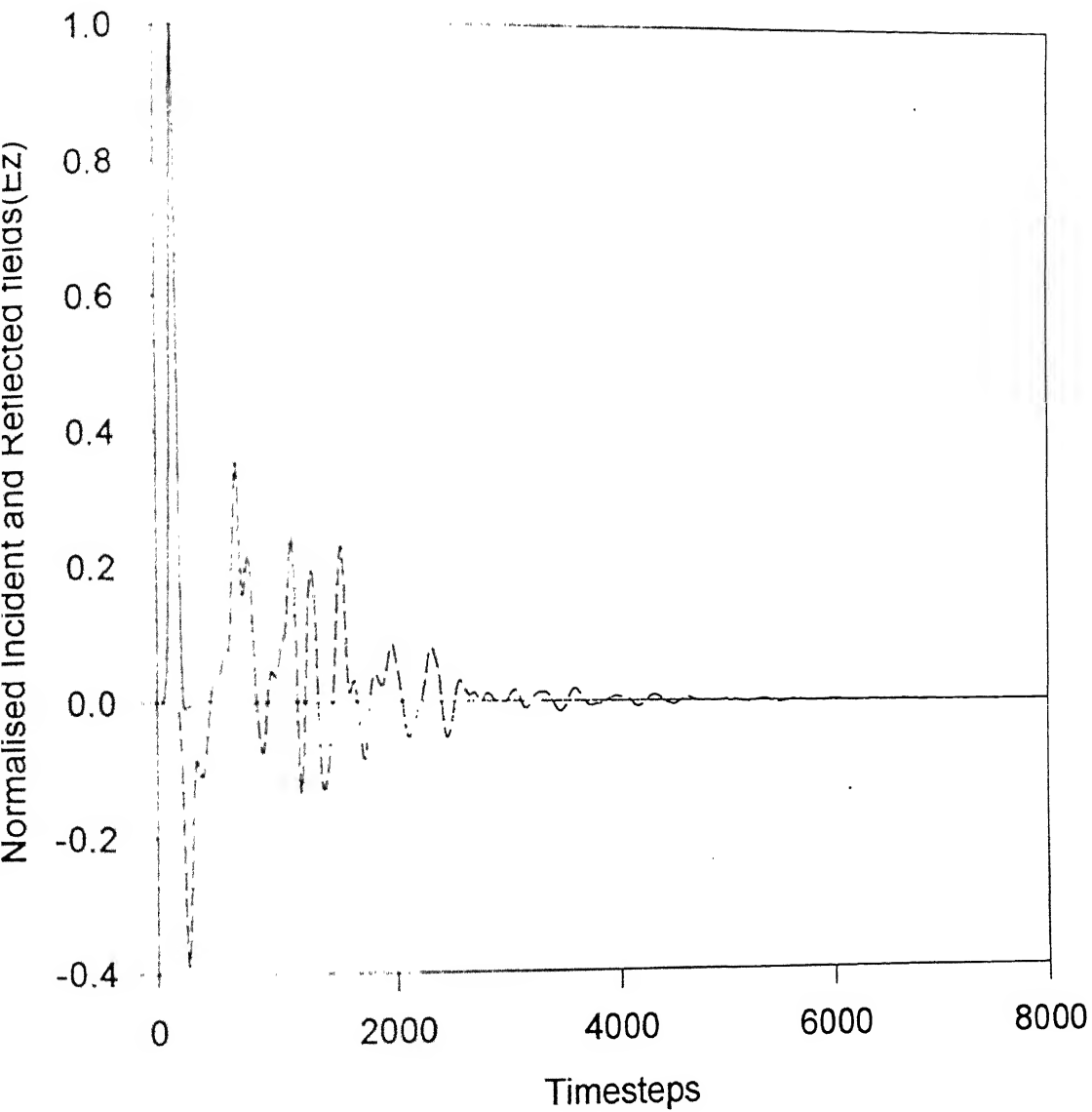Figure 8 5 Patch Antenna on an arbitrary anisotropic substrate

Wave Forms

Figure 8 6 Results obtained by Simulator MIPML for propagation of the pulses

e incident pulse is the reference pulse through the microstrip. Reflected pulse is the

eform of the reflected field from patch antenna.
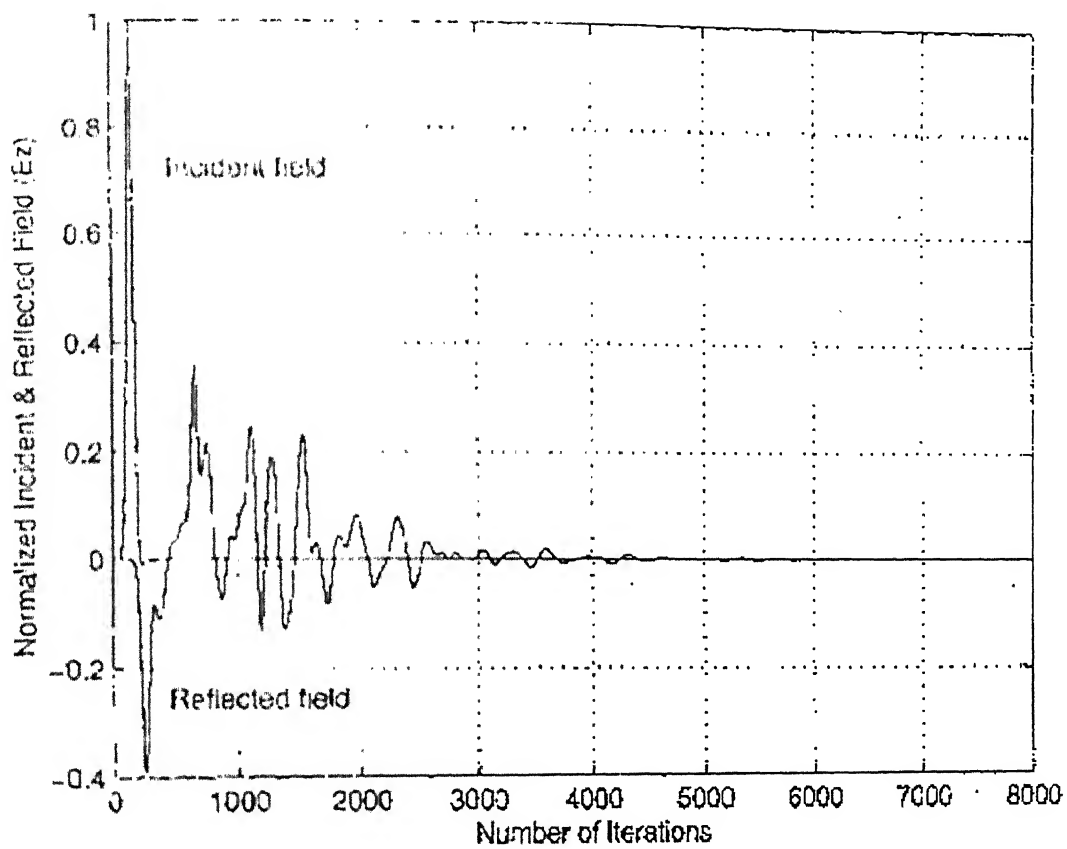
Figure 8 7 Zhao's result [43] for incident and reflected pulses

Chapter 9

Microstrip Transmission Lines on Anisotropic Substrates: MIPML Analysis

Introduction

Demand for high-speed pulse circuits has increased need for highly accurate full wave analysis of microstrip transmission lines. Till 1978 analysis were mostly TEM in nature for anisotropic substrates [34, 35]. Disadvantage of TEM analysis is that it does not take dispersion into account. These effects have to be included empirically. Later Full wave analysis method based upon waveguide model appeared [6]. Disadvantage of this method was that it did not take into account radiation effect and the surface wave generation. Also mode-matching step involved error because modes generated in model are not the same those generated in microstrip and microstrip discontinuities. For Anisotropic substrates, in 1985, approach based on TLM method appeared [36]. Also Koike [37] using Bergeron's method presented his analysis. TLM is not as efficient as FDTD method is and with the invention of PML, FDTD results are far more accurate than those presented in [35] and [36]. Disadvantages of These methods have been discussed in Chapter one.

Salient features of our EM simulator are that it is using MIPML, so capable of analyzing any material [chapter 8], Virtually reflection free domain truncation [chapter 8] and this reflection free boundary has certain advantages, which have been highlighted in next section and any kind of planar circuit can be analyzed without any modification to basic algorithm. For a new geometry, its dimensions are to be specified in subroutine DATAIN, implement boundary conditions for D in Subroutine CONDBND, implement boundary condition for E in Subroutine EFIELDS. The same routine also has to be modified for specifying dielectric constant in computing domain so fields may be calculated from flux. In subroutine EXCITATION we have to specify distribution of stimulus for the given geometry. We have already included a wide range of sources so any kind of stimulus just needs to be specified by entering choice.

For calculating dispersion characteristics of relative effective dielectric constant (REDC) of microstrip Zhang et al. [42] have used multiple cell method (MCM). We also use the same and also proposed a new method of single cell (SCM), which is based upon transmission line analogy and contrary to the method proposed by liou [12], our method does not require calculation of flux and charge.

9.1 Methods of Calculating Z_o and Effective Dielectric Constant

Koike [37] used following definition for characteristic impedance.

$$Z_o = 2P_z / I_o^2 \qquad (9.1)$$

For evaluating REDC he used ratio of free space wavelength to guide wavelength. This was possible because his analysis was at single frequency. Though power definition can be used for signals containing wide frequency range. The only problem is that E_x, E_y, H_x and H_y over a complete xy plane are to be stored and poynting vector is to be calculated by integrating sum of E_x*H_y and $E_y*(-H_x)$ over xy plane and averaging over one period is to be done.

Definition used by Zhang [2] for characteristic impedance is

$$Z_o = \frac{V(\omega)}{I(\omega)} \qquad (9.2)$$

And for REDC, they took the Fourier transforms of E_x (t) at two different locations (just underneath the center of strip), with a separation of L, along the propagation direction:

$$E_x(\omega, z = 0) = \int_{-\infty}^{\infty} E_x(t, z = 0) e^{-j\omega t} dt \qquad (9.3a)$$

$$E_x(\omega, z = L) = \int_{-\infty}^{\infty} E_x(t, z = L) e^{-j\omega t} dt \qquad (9.3b)$$

Taking ratio of (9.3a) and (9.3b), we get transfer function of this section of transmission line, which is

$$e^{-\gamma(\omega)l} = \frac{E_x(\omega, z = L)}{E_x(\omega, z = 0)} \qquad (9.4a)$$

$$\gamma(\omega) = \alpha(\omega) + j\beta(\omega) \qquad (9.4b)$$

$$\beta(\omega) = \omega\sqrt{\mu_0 \varepsilon_0 \varepsilon_{reff}(\omega)} \qquad (9.4c)$$

$$\varepsilon_{reff}(\omega) = \frac{\beta^2(\omega)}{\omega^2 \mu_0 \varepsilon_0} \qquad (9.4d)$$

Results of both approaches in FDTD method are almost identical but second approach is simpler. It is because evaluating V and I is much simpler. This method is multiple z method as propagation of the wave is to be monitored at many locations along direction of propagation (z-direction). Advantage of this method is that results are accurate over a large frequency band, as it does not rely upon TEM approximation. Therefore, for frequencies where deviation from equivalent circuit model, from transmission line analogy, takes place results provided by the method used by Zhang et al. [42] are still acceptable.

9.2   Shortcomings of Above Methods and Single Cell Method

Biggest disadvantage in FDTD analysis is that the frequency dependence (dispersion relation) of the microwave parameters of the wave characteristic impedance and the relative effective dielectric constant (REDC) show oscillatory behavior. This behavior may be attributed to following reasons:

(A) Imperfect ABCs that generate artificial reflection at computational boundary

(B) The excitation source can contain mixed modes of propagation and evanescent waves

(C) The continuous radiation loss spectrum that was taken into account in FDTD, but failed to be implemented properly in the multiple–z method for phase velocity determination

(D) Possible numerical errors due to the numerical approximation of the Fourier integration.

The first reason is supposed to be the biggest contributor to the oscillatory behavior. By using MIPML formulation we have reduced it. Our results for multiple z method show no oscillatory behavior. A slight droop at very low frequency is observed in REDC. We used a modified single cell model to correct this small droop to get perfect characteristics. The

other biggest nuisance in multiple z method is due to the multiple of an integer with 2π in phase difference, when trying to determine a unique propagation constant. Liou et al. [12] have tried to overcome above problem by introducing a new method.

The method used by Liou [12] requires charge Q and magnetic flux for evaluation of L and C per unit length of transmission line. He used following formulation

$$L\delta z = \frac{\psi}{I} \qquad (9.5a)$$

$$C'\delta z = \frac{Q}{V} \qquad (9.5b)$$

$$LC' = \frac{\psi}{I}\frac{Q}{V}\cdot\frac{1}{\delta z^2} = \frac{1}{v_p^2} \qquad (9.5c)$$

$$\varepsilon_{eff} = c^2 LC \qquad (9.5d)$$

$$Z_o = \left(\frac{L}{C'}\right)^{\frac{1}{2}} \qquad (9.5e)$$

We use different method of evaluating L and C. we have straightaway discretised transmission line equations.

$$\frac{dV}{dz} = -j\omega LI \qquad (9.6a)$$

$$\frac{dI}{dz} = -j\omega CV \qquad (9.6b)$$

$$-\frac{V(z) - V(z + \delta z)}{j\omega\,\delta z\,I(z)} = L \qquad (9.6c)$$

$$-\frac{-I(z) + I(z + \delta z)}{j\omega\,\delta z\,V(z)} = C' \qquad (9.6d)$$

Once L and C are known we use equations (9.5d) and (9.5e) for REDC and Z_o. We have observed distinctive improvement in REDC results. Z_o results are same as those worked out with V/I method. It shows accuracy of this method . Here caution is to be exercised that for frequencies where equivalent circuit approach holds, results obtained by a single cell method are accurate but for higher frequencies, where assumptions of equivalent circuit approach deviate multiple z method gives accurate results. For this reason we have preffered to give results by both method.

9.3 Results

We have enclosed results from Reinmut K. Hoffman for Crystal main axis perpendicular to the substrate surface. These results have been calculated by the methods of lines with equivalent transformation in figure (9.2). In the same figure we have compared our results. We have enclosed our results for various w/h ratios. It is observed that results for characteristic impedance are in excellent agreement with published results. There is slight discrepancy in REDC but this is owed to the fact that our results are for full wave analysis and those given by Hoffman are calculated with TEM approximation. To rule out possibility of spurious modes affecting our results, which have been calculated by sampling fields at approximately 1.5 λ, we compare them with results calculated at 4 λ.

Sr. No.	Method	Zo	REDC
1.	Hoffman's results	46.5000	7.3750
2.	Results sampled at 1.5 λ		
2.1	MCM method	43.0943	7.7240
2.2	SCM method	43.4312	7.6734
3.	Results sampled at 4 λ		
3.1	MCM method	43.1011	7.5487
3.2	SCM method	43.1028	7.5451

In above table we see that results at 4 λ by MCM and SCM are exactly same. The results are not very different from the results at 1.5 λ. So results at 1.5 λ are well within reasonable accuracy. This reduction of computing domain enables MIPML to be run on a Personal computer and still get accurate results. We have also worked out effect of angle of optical axis with respect to X-axis in figure (9.3). Results of Koike [37] have also been enclosed figure (9.4). Our results show the same pattern of variation. Details of structure are shown in figure (9.1). SIMULATOR MIPML produces results, which are most accurate of all. This is due to most accurate boundary conditions and because of the use of single cell method. These reasons have already been mentioned above in details. We

have enclosed results at 1.5 λ though the results at 4 λ or farther would have been more accurate. The reason is that for very odd w/h ratios the size of computational domain would have become so large that it would have been impossible for us to calculate results on the computer available to us. To maintain uniformity in the results for all w/h ratios we have calculated them at 1.5 λ. Even there also our results are very accurate. For any specific applications results can be calculated with larger domain.

It is demonstrated in the results for w/h ratio of 0.8 (figure 9.6) that nuisance is faced in MCM because of multiplication of an integer with 2π in the phase difference when trying to determine a unique phase difference. So selection of sampling points should be carefully done. In SCM, We demonstrate in the results mentioned above that there is no such problem. This gives capability to calculate results upto a larger bandwidth with the same cell size and time step. This is quite a significant improvement. The same is again demonstrated in figure (9.7) that if sampling points are not properly selected in MCM than results could be disastrous. But SCM does not pose this problem. From figures (9.11) and (9.12) capability of SCM to reduce oscillatory behavior is very clear. These properties of SCM make it quite attractive.

9.4 Conclusions

Though we have tried to compute results for a wide range of w/h ratio which has never been attempted earlier. The reason is for very odd ratio requirement of a large computing domain makes it very difficult to do it with a reasonable amount of computer memory. Also increased computing time compounds the problem. These difficulties come into picture because of adequate sampling of microstrip geometry dimensions make it necessary to keep size of space sample very small. Also sampling needs to be done atleast one wavelength away for spurious modes to die down. These are generated because it is not always possible to give excitation in pure dominant mode and because of inhomogeneous medium, evanescent waves are generated. If sampling points are kept at one wavelength away with very small space step due to geometrical constraints, then we have a large computing domain. Also thickness of substrate or width of strip should be a fraction of wavelength and this requirement also leads to above mentioned problem of taking very small steps which may not be required for the given frequency range and this means a burden on computing resources. In fact it required extensive experimentation for

a very long period of time by us to determine optimum sizes of computing domain for various w/h ratios for the given computer memory.
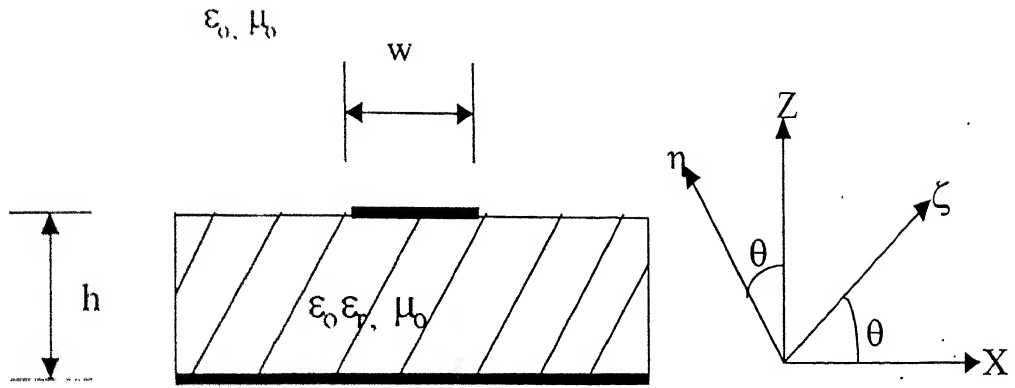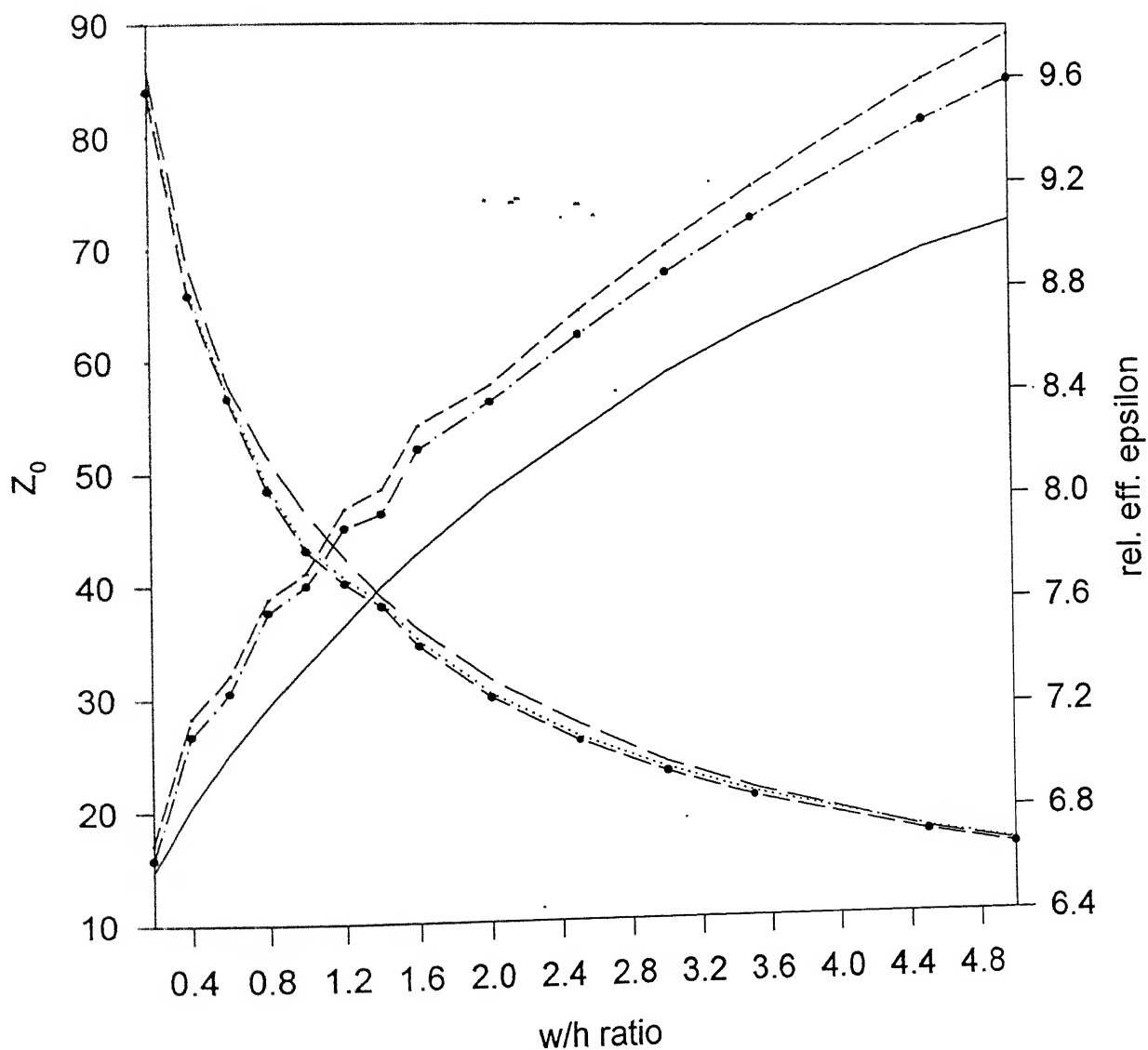

Figure 9.1 Cross section of microstrip line along with orientation of crystal axes ζ, η with respect to XZ axes.

- — Hoffman's results for dielectric constant
- — - Hoffman's results for Z_o
- · Our results for Z_o using SCM
- — → Our results for Z_o with MCM
- — - - Our rsults with MCM for REDC
- - — • Our results for REDC with SCM

Figure 9.2
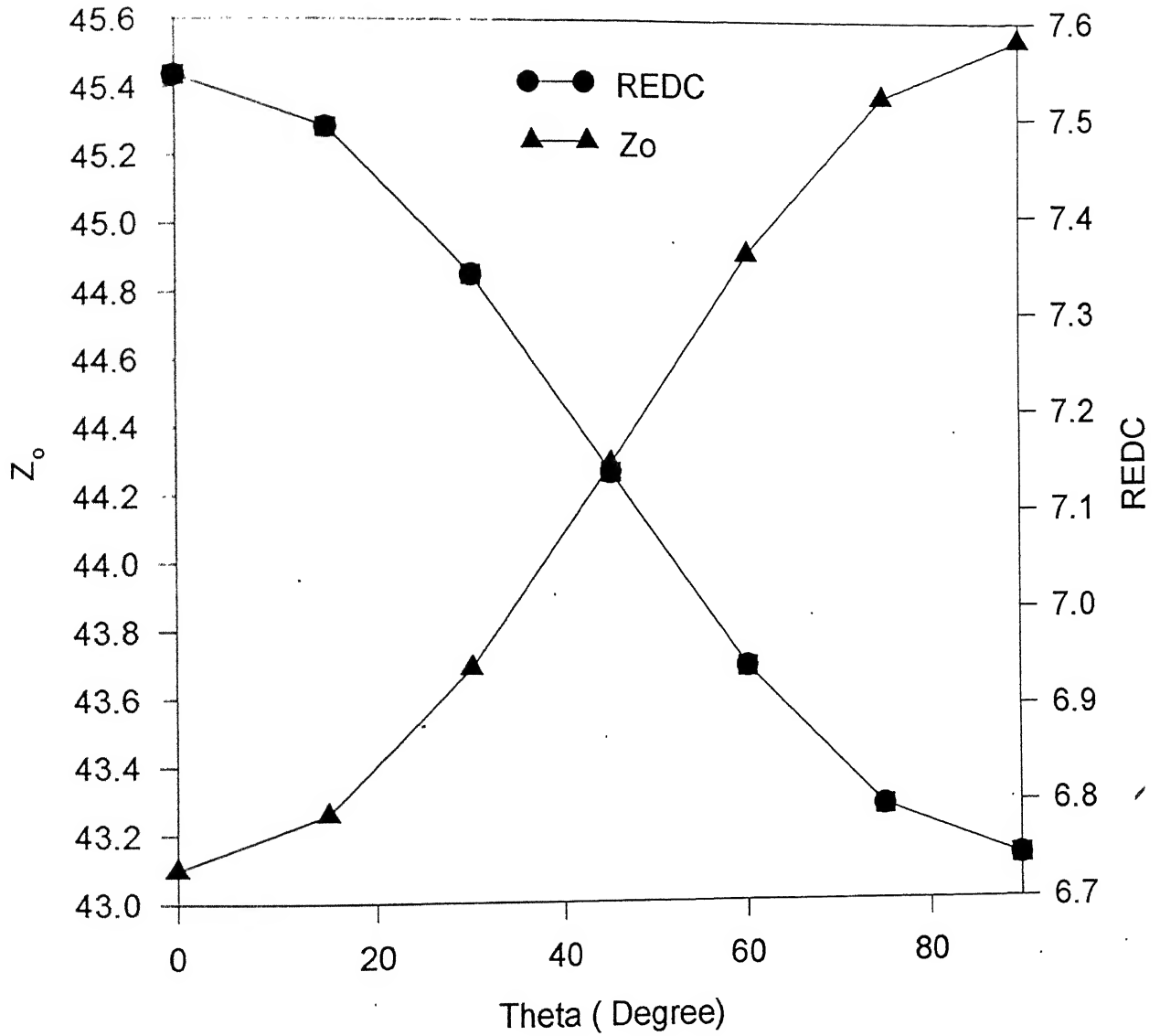
Figure 9.3 Effect of Theta for W/H ratio = 1
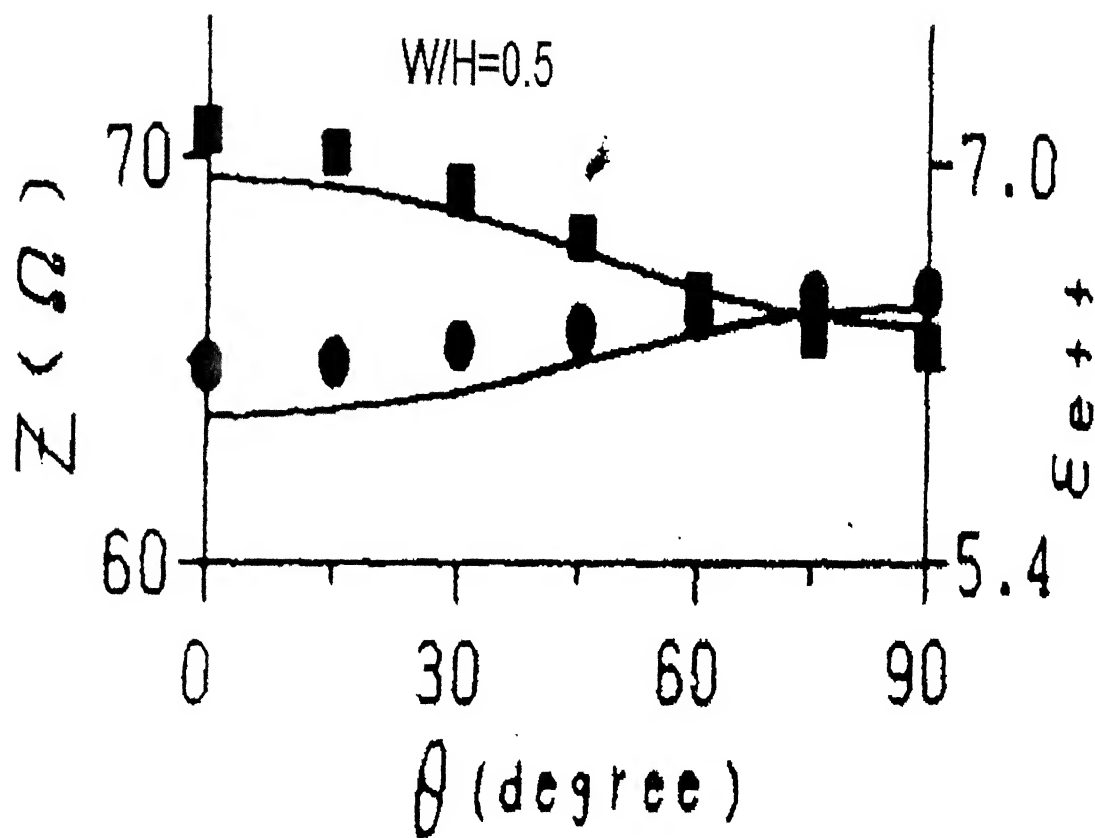
Fig. 9.4 ch'acteristic impedance and effective dielectric constant of microstrip line as a function of tilt angle.

w/h = 0.2 theta = 0°
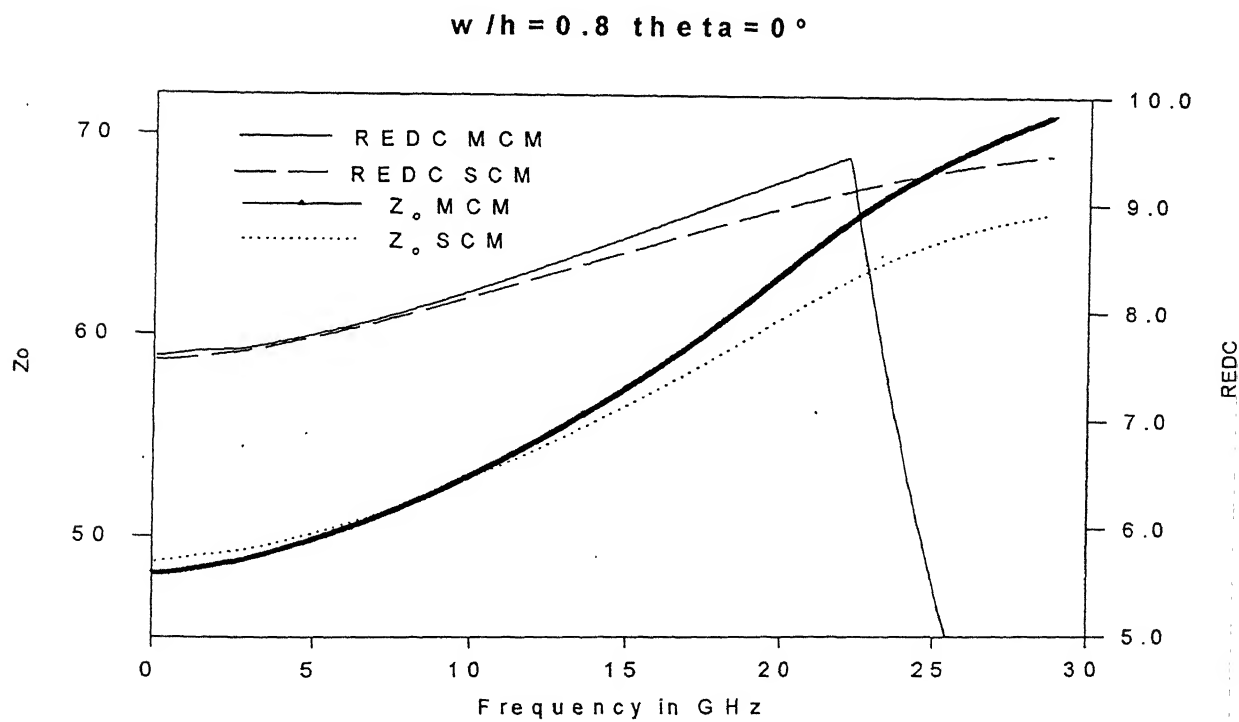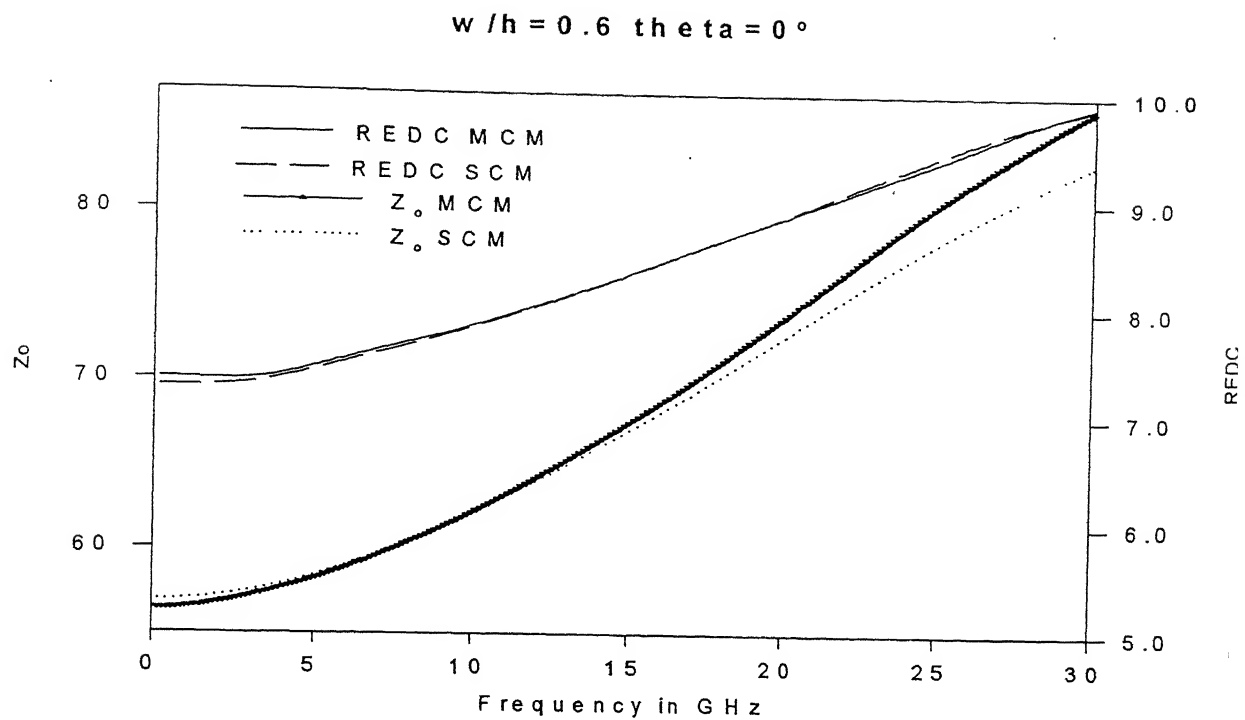
w/h = 0.4 theta = 0°

Figure 9.5

w / h = 0 . 6   t h e t a = 0 °

w / h = 0 . 8   t h e t a = 0 °

Figure 9.6

w /h = 1.0 y = 90 y1 = 109 theta = 0°
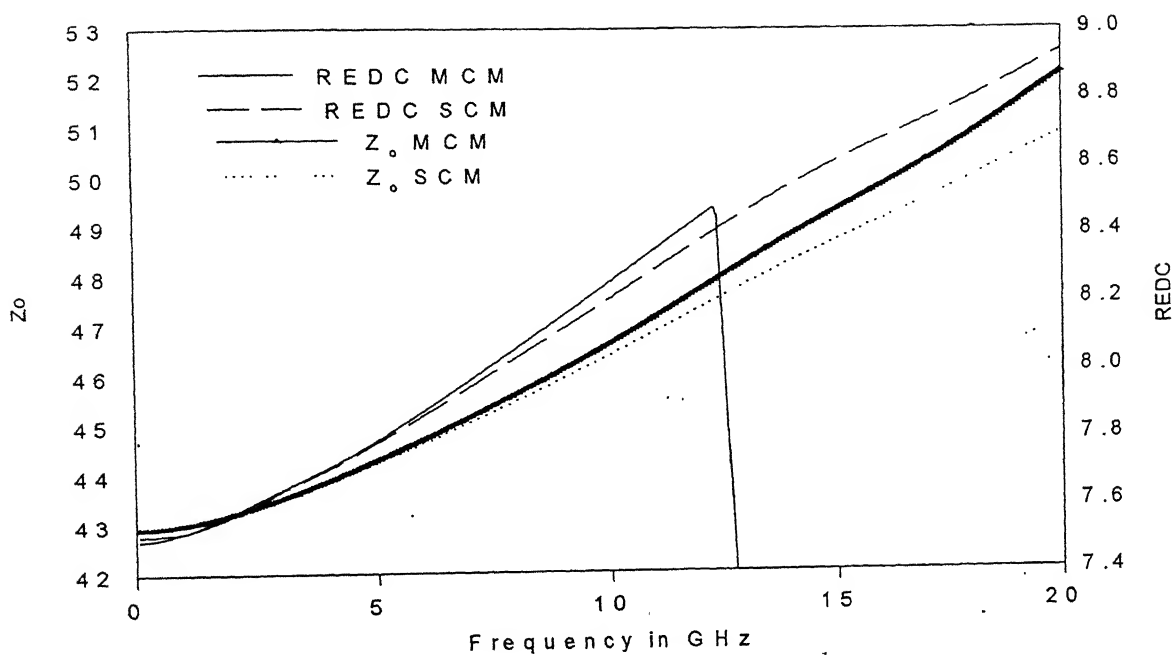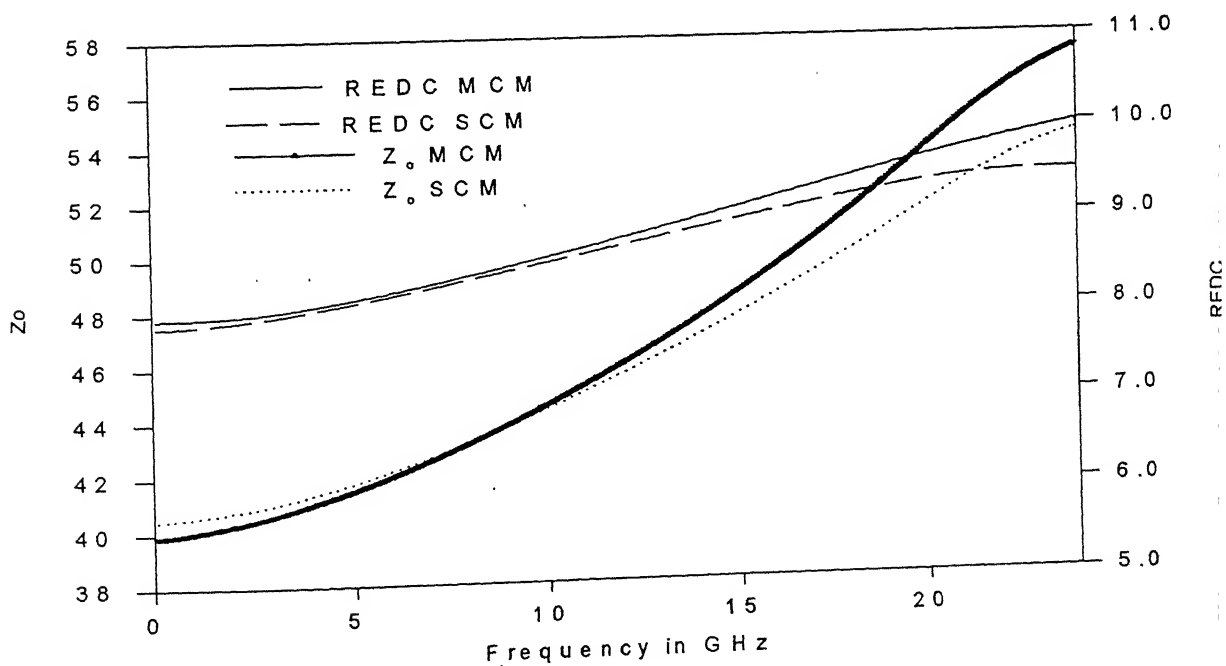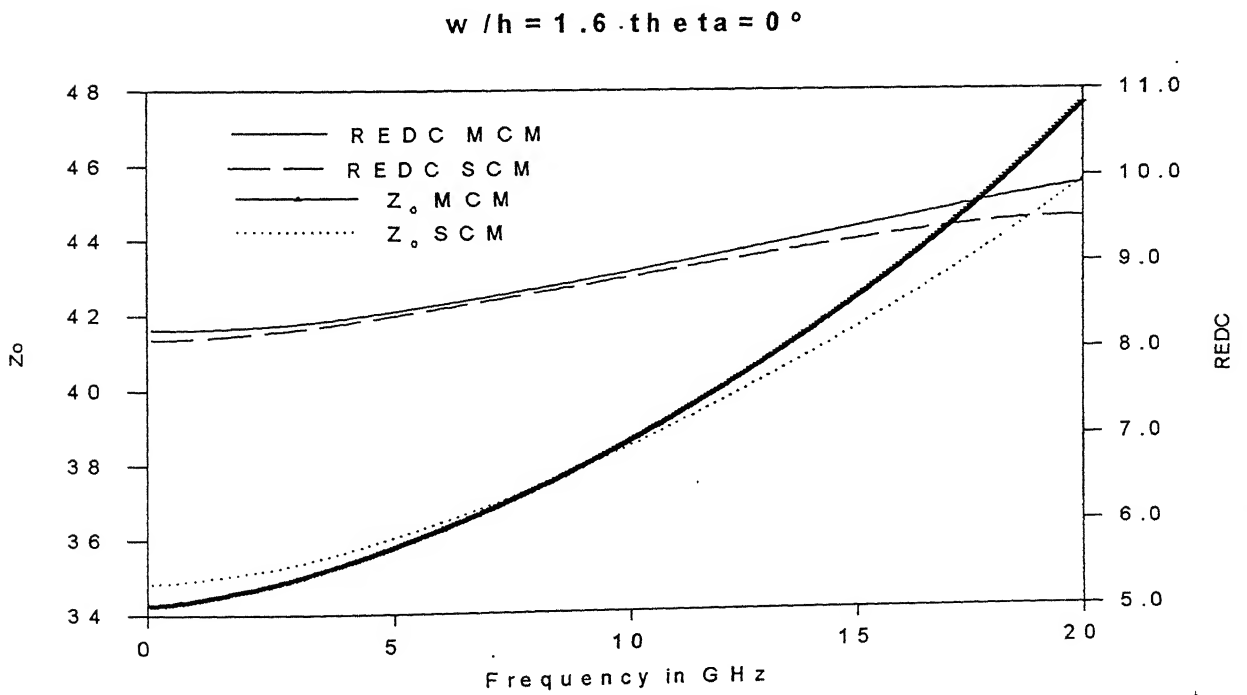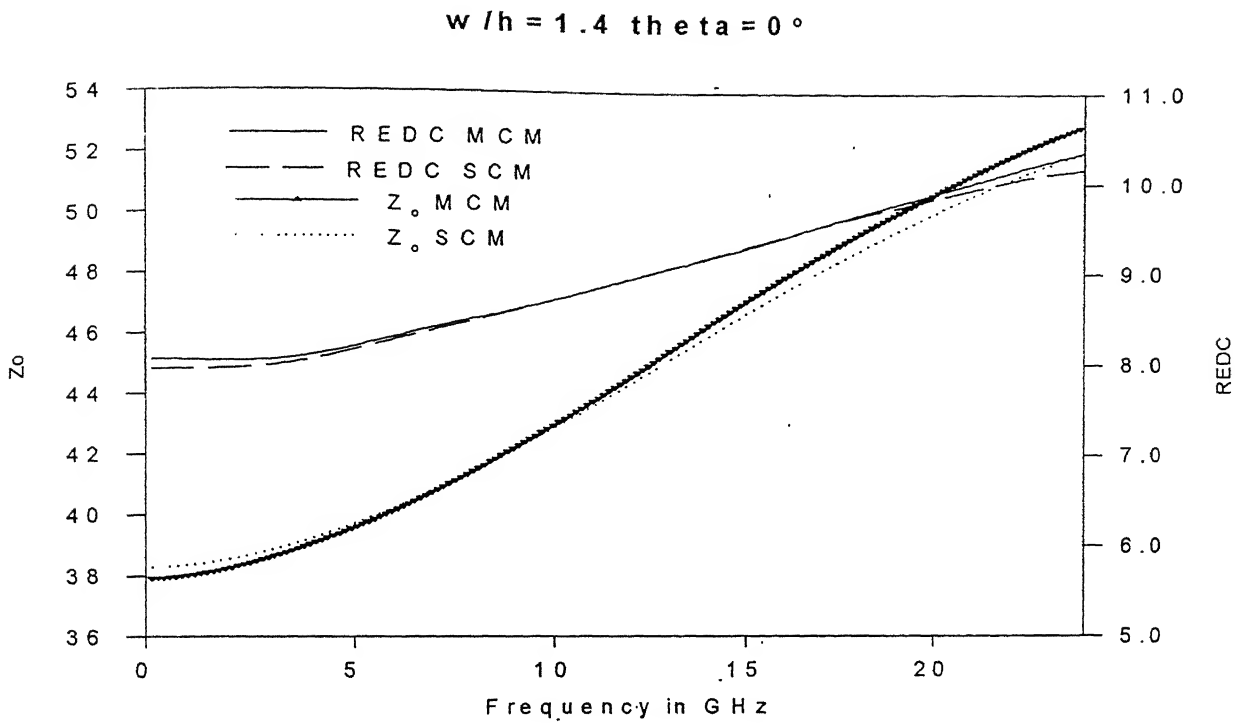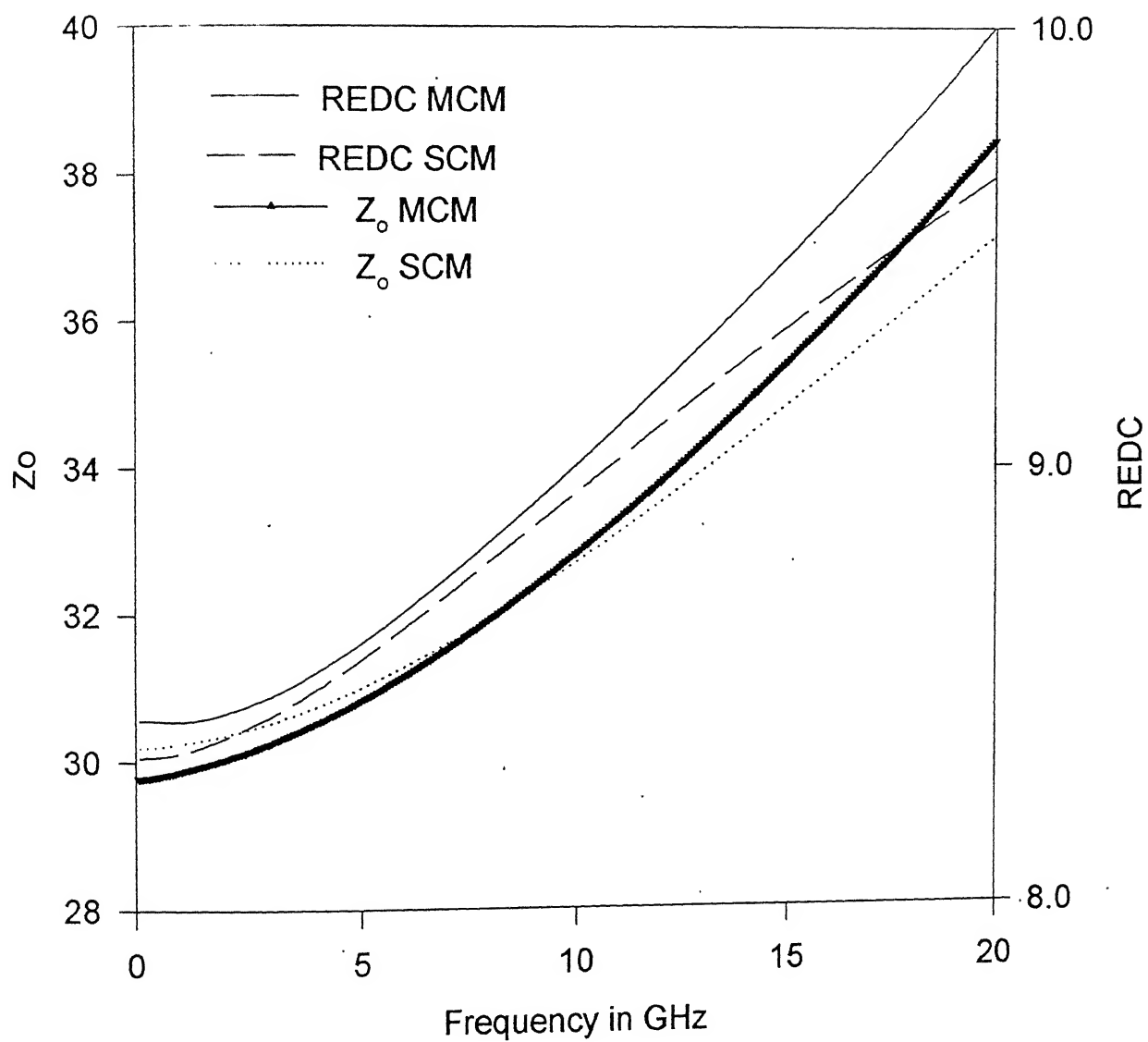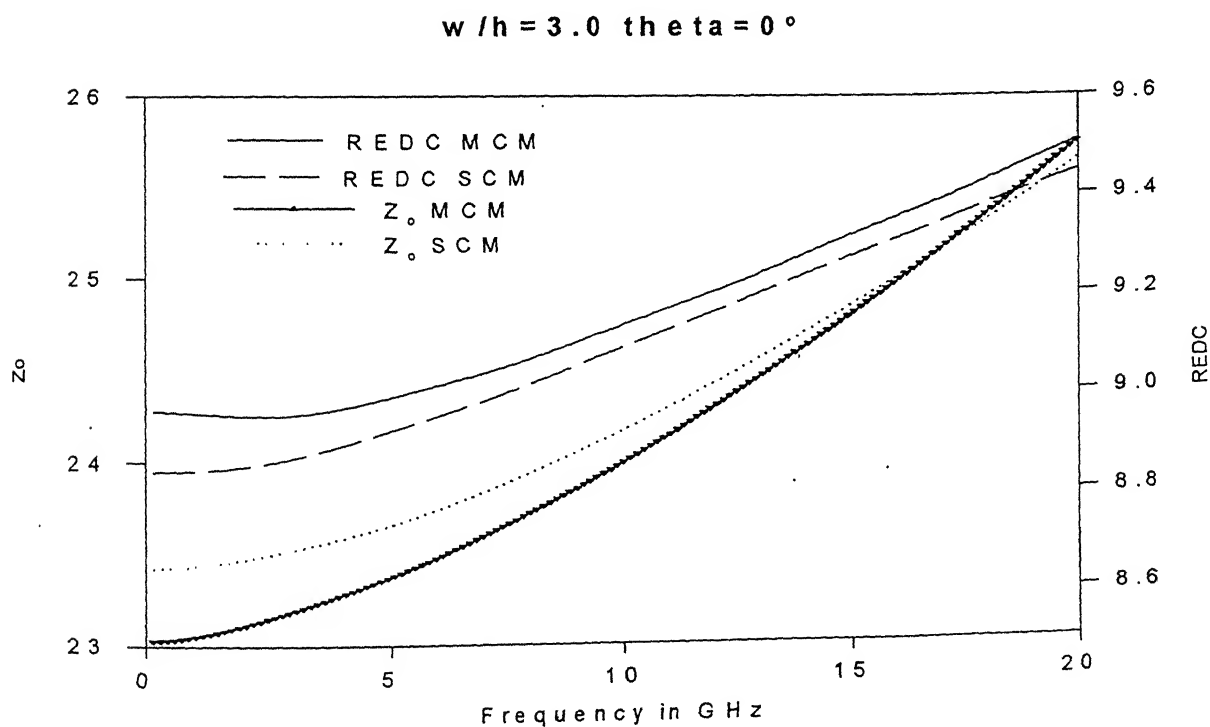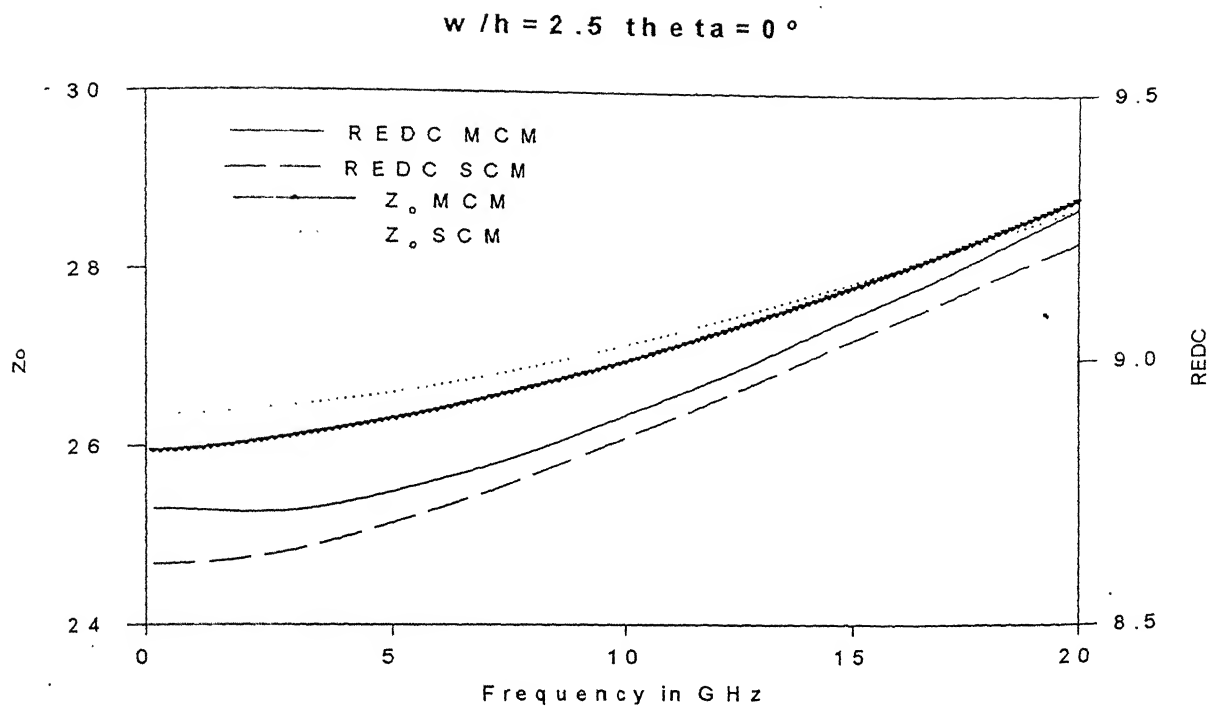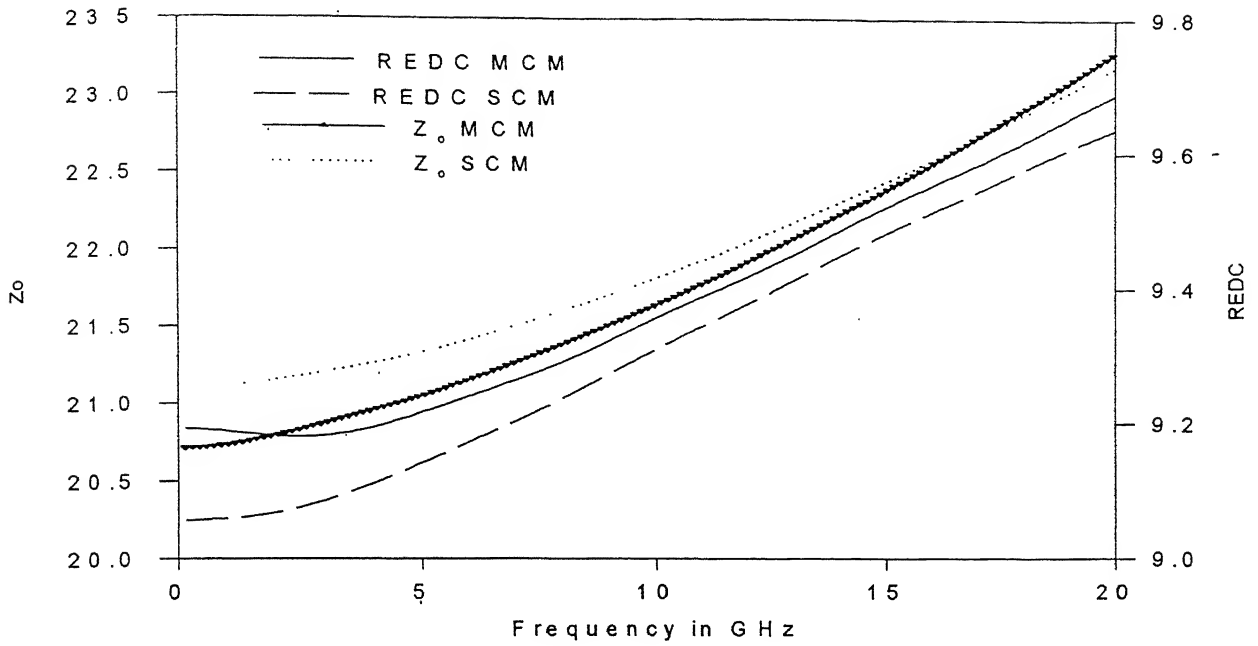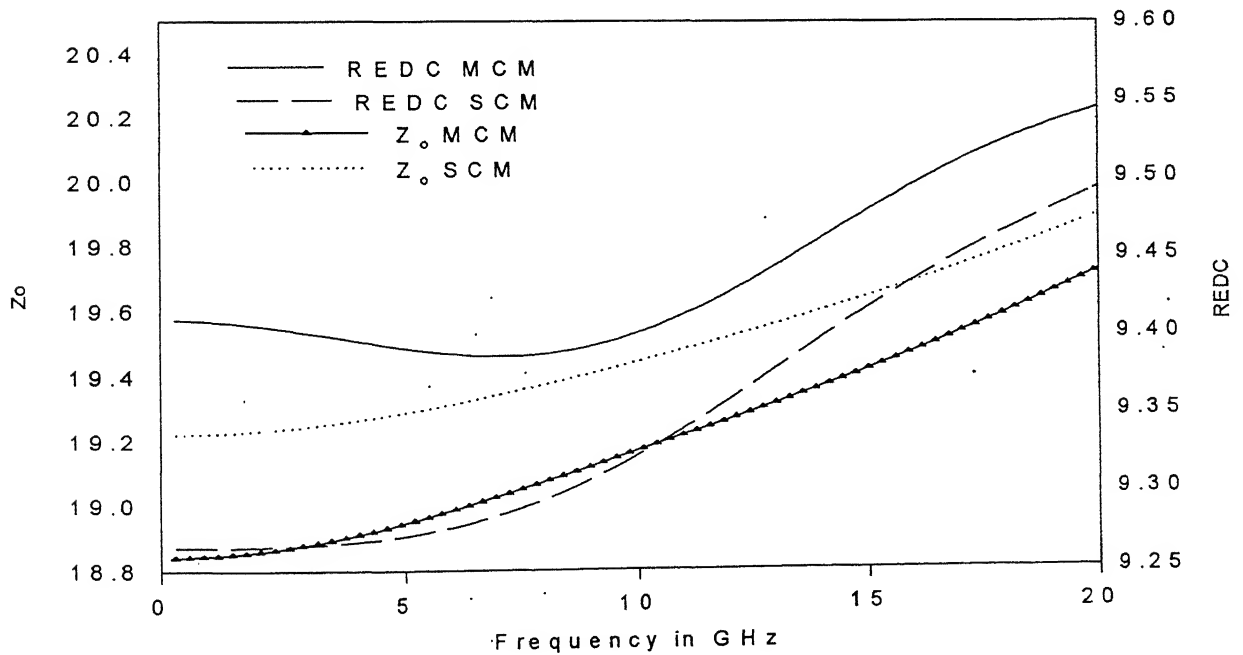
w /h = 1.2 theta = 0°

Figure 9.7

114

Figure 9.8

w/h=2.0 theta=0°

Figure 9.9

116

w /h = 2.5 theta = 0°

w /h = 3.0 theta = 0°

Figure 9.10

Figure 9.11

w /h = 4 .5 t h e ta = 0 °

Legend:
- REDC MCM
- REDC SCM
- Z₀ MCM
- Z₀ SCM

(Top plot: Zo vs Frequency in GHz; left axis Zo from 17.2 to 18.4, right axis REDC from 9.40 to 9.75)

w /h = 5 th e ta = 0 °

Legend:
- REDC MCM
- REDC SCM
- Z₀ MCM
- Z₀ SCM

(Bottom plot: Zo vs Frequency in GHz; left axis Zo from 15.8 to 17.0, right axis REDC from 9.5 to 9.9)

Figure 9.12

119

w /h = 1.0   y =   1 0 0 y 1 = 1 0 9 th e ta = 0 °

Legend:
- REDC MCM
- REDC SCM
- Z_0 MCM
- Z_0 SCM

Y-axis (left): Zo
Y-axis (right): REDC
X-axis: Frequency in GHz

w /h = 1.0   y =   9 0 y 1 = 1 0 9 th e ta = 1 5 °

Legend:
- REDC MCM
- REDC SCM
- Z_0 MCM
- Z_0 SCM

Y-axis (left): Zo
Y-axis (right): REDC
X-axis: Frequency in GHz

Figure 9.13

128
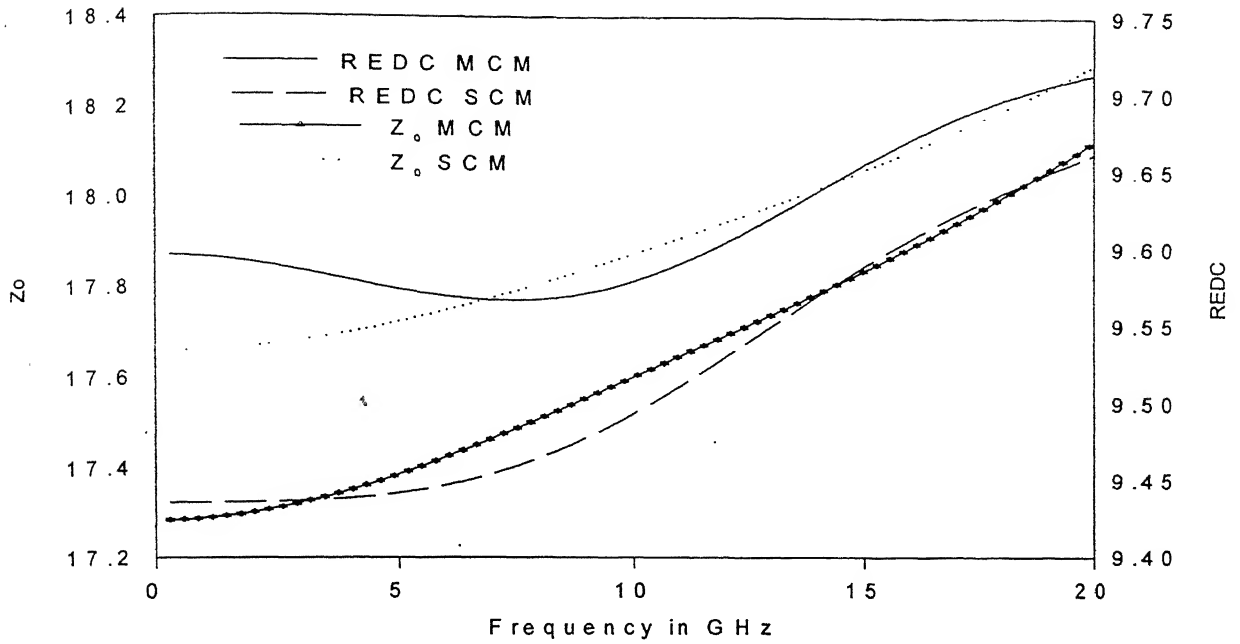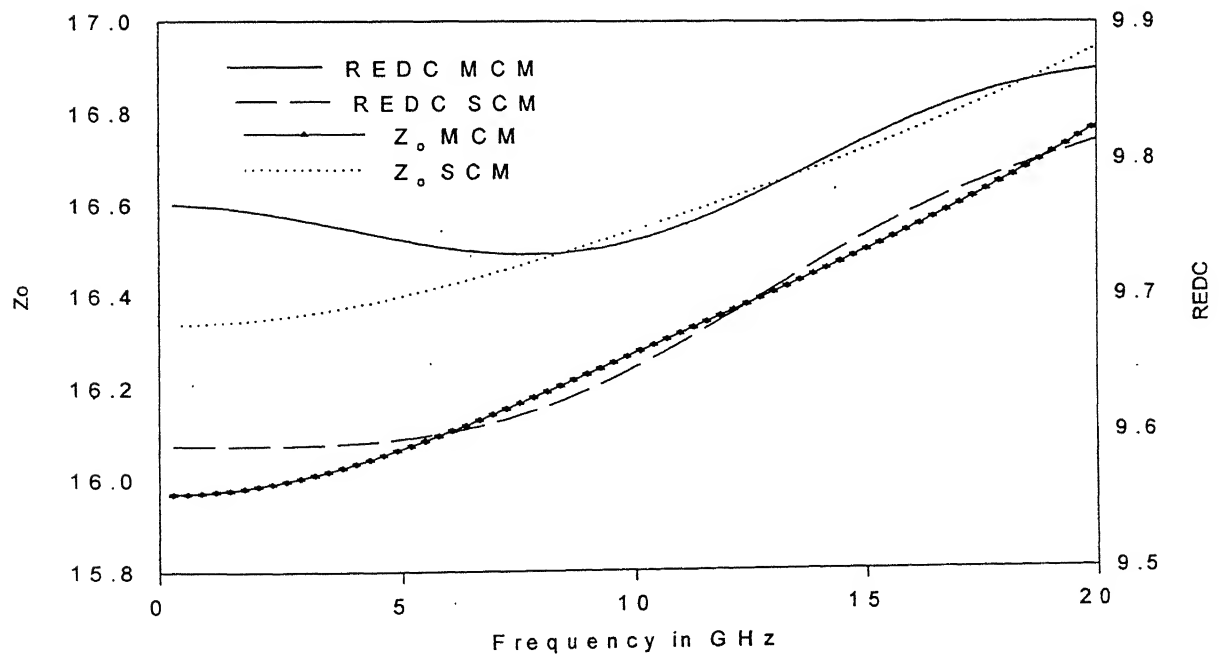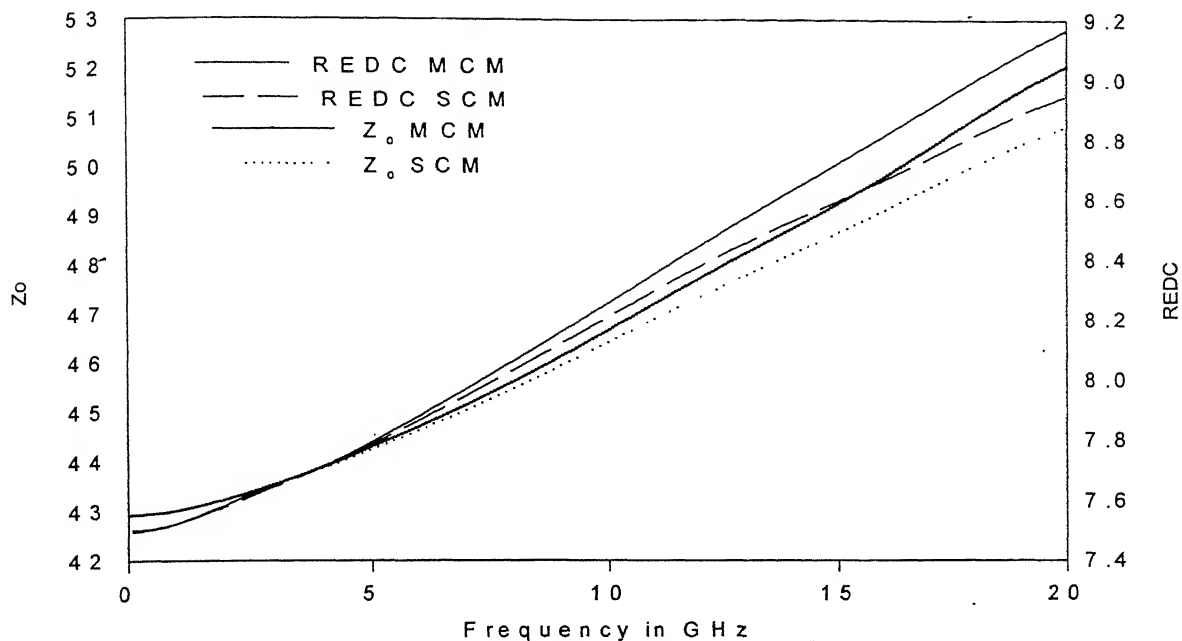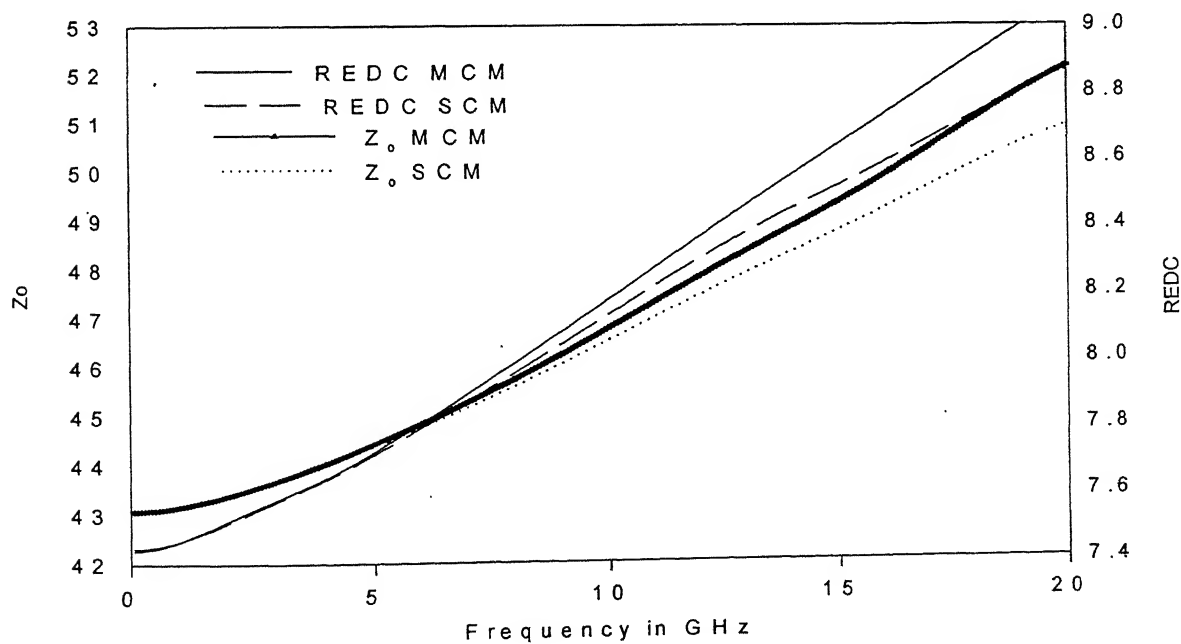
w /h = 1.0 y= 90 y1=109 theta=30°
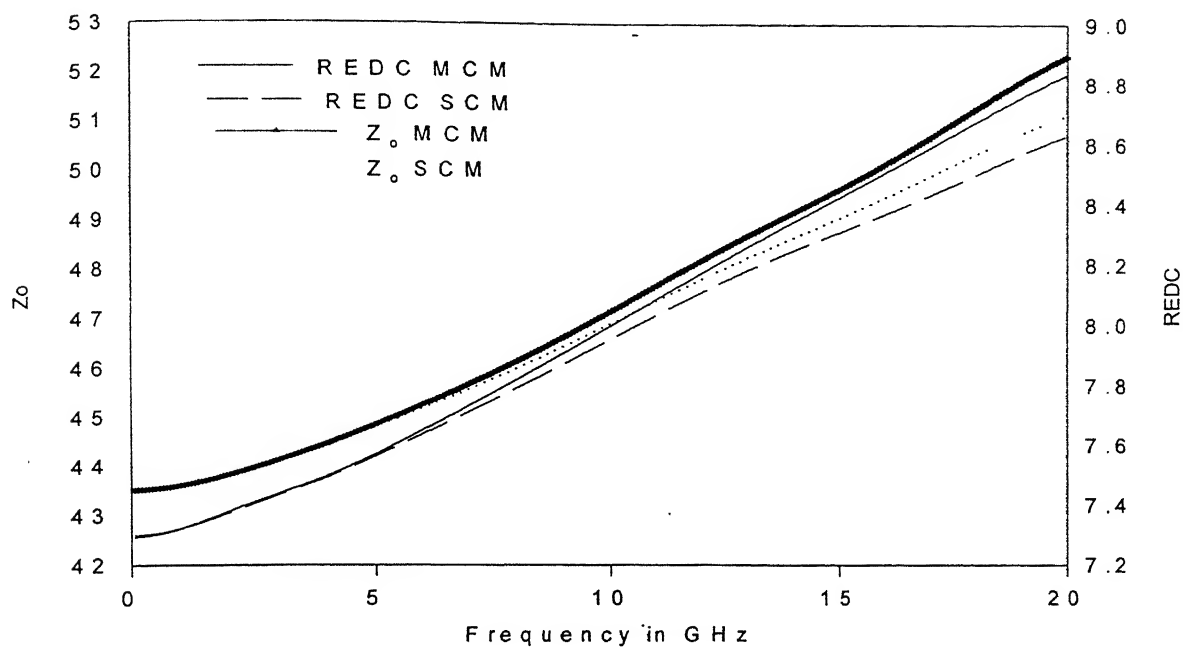
w /h = 1.0 y= 90 y1=109 theta=45°

Figure 9.14

w / h = 1.0   y = 90 y1 = 109 theta = 60°

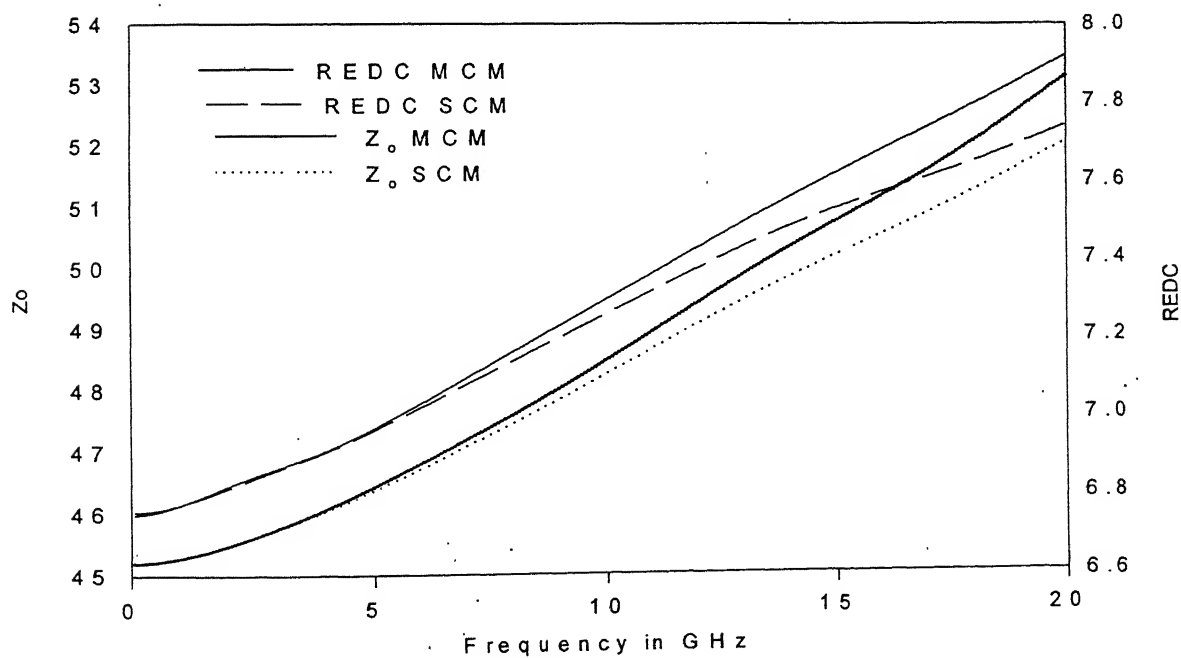w / h = 1.0   y = 90 y1 = 109 theta = 75°
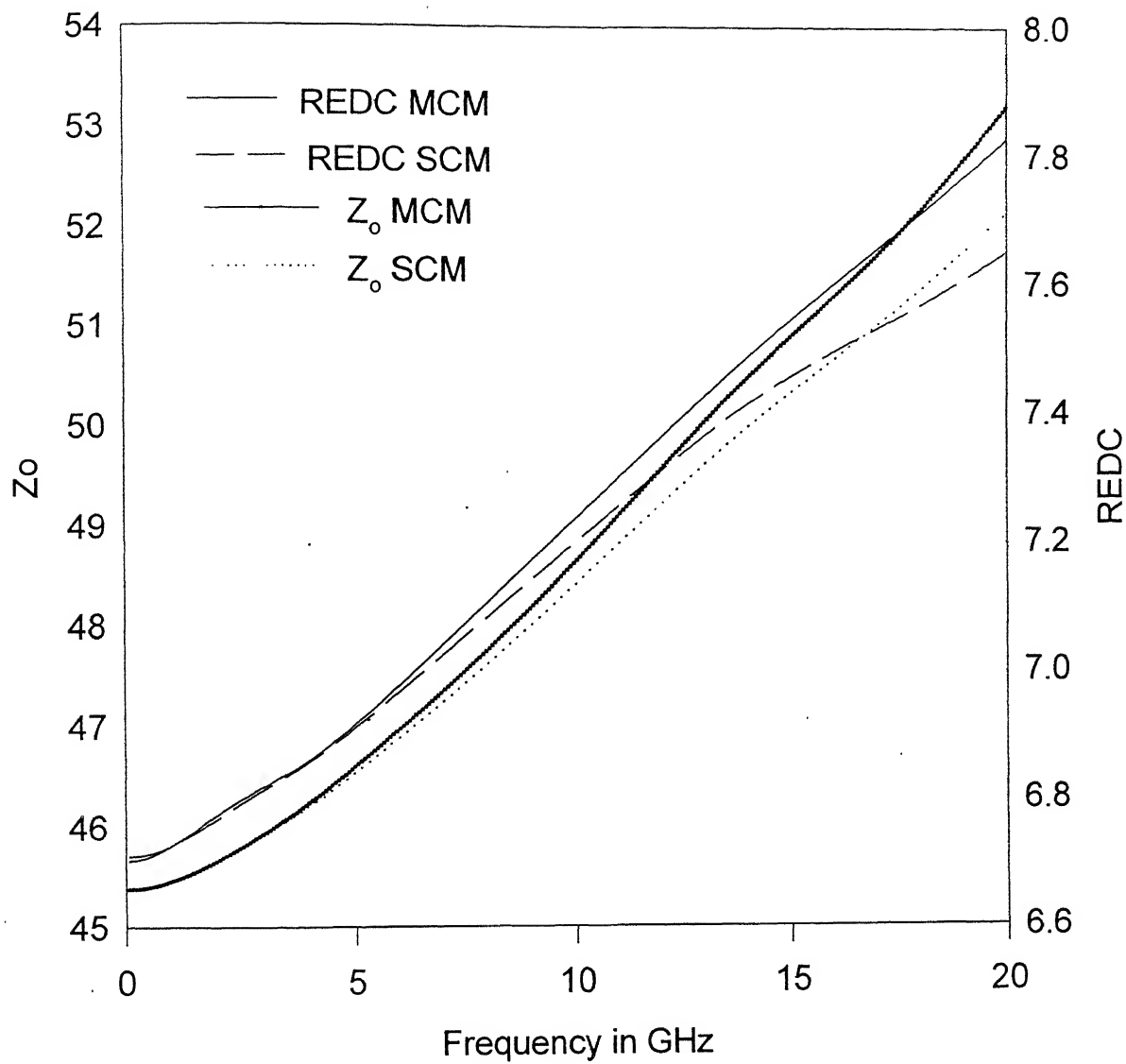
Figure 9.15

122
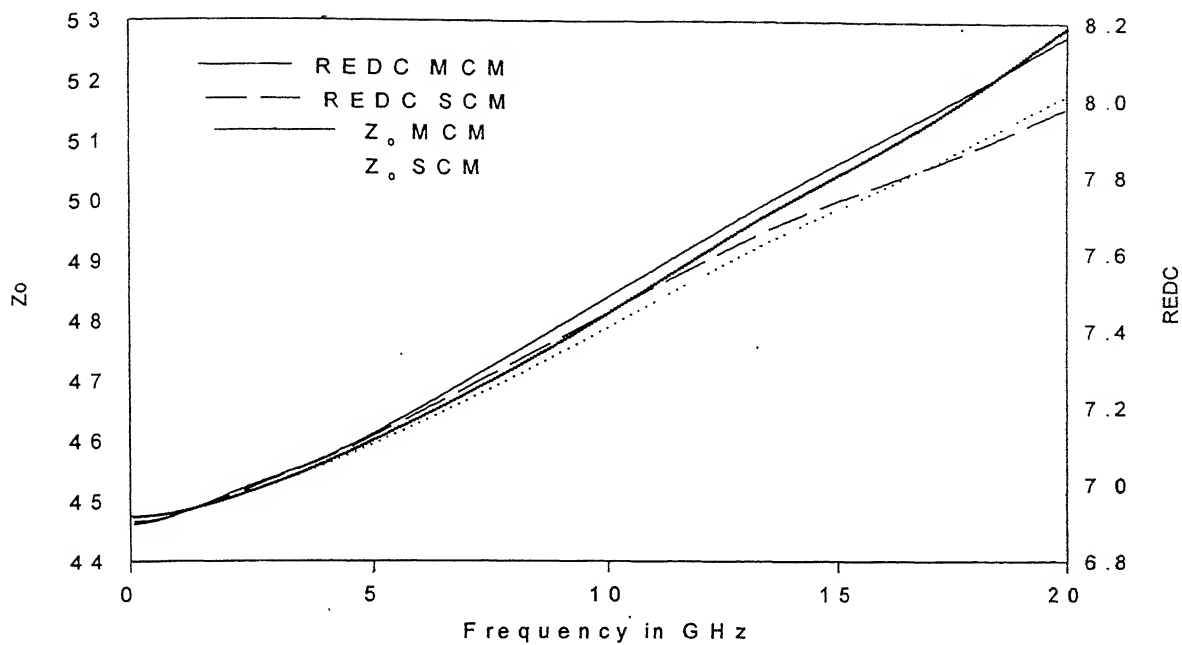
w/h=1.0 y= 90 y1=109 theta=90°

Figure 9.16

Conclusions and Further Developments

In this thesis work we have proved that any field quantities, if they can be expressed in Maxwellian form, can be matched using unsplit formulation of PML. This is possible due to material independent nature of the PML equations. We have also demonstrated that in 2-D space any incident plane wave irrespective of its polarization, frequency and angle of incidence can be matched at the interface of PML and Anisotropic medium without any reflection. Our results clearly demonstrated that because of virtually transparent boundary conditions, there is no oscillatory behavior in frequency dependent characteristics of transmission line and results are highly accurate. Since by using MIPML formulation it is possible to truncate computing domain (compare the size of domain used by Zhang et al. [2] and by us for similar w/h ratio), by using reasonable sizes of computing domains, very small w/h or very large w/h ratios can be analyzed. For example we have analyzed w/h ratios from 0.2 to 5. We could have gone for even smaller or bigger ratios then this if computer system with slightly larger memory were available.

After formulating MIPML for anisotropic media and preparing simulator for it, we tested it thoroughly for various planar circuits and for a uniform 3-D anisotropic space. We could achieve very good absorption with worst case figure well above –75 dB in case of uniform arbitrary anisotropic media.

We also simulated propagation of a Gaussian pulse and calculated characteristics of a patch antenna. Our results were in excellent agreement with Zhao who calculated them using split formulation.

After making sure that simulator MIPML properly and gives accurate characteristics we used it for our ultimate goal of finding dispersion characteristics of Microstrip on an anisotropic substrate. We have chosen it for several reasons. One of the main reasons was that most of the researchers [34, 35] so far used TEM mode approximation as the mode of propagation while calculating characteristic impedance. They did not give dispersion characteristics in their results. As frequency increases mode of propagation does not remain TEM. Mariki [36] calculated dispersion of characteristic impedance for w/h ratios of 1.5,3,3.5 and 5 but as far as relative effective dielectric constant was concerned he gave characteristics only for single ratio of one.

We have worked out ratios as wide as 0.2 to 5 and for all these ratios, we have given dispersion characteristics of relative dielectric constant and characteristics impedance. This data is very useful for designing microstrip circuits on anisotropic substrate.

We have also worked out effect of angle of crystal optical axis with X-axis. Thus effect of angle has also been taken into account. This shows that our simulator is capable of working and providing accurate results for microwave CAD in non-homogeneous, arbitrary anisotropic media.

We have also used a new method, which is very simple and provides highly accurate data, for dispersion characteristics by reducing oscillatory behavior. Here we use data over a single cell. So nature of errors in time domain which are already very little because of excellent boundary conditions is identical and magnitude is almost same as they are over a cell only. Since we are Subtracting voltages and currents, these errors also tend to get cancelled. This accounts for non-oscillatory behavior. Our method is simpler than liou et al. [12] as it does not require calculation of charge and flux. Also conceptually it is very simple, as it is just descretization of equivalent circuit of transmission line analogy. However, pinch of caution is that in frequency range, as long as above-mentioned model is valid, results of this method are valid. For further frequency range above 25 GHz, multiple cell method [2] is to be used.

Further Developments and Suggestions

In this simulator we have kept provision of taking care of evanescent waves and lossy media. To do so Kappa factor in DATAIN subroutine has to be kept more than one. Though we did not do any experimentation with this because of shortage of time but it can further reduce size of computing domain, as we need not to provide space for attenuation of evanescent waves. Some very exciting experimentation will be done in near future for calculating S parameters of basic microwave discontinuities on arbitrary anisotropic substrate with very small computing domain. As we have already mentioned that this simulator can analyze any planar geometry without any modification.

We also plan to analyze scatterers, which are not planar. For that slight modifications in the subroutines responsible for implementing boundary conditions for D and E are to be done. There is no need for doing any other modification in the core algorithm. With this addition it will be possible, to analyze DR circuits, Ferrite based circulator etc.

he most exciting area could be the analysis of multiconductor microstrip and stripline circuits, hot topic in the area of computer hardware. Our simulator can do that without any odification. Only geometry needs to be specified.

research the trend is to build upon what others have done. Though our simulator has been sted in Cartesian Coordinates but as we stated earlier that shortage of computer memory, wsoever big computer may be, always comes into picture. In our case we faced it for very mall or very large w/h ratios. It will become a very potent simulator if in future, Subcellular, ubgridding techniques [4,5] and conformal coordinate [6] techniques in form of new broutines are included with this simulator. This will facilitate doing simulation for thin gaps, ints and wires. Also cylindrical DRs and cylindrical ferrite geometry based circulators can be esigned. This simulator, named MIPML will become a complete package for any kind of eometry

astly we would like to stress that this simulator does simulation for isotropic media also. This mulator can also do any problem of any planar circuit in any linear media including anisotropic edium.

ince this simulator has been developed using Material Independent properties of PML we have amed it MIPML Simulator.

References

1. K. S. Yee, " Numerical Solution of initial boundary value problems involving Maxwell's equations in isotropic media." *IEEE Trans. Antennas and Propagation*, Vol.14, 1966, pp. 302-307.

2. X. Zhang, J. Fang, K. K. Mei and Y. Liu, "Calculation of Dispersive Characteristics of Microstrip by the Time Domain Finite Difference Method." *IEEE Trans. Microwave Theory and Techniques*, Vol.36, 1988, pp.263 -267.

3. Holland R. And J. W. Williams, " Total field versus scattered –field finite difference Codes: a comparative assessment," *IEEE Trans. Nuclear Science*, Vol.30, 1983,pp.4583 -4588.

4. Zivanovic, S. S., K. S. Yee, And K.K. Mei, "A Subgridding method for the time domain finite difference method to solve Maxwell's Equations." *IEEE Trans. Microwave Theory and Techniques*, Vol.39, 1991, pp. 471-479.

5. Holland R. And L. Simpson. " Implantation and optimization of the thin – strut formulation in THREDE," *IEEE Trans. Nuclear Science*, Vol.27, 1988, pp.1625 - 1630.

6. Holland R., "finite difference solutions of Maxwell equations in non-orthogonal co-ordinates," *IEEE Trans. Nuclear Science*, Vol. 30, 1983, pp.4589 -4551.

7. Tirkas P.A. and K. R. Demarest, "Modeling of thin dielectric structures using finite difference time domain technique," *IEEE Trans. Antennas and Propagation*, Vol. 39,1991, pp. 1338-1344.

8. Molaney, J.G. and G.S. Smith, "The efficient modeling of thin material sheets in the finite difference time domain method (FDTD)," *IEEE Trans. Antennas and Propagation*, Vol.40, 1992, pp.323 330.

9. Krumpholz, M., H. G. Winful, L.P.B. Katehi, "Non Linear time domain modeling by Multiresolution time domain," *IEEE Trans. Microwave Theory and Techniques*, Vol.45 , 1997 , pp. 385-393

10. Taflove A., and K. Umashanker," A hybrid moment method /finite difference time domain approach to electromagnetic coupling and aperture penetration into complex geometries," *IEEE Trans. Antennas and Propagation*, Vol.30, 1982, pp.617-627.

11. David M.Sheen, Sami M. Ali, Mohammed D. Abouzahra and Jin Au Kong, " Application of the three dimension finite difference time domain method to the analysis of planar Microstrip Circuits," *IEEE Trans. Microwave Theory and Techniques*, Vol. 38, 1990, pp. 849-856.

12. L. L. Liou and M. Mah, " An equivalent Circuit Approach for Microstrip Component Analysis Using the FDTD Method." *IEEE Microwave and Guided wave lett.*,Vol.8, 1998,pp.330 –332

13. Jean-Pierre Berenger, " A Perfectly Matched Layer for the Absorption of Electromagnetic Waves." *J. Computational Physics*, Vol.114, 1994, pp.185 -200.

14. Michael A. Gribbons, William P.Pinello, and Andreas C. Cangellaris, " A stretched Co-ordinate Technique for Numerical Absorption of Evanescent and Propagating Waves in Planar Waveguiding Structures." *IEEE Trans. Microwave Theory and Techniques*, Vol.43, 1995, pp. 2883-2889.

15. Zhonghua Wu and Jiayuan Fang, " Numerical Implementation and Performance of Perfectly Matched Layer Boundary Condition for Waveguiding Structures." *IEEE Trans. Microwave Theory and Techniques*, Vol.43, 1995, pp. 2677-2683.

16. Jiayuan Fang and Zhonghua Wu, "Generalized Perfect Matched Layer for the Absorption of Propagating and Evanescent Waves in Lossless and Lossy Media." *IEEE Trans. Microwave Theory and Techniques*, Vol. 44, 1996, pp. 2216-2222.

17. Li Zhao and Andreas C. Cangellaris, " A General Approach for the Development of Un-split Field Time-Domain implementations of Perfectly Matched Layers for FDTD grid truncation." *IEEE Microwave and Guided wave lett.*,Vol.6 , 1996,pp.209 -211.

18. Weng Cho Chew and William H. Weedon, " A 3-D Perfectly Matched Medium from Modified Maxwell's Equations with Stretched Coordinates," *Micro. Opt. Tech. Lett.* , Vol. 7,pp. 599-604.

19. Zachary S. Sacks, David M. Kingland, Robert Lee, and Jin-Fa lee, " A Perfectly Matched Anisotropic Absorber for Use as an Absorbing Boundary Condition." *IEEE Trans. Antennas and Propagation*, Vol.43, 1995, pp.1460-1463.

20. Gedney, S.D., "An anisotropic Perfectly Matched Layer Absorbing Media for the Truncation of FDTD Lattice." *Technical Report EMG.95-006*, Dept. Of Electrical Engineering, University of Kentucky, March 1995.

21. Gedney, S.D., "An Anisotropic PML Absorbing Media for FDTD Simulation of Fields in lossy Dispersive Media," *Electromagnetics*, Vol.16, 1996, pp. 399-415

22. An Ping Zhao and M. A. Rinne, " Theoretical proof of Material Independent PML Absorbers Used for Arbitrary Anisotropic Media." *Electronics Lett.*, Vol.34, pp.48-49

23. An Ping Zhao, "Generalized –Material –Independent PML Absorbers used for the FDTD Simulation of Electromagnetic Waves in 3-D Arbitrary Anisotropic Dielectric and Magnetic Media." *IEEE Trans. Microwave Theory and Techniques*, Vol.46, 1998, pp.1511 -1513.

24. An Ping Zhao and Antti V. Raisanen, "Generalized Material Independent PML Absorbers for the FDTD Simulations of electromagnetic Waves in Arbitrary Anisotropic Dielectric and Magnetic Media." *IEEE Microwave and Guided wave lett.*, Vol.8 , 1998, pp.52 -54 .

25. Katz, D.S., E. T. Thiele, And A. Taflove, " Validation and Extension to 3-Dimesions of the Berenger's PML Absorbing Boundary Conditions for FDTD meshes." *IEEE Microwave and Guided wave lett.*, Vol.4 , 1994, pp.268 -270 .

26. Christopher E. Reuter, Rose M. Joseph, E. T. Thiele, D. S. Katz and Allen Taflove. "Ultra Wide Band Absorbing Boundary Condition for Termination of Waveguiding Structures in FDTD Simulation." *IEEE Microwave and Guided wave lett.*, Vol.4 , 1994, pp.344 -346 .

27. An Ping Zhao And Antti V. Raisanen, " Application of a Simple and Efficient Source Excitation Technique to the FDTD Analysis of Waveguide and Microstrip Circuits." *IEEE Trans. Microwave Theory and Techniques*, Vol.44, 1996, pp. 1535-1538.

28. An Ping Zhao, Antti V. Raisanen, and Srba R. Cvetkovic, "A Fast and efficient FDTD Algorithm for the Analysis of Planar Microstrip Discontinuities by Using a Simple Source Excitation Scheme." *IEEE Microwave and Guided wave lett.* , Vol.5, 1995, pp.341-343.

29. Deane T. Prescott and Nicholas V. Shuley, " Reflection Analysis of FDTD Boundary Conditions –Part I: Time-Space Absorbing Boundaries." *IEEE Trans. Microwave Theory and Techniques*, Vol.45, 1997, pp. 1162-1170.

30. Deane T. Prescott and Nicholas V. Shuley, " Reflection Analysis of FDTD Boundary Conditions –Part II: Berenger's PML Absorbing Layers." *IEEE Trans. Microwave Theory and Techniques*, Vol.45, 1997, pp. 1171-1178.

31. Garcia S.G., Perez I. V., R.G. Martin and B. Garcia Olmedo, "Applicability of the PML Absorbing Boundary Condition to Dielectric Anisotropic Media." *Electronics Letters*, Vol.32, 1996, pp.1270-1271.

32. An Ping Zhao And Antti V. Raisanen, "Material Independent PML Absorbers for Arbitrary Anisotropic Dielectric Media'' *Electronics Letters*, Vol.33, 1997, pp.1535-1536.

33. An Ping Zhao And Antti V. Raisanen, "Extension of Berenger's PML Absorbing Boundary Conditions to Arbitrary Anisotropic Magnetic Media," *IEEE Microwave and Guided wave lett.* , Vol.8, 1998, pp.15 -16.

34. Owens R. P., James E. Aitken, and T.C. Edwards, " Quasi-Static Characteristics of Microstrip on an Anisotropic Sapphire Substrate." *IEEE Trans. Microwave Theory and Techniques*, Vol. 24, 1976, pp.499 - 505.

35. N.G. Alexopoulos and C.M. Krowne, " Characteristics of Single and Coupled Microstrips on Anisotropic Substrates." *IEEE Trans. Microwave Theory and Techniques*, Vol.26, 1978, pp.387 -393.

36. G. E. Mariki and C. Yeh, "Dynamic Three-Dimensional TLM Analysis of Microstriplines on Anisotropic Substrate." *IEEE Trans. Microwave Theory and Techniques*, Vol.33, 1985, pp. 789-799.

37. Shoichi Koike, Norinobu Yoshida and Ichiro Fukai, "Transient Analysis of Microstrip Line on Anisotropic Substrate in Three-Dimensional Space." *IEEE Trans. Microwave Theory and Techniques*, Vol.36, 1988, pp.34 -43.

38. Enquist, B., and A. Majda, "Absorbing Boundary Conditions for the Numerical Simulation of Waves." *Mathematics of Computation*, Vol.18, 1975, pp.66-78

39. Mur, G., "Absorbing Boundary Conditions for the time dependent wave equation." *IEEE Trans. Electromagnetic Compatibility*, Vol.23, 1981, pp.377 -382.

40. M. A. Morgan, "Finite Element and Finite Difference Methods in Electromagnetic Scattering." *PIER, Elsevier* , 1989

41. Allen Taflove and Morris E. Brodwin, " Numerical Solution of Steady-State Electromagnetic Scattering Problems Using the Time dependent Maxwell's Equations." *IEEE Trans. Microwave Theory and Techniques*, Vol.23, 1975, pp.623-630.

42. Trefethen, L. N., and L. Halpern, "Well-posedness of One-way wave Equations and Absorbing Boundary Conditions," *Inst. Computational Appl. Sci. And Engrg.* (ICASE), NASA Langley Res. Ctr., Hampton, VA, Rept. 85-30,1985.

43. An Ping Zhao, "Figures of Characteristics of Patch antenna on an arbitrary anisotropic substrate." *In a personal communication*